FACULTY OF SCIENCES

EVALUATION OF THE DETECTION AND QUANTIFICATION OF SEDIMENT PLUMES CAUSED BY DREDGING ACTIVITIES USING A MULTIBEAM ECHOSOUNDER

Nils Lowie
Student number: 01200387

Promotor: Prof. dr. David Van Rooij
Copromotor: Koen Degrendele

Jury: Prof. dr. Marc De Batist, dr. Michael Fettweis

Master's dissertation submitted in partial fulfilment of the requirements for the degree of Master of Science in Geology

Academic year: 2016 – 2017

GHENT UNIVERSITY

KU LEUVEN

ACKNOWLEDGEMENTS

Writing a master thesis is a work to which a lot of people contributed in a direct or indirect way. It is also the crown on my education of five years. It would therefore like to use this page to thank everyone who helped and supported me in this journey, including you, the reader, for taking interest in this.

Several times throughout the process of writing this work and more in general my study I could make the comparison with a multibeam survey. Therefore I'll tell this story in analogy to a survey vessel.

Firstly I have to thank the captains who guided the vessel through the weather. I would like to thank my promotors who helped me getting this thesis written in particular. Thank you prof. Van Rooij for the reads of the drafts, constructive comments and trusting me into doing my own thing in a relatively unsearched field under the good guidance of my co-promotors. One of the most important guys I have to thank for this work, probably the head-captain of this ship, is my co-promoter Koen Degrendele. Thank you for the discussions on this topic and other, for letting me write at my own (slow) pace, and thank you for the reading and corrections. Together with Marc you gave me every possible chance (I refer to the 'Story of My Research' part for this). I learned a lot from all the presentations in which you guided me and it helped me to be more confident in presenting. It even helped me to get the dream job I wanted at one of my dream companies, and therefore I am forever grateful to the both of you.

A vessel is nothing without its crewmembers to operate everything and keep things going. I would like to thank prof. Bertrand, Elke and Loic for guiding me into the world of grain size analysis and thank them for their time explaining everything related to it. Thank you to the crew of RV Simon Stevin and thank you to my colleagues at the CSS for their pleasant company at noon when eating.

A vessel cannot navigate without fuel, which I consider as both emotional as financial support. For the latter I would like to thank the FPS Economy for paying my trip to Rennes and travel expenses. Lastly as for emotional support I would like to thank the following people.

Lies(beth), although our ways have parted now, I thank you for the first four years of my study in which you were my biggest support. Not mentioning you here would be unfair to the truth and I will not forget the big part of you in this story.

Thank you to my friends, for all the (un)forgettable nights out and the stud(ie)ing together. Thank you to my classmates and Geologica friends for the nice moments and excursions. Thank you to some best friends in particular: Simon, Dolf, Ricardo, Mathias, Rob and Stan, especially for your special support during the beginning and first semester of this last studying year. Thank you Eline for your recent support!

Merci oma en pepe en de rest van mijn familie voor de steunende berichtjes voor een examen. Lars, Amber en Jinte, merci om mijn soms rare stressdansjes te verdragen, mijn plagende opmerkingen en meer gedurende examenperiodes en periodes van stress (dat wil niet zeggen dat jullie er nu van af zijn!).

Mama en papa. Deze campagne was een campagne met veel storm en mooi weer afgewisseld. Weer is altijd de onzekere factor, maar er was doorheen mijn studie één zekerheid: jullie waren de sterke mast van het schip die alles overeind hield, ervoor zorgde dat het schip niet zonk, het onderdeel van het geheel waar ik altijd kon op rekenen. Bedankt om doorheen woelige periodes met veel stress en mijn niet altijd vriendelijk zijn toch achter mij te blijven staan en mij onvoorwaardelijk te steunen. Merci om mij de kans te geven om te studeren en dus de financiële support. Ik kon mij geen betere ouders/houvast voorstellen.

LIST OF FIGURES

LIST OF TABLES

LIST OF ABBREVIATIONS

ADCP	Acoustic Doppler Current Profiler
BCS	Belgian Continental Shelf
BD	Backhoe Dredger
BPNS	Belgian Part of the North Sea
CSD	Cutter Suction Dredger
CTD	Conductivity, Temperature and Depth
CUBE	Combined Uncertainty and Bathymetry Estimator
dB	Decibel
EEZ	Exclusive Economic Zone
FMGT	FlederMaus Geocoder Toolbox
IFREMER	Institut Français de Recherche pour l'Exploitation de la Mer
MBES	Multibeam Echosounding System
PSU	Practical Salinity Unit
RTK	Real Time Kinematic
RV	Research Vessel
SBS	Seafloor Backscatter
SPI	Sediment Profile Images
SPM	Suspended Particulate Matter
SVP	Sound Velocity Probe
TSHD	Trailing Suction Hopper Dredger
WCBS	Water Column Backscatter

TABLE OF CONTENTS

THE STORY OF MY RESEARCH

The story of my research can be told from the initial beginning, which probably even dates back to when I was 13 to 14 years old. As a young student in secondary school I was always fascinated by nature, watching a lot of documentaries on television, always interested in how things worked. I studied Latin in my first four years of middle school, followed by a transition to the science-mathematics direction in my last two years. I was very interested in the whole of sciences with mainly physics and geography as highest interests. This preference for sciences made me after a long consideration choose for trying to obtain a bachelor's degree in geology at Ghent University because of its combining of biology, chemistry, physics, geography, geology and a bit of mathematics.

It was only in my third bachelor year that I really came in contact with my main interest in geology: the marine geology branch. Courses such as geophysics, marine geology and tele-detection were my favourite ones back then. Moreover, in our last bachelor year we were given the chance to choose our own topic for our bachelor thesis. I chose for a topic outside the university about sand and gravel extraction on the Belgian Continental Shelf with Lies De Mol from the Continental Shelf Service (CSS) as my tutor. I had to work with them for almost six weeks, a period in which I learned a lot about acquiring bathymetric data, processing and interpreting it. I was even given the chance to go on a surveying campaign on RV Belgica for some days which only enhanced my interest in surveying and marine geology even more. At the Continental Shelf Service I also met Koen Degrendele and Marc Roche for the first time who now helped me for this master thesis.

After my bachelor thesis I started a master in geology of basins. In the second term of the first master I had a window I which I had to choose 30 credits of elective courses. I chose to maximise the courses related to marine geology and learned a lot of new things from 'Marine surveying', 'Ocean drilling', 'Dredging and offshore' and several other courses. It was also at that time that the master thesis subject came available. I had already thought about which direction I wanted to specialize myself in and it was back then that I decided to ask Koen and Marc of the CSS if they had any topic for me. Gladly for me they indeed could propose me a subject about water column backscatter which I happily accepted.

For the last year now I have been writing my thesis. During that period I spent around five days on sea, acquiring my own data on board of RV Simon Stevin which is always a pleasant experience. The most interesting part of it is exploring and working on it at your own pace and time. Exploring new fields comes with new challenges and limitations which make the work even more enjoyable. In January Marc and Koen encouraged me to send in an extended abstract of my ongoing research with which I was selected to do a pitch presentation on the VLIZ Marine Science Day. In April I even had the opportunity to go with them to the Catalyst Workshop on Water Column Data to present some more of my research. Both presentations helped me to become more experienced and confident in presenting. In the end all these things told here helped me to already sign a contract signed as surveyor at one of the world's biggest dredging firms, and therefore my next challenge already awaits in October.

CHAPTER I INTRODUCTION

1.1. Sand extraction on the Belgian Continental Shelf

Sand extraction on the Belgian Continental Shelf (BCS) started in 1976 and has increased ever since (FPS Economy S.M.E.s Self-employed and Energy, 2014). The extraction of sand on land is becoming more difficult because of environmental and spatial policies as legislation and laws got stricter over these 40 years of extraction. Moreover sand from the sea has some advantages over sand gained on land. It is easier to extract in general, cheaper and the composition is more consistent (FPS Economy S.M.E.s Self-employed and Energy, 2014). Almost no clay and silt is present and only the most resistant particles are concentrated, the sand fraction itself (Mathys, 2009). This sand is mainly used for two purposes (Van De Kerckhove, 2011). In the construction industry sand is used as one of the main components of concrete, but also for foundations and asphalt. Another important use of the Belgian marine sand is coastal defence. Due to big storms (the so called superstorms) and a generally rising sea level (Lebbe et al., 2008), the Belgian beaches could erode and be destroyed. On the 10th of June 2011 the Flemish government approved a Masterplan of Coastal Defence (Flemish Government Department Coastal Safety, 2014) in which the beaches and dunes of the 10 Flemish coastal cities will be enforced against the erosion due to the sea.

Since 1999 the Continental Shelf Service (CSS) of the Belgian Federal Government is responsible for the monitoring and regulation of all the extraction. The CSS issues the exploitation permits and monitors the impact of the extraction by gathering and processing multibeam echosounding system (MBES) data and by comparing this with data from Electronic Monitoring Systems (EMS), the so called 'black box' data of the dredging vessels. Moreover they can advise the closure of certain extraction areas where more than five meter of sand is extracted compared to a reference level (FPS Economy S.M.E.s Self-employed and Energy, 2014). The extraction areas mainly lie on the Flemish banks (sector 1), the Hinder banks (sector 4) and the Thorntonbank (sector 3) (Fig. 1). Monitoring zone TBMAB situated on the Thorntonbank is the zone in which this study is situated.

The sand used from the BCS is not unlimited and is getting scarcer (Roche et al., 2017). An estimation along a profile inside zone TBMAB shows that since 2008 the extracted volume per month has risen from 1 000 m³ to 7 000 m³ on the Thorntonbank, with a sharp increase since 2013 (Fig. 2). Studies have recently been succeeded to map the exploitable sand reserves and based on this several manageable changes for the limits of sand extraction have been proposed (Degrendele et al., 2017).

On the BCS, exploitation is only allowed with trailing suction hopper dredgers (TSHD) (FPS Economy S.M.E.s Self-employed and Energy, 2014). This type of dredging vessel is obliged to be constantly moving when extracting and sucks up the sand by means of a suction head. This way of dredging has both direct and indirect impacts for the seafloor and the water column. The aim of this work is to find a more extensive way to monitor these changes in space and in time through the use of a MBES.

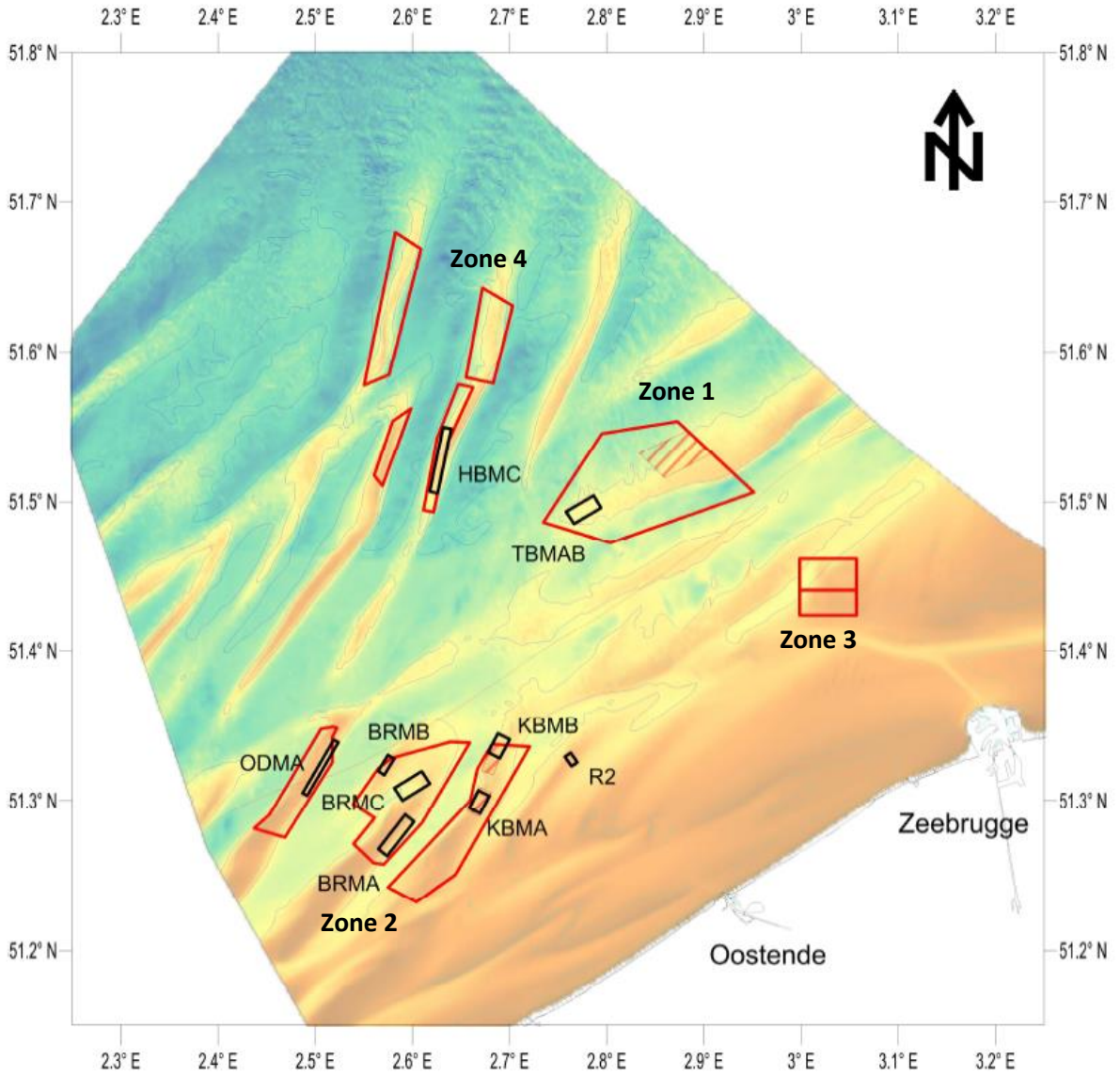

Figure 1. The Belgian Continental Shelf with the sandbanks and the sectors of monitoring on it. Zone 1: Thorntonbank, zone 2: Flemish Banks, zone 3: Sierra Ventana, zone 4: Hinder Banks (Degrendele et al., 2014). *Projection of the map is WGS84.*

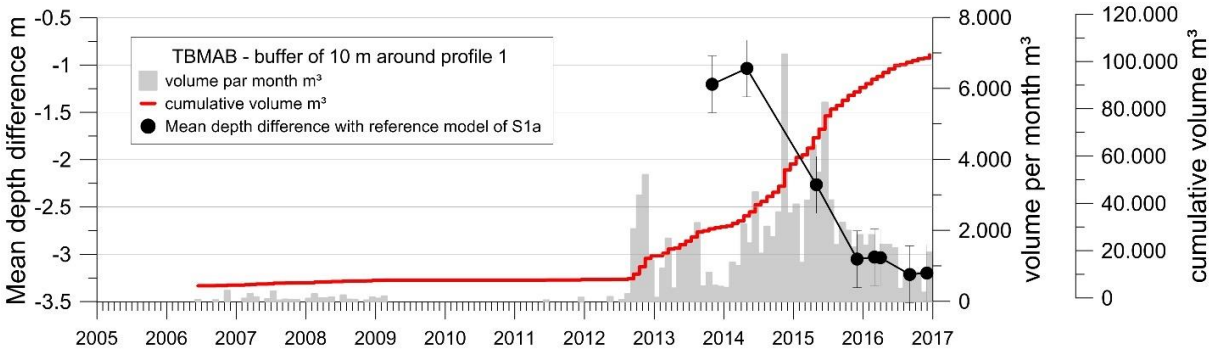

Figure 2. Extracted volume per month, cumulative volume and mean depth difference with reference model of S1a (2001-2004) calculated along a profile in monitoring zone TBMAB (Roche et al., 2017).

1.2. Objectives

To be able to more extensively monitor dredging, several topics will be investigated. Firstly the real-time impact of a TSHD on seafloor bathymetry and backscatter properties will be investigated and an identification and characterisation of the real-time dredging track will be carried out. These represent the direct impact of dredging. The eventual fading or replenishing of the dredging track will be investigated during the next step in the investigation. This will be studied by using bathymetric and backscatter data, obtained during campaigns before and after the dredging.

The water column is also affected by dredging, representing the indirect impact of sand extraction. A TSHD causes sediment plumes which will disperse scatters (so the fine dredged fraction itself) in the water column. A differentiation is made between a sediment plume caused by the overspill of the TSHD, which is seawater with suspended particulate matter (SPM) and the sediment plume caused by dragging the suction head on the seafloor (Spearman et al., 2011). This will lead in the end to two sorts of plumes: the active plume and the passive plume (Fig. 3). Sediment plumes due to dredging have already been studied before (Duelos et al., 2013; Evangelinos, 2015; Nieuwaal, 2001; Spearman et al., 2011; Van Lancker et al., 2014).

But sediment plumes are also formed in other circumstances. Next to dredging they are also formed during bottom trawling (Jones, 1992; Palanques et al., 2001; Pilskaln et al., 1998), under influence of wind farms (Booth et al., 2000; Vanhellemont and Ruddick, 2014) and even natural conditions (storms, river run off) (Gabrielson and Lukatelich, 1985; Richards and Leighton, 2003).Water column data of MBES is up until now mostly used to detect gas venting, near surface bubbles, imaging of internal waves and imaging of turbulence. Also large applications are to be found in fishery research and detection of shipwrecks (Colbo et al., 2014).

The cumulative influence of sediment plumes can have big consequences for marine life. Negative impacts of sediment plumes are related to marine ecology, the overall quality of the water, and influence on fish communities (Nieuwaal, 2001). Some examples of these negative impacts can be stated. SPM will trouble the water near the dredging site, leading to light attenuation, light that is needed for corals to survive (Erftemeijer et al., 2012). Also interference of SPM with respiration and the filter feeding systems of some organisms should be avoided (Taylor et al., 2011). SPM causes reduction of photosynthesis by plankton, algae and vegetation. This reduction eventually disturbs the food chain (Nieuwaal, 2001). Increases in SPM concentration will cause reduction of oxygen in the water and eventually the release of heavy metals (Kim, 2011).

Up until now most research and knowledge of water column data is specific to these cases and could not really be used for the specific case of sediment plumes. Moreover when sediment plumes are studied in most cases Acoustic Doppler Current Profilers (ADCP) or Optical Backscatter (OBS) is used (Battisto and Friedrichs, 2003). Therefore this work will give a first insight in the early possibilities of usage of water column data derived from MBES for the detection of sediment plumes. This research should in the end be part of a bigger research question in which the feasibility to use MBES to obtain a SPM concentration will be investigated, which is currently ongoing (Best et al., 2010; Simmons et al., 2010)

By using the water column data an evaluation will be made of the parameters that affect the water column backscatter (WCBS) using a MBES in order to obtain a better comprehension of the sediment plumes and to better map these sediment plumes in the future. As there is a dataset at hand which represents the real time dredging changes, several correlations will be investigated to obtain an insight

in this. The distance in space and time between dredger and survey ship will be used to assess the impact on the WCBS. For this, correlations of time differences between vessels and the WCBS value will be investigated. In other words the speed at which the sediment plume fades will be researched. Also the importance of at what distance the dredger should be followed to capture the plume will be researched. Additional samples are available to be used for information of the sediment itself.

A last goal of this work is to visualize the sediment plumes using the water column data and convert this to maps of plume intensity and even a three-dimensional model of the plume. The possibilities of treating raw water column data will be given with the problems encountered and the advantages and disadvantages of the used software.

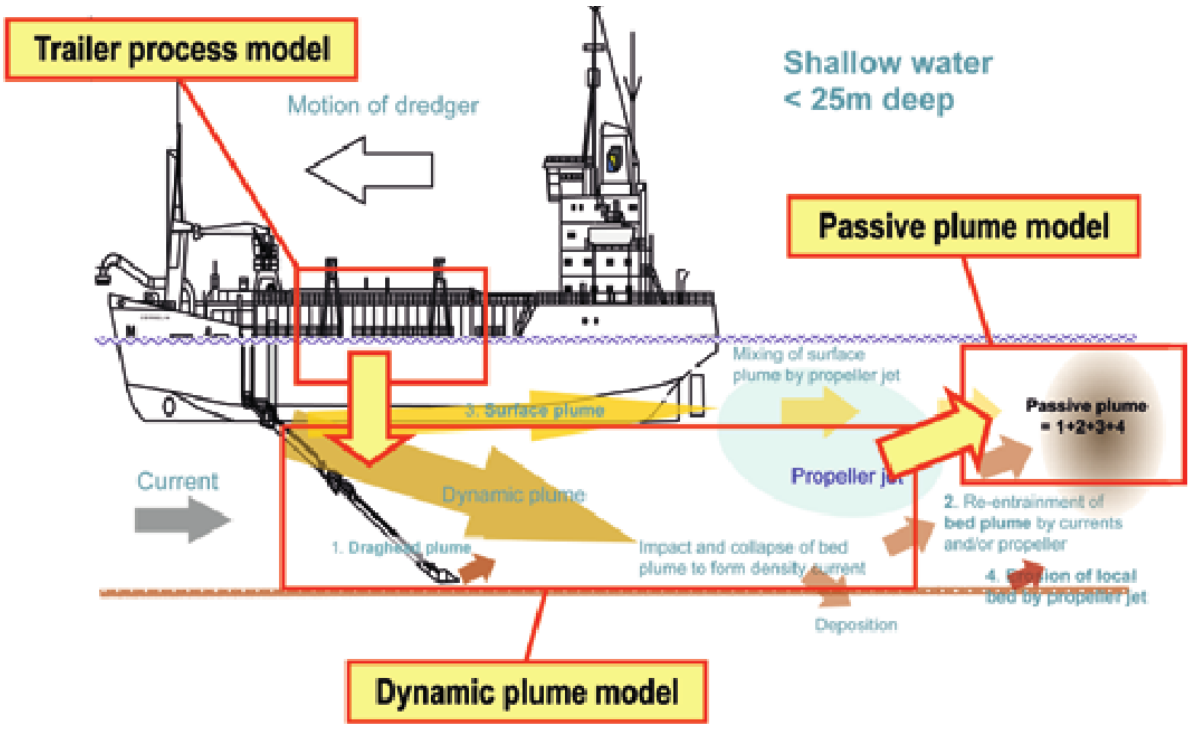

Figure 3. Illustration of the overspill from the barge and the dragging of the suction head, which will lead to a dynamic sediment plume and a passive sediment plume (Spearman et al., 2011).

2.1. The North Sea

The North Sea is an epicontinental shelf sea and lies in between France, Belgium, The Netherlands, Denmark, Germany, Norway and Great Britain (Fig. 4). It has exchanges with the Atlantic Ocean in the north, through the Norwegian Sea, as well as in the south where the Strait of Dover (40 km wide in between Calais and Dover) and The Channel form a corridor to the Atlantic Ocean. The Kattegat in between Denmark and Sweden forms the connection with the Baltic Sea in Scandinavia. The surface area of the North Sea is 575 000 km² with an estimated water volume of 54000 km³ (De Moor, 1986). The water depth of the North Sea ranges mainly from several meters to 100 meters in the central part of the North Sea, with deeper parts (till 200 m depth) at the coast of Norway and in the Kattegat (Fig. 4). The average depth of the North Sea is 80 m, the maximum water depth is 800 m in the Norwegian Trench (Pohlmann and Sündermann, 2011).

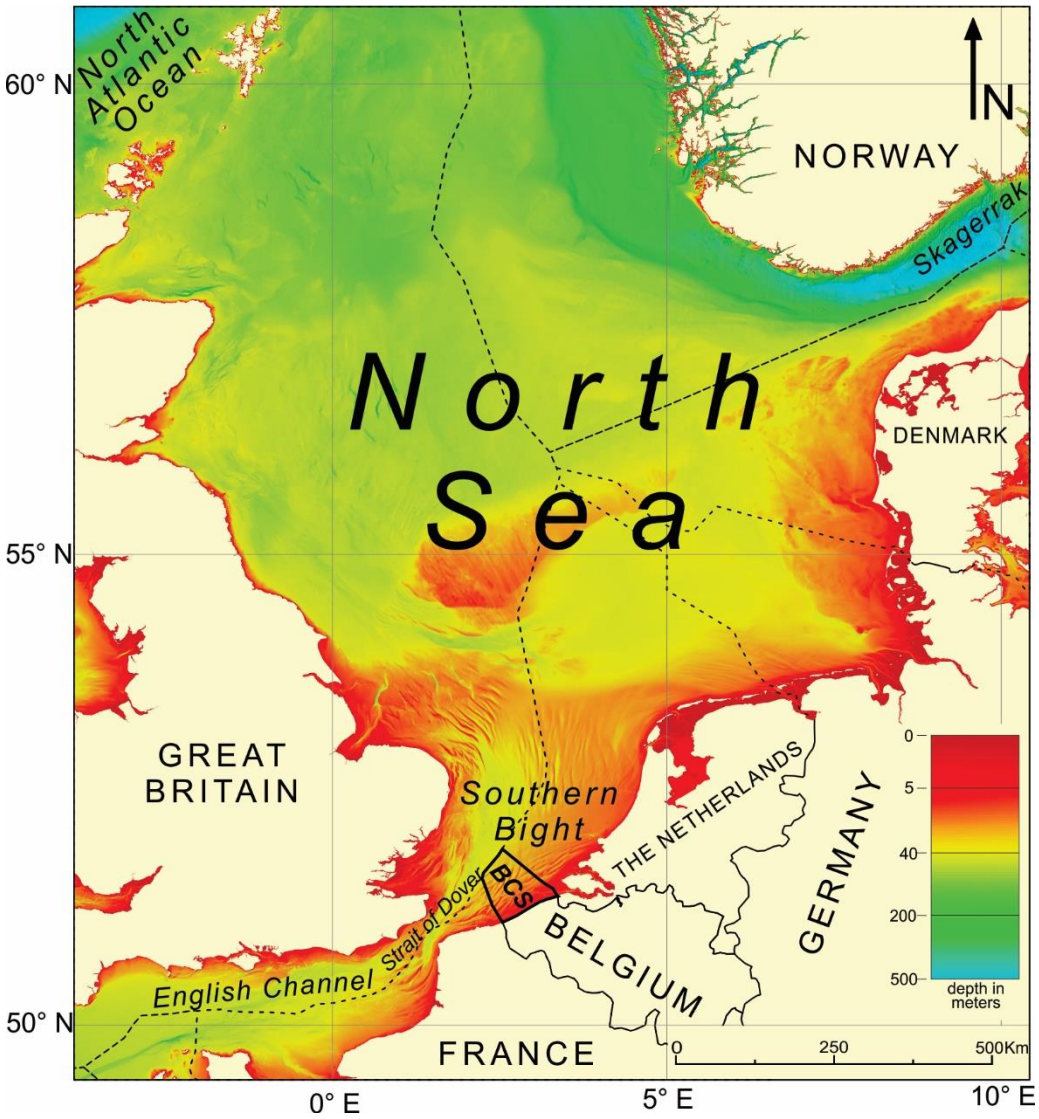

Figure 4. Location and bathymetry of the North Sea situated northwest of Europe. The boundary of the Belgian Continental Shelf is shown with a thick black line. Bathymetry is retrieved from EMODnet. UTM zone 31N WGS84.

In terms of geology the North Sea is a continental rift depression of Mesozoic age with a north-south axis (Mathys, 2009). It is underlain by Caledonian basement (Ziegler, 1992). Rifting started in the area during the Triassic-Early Jurassic and was related to the opening of the Atlantic Ocean. In the post-rift phase several Mesozoic and Cenozoic packages are deposited from the surrounding mountain ranges in mainly Scandinavia and the Alps (Mathys, 2009). These deposits make up the larger part of the North Sea geology.

During the Quaternary the above mentioned deposits were covered by major ice sheets when even Scottish and Scandinavian ice sheets covered large parts of the North Sea during the Last Glacial Maximum (Carr et al., 2006). During these glacial periods several rivers incised in the Mesozoic cover because the sea level was lower at those moments and relocation occurred of the rivers due to the far southward extension of the ice caps (De Moor, 1996). These large rivers (Thames, Meuse, Rhine) traversed the southern part of the North Sea basin during glacial stages and carried a lot of sediment into the southern North Sea Basin (Mathys, 2009). This led to the configuration of the North Sea basin as it is today. At present rivers provide a steady input of fresh water in the North Sea, with the main contributors the Rhine and Elbe. In Belgium the Meuse and the Scheldt rivers contribute to the fresh water input in the North Sea.

Characteristic for the whole North Sea is the large periodic variation in the sea level due to the tides (Fig. 5). Tide currents in general have two main causing forces: the gravitational forces of the sun and the moon. The lunar semi-diurnal constituent, M2 is of the most importance in the North Sea, followed by the solar semi-diurnal constituent, S2 (Briere et al., 2010). The M2 tide component has a period of 12 hours and 25.2 minutes whereas the S2 tide component had a period of 12 hours. These tide components together with some smaller components which cannot be neglected such as spring and neap tide (due to alignment or perpendicular position of sun, moon and earth) will interplay with the resulting tide as we observe it.

Figure 5. Semidiurnal tides M2 and S2 in the North Sea. Solid lines are co-phased lines (hours) whereas the dashed lines represent the co-range lines (meters) (Pohlmann and Sündermann, 2011)

2.2. The Belgian part of the North Sea

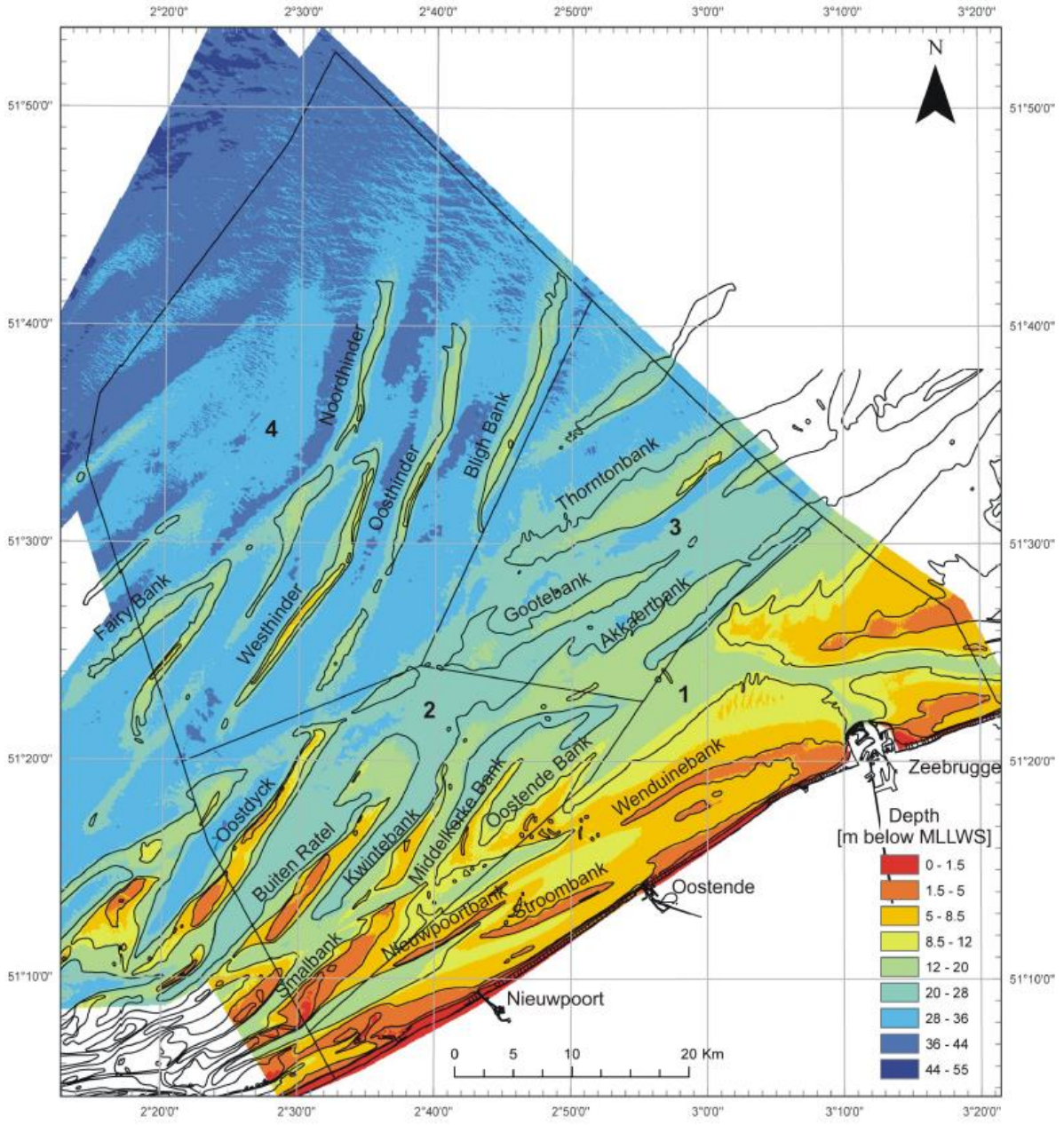

Figure 6. The Belgian Continental Shelf with its sandbanks. 1: the Coastal Banks; 2: the Flemish Banks; 3: the Thorntonbank, Grootebank and Akkaertbank; 4: the Hinderbanks. Mathys (2009) *modified from* Le Bot et al. (2003)*. UTM zone 31N, Projection: WGS84.*

The Belgian part of the North Sea (BPNS), commonly referred to as the Belgian Continental Shelf (BCS) is found in the southern part of the North Sea. The BCS occupies an area of 3500 km² (Mathys, 2009). The BCS also compromises the whole Exclusive Economic Zone (EEZ) of Belgium. This is the zone in which Belgium has rights for the usage of its marine resources and the exploration of it. It stretches out further seaward than the Belgian territorial waters that are limited to the 12 nautical miles boundary. At the boundary of Belgians EEZ lie the Exclusive Economic Zones of France, the United Kingdom and The Netherlands. The depth of the waters of the BCS is relatively shallow with an average depth of about 20 m (Fig. 6).

The BCS is composed of several layers. At a depth of 450 m at the Dutch border, and at a depth of 250 m the Paleozoic basement can be found (Le Bot et al., 2003). This London-Brabant Massif flooded since Late-Cretaceous times during which chalk layers were deposited. The top of this layer is nowadays found at a depth of 150 to 350 m (increasing to the NE) (De Batist, 1989). On top of this Paleogene deposits are found between the covering Quaternary sediments. These deposits were determined to be of Thanetian to Rupelian age and range from a -10 m to -60 m (MLLWS) depth (De Batist, 1989).

The Quaternary deposits are separated from the Paleogene substratum by an angular unconformity (De Batist, 1989). This is thought to be caused by both marine and fluvial circumstances over a long period of climatic changes during the Quaternary. In these deposits a striking feature was found called the 'Ostend Valley' which is thought to be the seaward extension of the Flemish and Coastal Valley (Henriet et al., 1989).

In terms of tides, current velocities were calculated for the whole BCS by mathematically deriving the tide curves to the time. Values of 75 to 125 cm/s peak velocity were found (Van Lancker et al., 2007).

2.3. The Thorntonbank

All the data acquired in this study is more specifically from monitoring zone TBMAB on the Thorntonbank in the eastern part of the BCS (Fig. 1). The Thorntonbank is the most northern sandbank of the Zeelandbanks. Neighbouring sandbanks are the Hinderbanks north of it, the Flemish banks west of it and the coastal banks with the traffic gullies to Antwerp and Zeebrugge in the south (Fig. 6). The crests of the Thornton sandbank in the study area lie at a depth of more or less -17 m lowest astronomical tide (LAT), whereas the gullies in between have a depth of around -25 m maximum. The overall orientation of the whole sandbank is ENE-WSW, with perpendicular current ripples with WNW-ESE orientation.

The eastern part of the Thorntonbank is occupied by windmill parks (Degraer et al., 2013) , but the western part is available for sand extraction. In the Belgian legislation this area is defined as extraction zone 1 (Fig. 3). The mean composition of the sand on the Thorntonbank is 400 µm and uniform on the whole bank (De Backer et al., 2014). The main grain size fraction is therefore medium sand and makes up for 60 % of the fractions, a coarse sand fraction amounts up to 20 % of the Thorntonbank.

In terms of geology the Thorntonbank is a Holocene tidal sandbank. This means that it consists of Quaternary deposits on top of the Tertiary substrate. The characterisation of this Belgian sandbank was mainly executed using seismic investigation. In this way at least three depositional sequences have been described (Le Bot et al., 2003). Qt1 represents the most lower sequences and is incised in the Tertiary substratum. It represents a complex channel infill facies. The maximum thickness of this layer can count up to 10 m. The Qt2 sequences can only be found in the south-eastern part of the Thorntonbank at places where Qt1 is absent. Maximum thickness of this layer is 8 m. The upper depositional sequence on of the Thorntonbank is called the Qt3. These layers represent the upper Quaternary sediments and strongly vary in thickness. It is subdivided in Qt3a, a reflection free facies and Qt3b, representing prograding clinoforms.

The most important campaign, in which the larger part of data was gathered, was cruise No 16-730 on board of RV Simon Stevin. This campaign (TBMAB16- 730) lasted from 13 September until 15 September 2016. The main objective of this campaign was to closely monitor the impact of sand extraction activities with the EM2040 MBES by Kongsberg mounted on RV Simon Stevin. Therefore during this campaign three TSHD's were followed namely the Interballast III, the Ruyter and the Schotsman. For this purpose all possible data was logged which means bathymetric data, seafloor backscatter (SBS) data and WCBS data is at hand. Also additional ground truthing was performed using a Reineck box corer along the track of the Schotsman.

As the CSS monitors the Thorntonbank frequently, also additional bathymetric and backscatter data is available from additional monitoring campaigns in 2016. All survey data is named by an acronym. In this case for the Thorntonbank surveys TBMAB stands for ThorntonBankMonitoringszoneAB. The following extra surveys were used:

- TBMAB1610; 10 March 2016: a campaign conducted using RV Belgica
- TBMAB16-310; 13 and 14 March 2016: a campaign conducted using RV Simon Stevin.
- TBMAB16-900; 22 and 23 November 2016: a campaign conducted using RV Simon Stevin.
- TBMAB16-930; 7 December 2016: campaign conducted using RV Simon Stevin

This chapter will in the first part give an overview of the dredging vessels followed and their specifications, the survey ship used and some main principles regarding MBES. In the second part the methodology of the processing will be given.

3.1. Dredging

Dredging includes extraction and is executed underwater to gather sediments going from clay, sand and even hard rock. In case of loose material these are then dumped somewhere else through the bottom of the ship itself or by transporting it to the shore through floating pipelines or simply by unloading with a crane. Also the extracted material can be used for land reclamation, a process in which new land is made by 'rainbowing' it elsewhere. Belgium is known for its dredging industry, as Jan De Nul and DEME, two big dredging companies, are based in Belgium.

3.1.1. Different kind of dredging vessels

In dredging activities several types of vessels can be used. Depending on which type of soil that has to be dredged, three main types of dredgers can be distinguished (Todd et al., 2015):

Cutter suction dredgers (CSD) have a rotating cutter head which is used to remove harder sediments to even hard rock. The fragments are sucked up and charged into a pipeline or in split hopper barges. These sort of vessels have two spud poles from which one is pushed into the ground. The suction head then makes a swinging movement around this spud pole. When a full swing is performed, the other spud pole is pushed in, the first one pulled up and the position of the whole vessel is shifted a bit relative to the spud pole. In this way the suction head advanced some meters and then the whole process is repeated again (Todd et al., 2015).

Backhoe dredgers (BD) are used for digging trenches and channels. They consist of an excavation crane on the back of a small vessel which can be stabilized with spud poles. The excavated material is again dropped in a barge vessel. In this way depths to up to 25 m can be dredged.

TSHD's are dredging vessels where big suction heads are dragged rearward next to the vessel on the seafloor to excavate (Todd et al., 2015). These type of vessels are mainly used for unconsolidated material, mainly sand and gravel. The material is brought up from the suction head to the loading space of the vessel by large dredging pumps which create an under pressure in order to suck up the material into the hopper. Once in the loading space the dredged material settles and the additional water will discharge again into the ocean by means of an overflow. TSHD's are the most common dredgers and exist in different sizes. Whereas some of the biggest TSHDs in the world have a capacity of 46 000 m³ (i.e. Cristobal Colon and Leiv Eiriksson) (Jan De Nul, 2017), the TSHDs used to extract sand from the BPNS only have a capacity of 1500 to 2000 m³.

3.1.2. Dredging vessels followed in this work

The Interballast III is a TSHD owned by Group De Cloedt n.v. and its main harbour is in Ghent (Group De Cloedt N.v., 2011). It was built in 1980 and sails under the Dutch flag. The vessel has an overall length of 69.89 m and can reach a speed of 12 knots. It has accommodation for 9 crew members. The capacity of the vessel is 1886 m³ (the largest capacity of all three) and the suction pipe has a width of 600 mm. The vessel can be used for excavations up to 20 m at an angle of 45 degrees of the suction pipes. The capacity of the dredging system is set to 700 m³ per hour. It has hydraulic bottom door for unloading.

The Ruyter is a TSHD owned by Noordzeezand BV. Since it was built in 1994, it sails under the Dutch flag (Dredgepoint, 2017a). The length of the vessel is 82 m and it has a hopper capacity of 1600 m³. The Ruyter can dredge up to 30 meters depth and has one dredging pipe with a suction pipe diameter of 0.65 m.

At last in this research also the Schotsman was followed, which is also a TSHD. This vessel was built in 1983 and is currently owned by Transport Maatschappij "Terneuzen" B.V (Dredgepoint, 2017b). It is the longest of all three, with a length of 89.97 m. The hopper volume on the other hand is the least: 1500 m³. The vessel can dredge to up to 25 m, has one dredging pipe with a suction pipe diameter of 0.6 m.

3.1.3. Electronic Monitoring Systems

The data used in this work coming from the TSHD's is stored by an Electronic Monitoring System (EMS) (Van den Branden et al., 2014). Licenses to extract sand from the BCS allow a maximum extraction of 15 million m³ sand over a time span of 5 year, within the control zones that are granted to the dredger (FOD Economie, K.M.O. Middenstand en Engergie, 2014). In control zone 1, 2 and 4 (Fig. 1) only TSHD's are allowed. Additionally a mean speed relative to the seafloor of 0.5 knots has to be maintained. This extraction is controlled by using EMS. It automatically registers the following parameters: ID of the extraction vessel, date of the registration, time (U.T.C.) of the registration, position of the extraction vessel, speed of the extraction vessel, status of the pumps (on/ off) and status of extraction (yes/ no). The effective load has to be added manually in cubic meter as soon as it is calculated. This EMS- data is available for the Interballast III, Ruyter and Schotsman the September campaign and will be used to research the key correlations of plume intensity in function of time/distance.

3.2. Surveying

In all the campaigns discussed in this work, either research vessel (RV) Belgica or RV Simon Stevin was used. Campaign TBMAB1610 was conducted using a Kongsberg EM3002D shallow water MBES on board of RV Belgica. This vessel is owned by the Federal Science Policy Office and has been in use since 1984 (OD Nature, 2014). The EM3002D was operated at a frequency of 300 kHz and has a range of 1 m up to 150 à 300 m. The sonar heads on RV Belgica are installed on blisters on each side of the ship for the best acoustic conditions during sailing.

All other data from the other campaigns (TBMAB16-310, TBMAB16-730, TBMAB16-900 and TBMAB-930) were retrieved using the Kongsberg EM2040 MBES on board of RV Simon Stevin. Operating since 2012, the vessel is owned by VLOOT whereas VLIZ (Flanders Marine Institute) is responsible for the management and installation of all the equipment of the vessel. The vessel is constructed with funds of the Flemish Government (Flanders Marine Institute, 2017).

3.2.1. Principle and calibration of MBES

A MBES is based on SONAR (Sound Navigation And Ranging) principles (Lurton, 2002). By means of a transducer, sound pulses are sent out into the water . These interact with the seafloor and water column and reflect. Between emission and receival of the reflected sound pulse, the time is recorded. This is called the two-way travel time, so the time to go back and forth between transducer, seafloor and again transducer. Additionally the intensity of this reflected pulse is recorded, which is used to make backscatter maps. When taking into account the geometry of the array of beams, and using the sound velocity of the beam in the water, a depth value can be calculated to make bathymetric maps:

$$d = \frac{v * t}{2}$$

With d = depth (m), v = sound velocity in water (m/s), t = two-way travel time (s). Note that this formula is only valid for depth right underneath the ship. Beams can also be sent out under an angle to focus the beam over a broader swath. Therefore with one ping a broader swath width can be achieved. This ‘steering of the beam’ can be performed by using a shift in phase in the hydrophone to strengthen it into one direction.

As the sound velocity changes throughout the water column, a sound velocity profile has to be made. Sound velocity is already being measured at the transducers, but differences in salinity or temperature can create water bodies with different sound velocity properties. This can lead to refraction of the beam at the boundary between water bodies and therefore a wrongly calculated depth. A sound velocity profile is the solution to account for this problem. It can be made in two ways: by measuring the three main variables that affect sound velocity (conductivity/ salinity, temperature and depth) or by directly measuring the sound velocity with a Sound Velocity Probe (SVP). In the first case a Conductivity, Temperature & Depth Probe (CTD Probe) is lowered throughout the water column. By measuring conductivity, a salinity in Practical Salinity Unit (PSU) can be calculated, temperature is measured using a normal thermometer in degrees Celsius and depth in meter can be calculated using a pressure value. Eventually the sound velocity in function of depth can be calculated by using one of many formulas.

The frequently used formulas are:

$$v = 1448.96 + 4.59t - 0.053t^2 + 1.34(S - 35) + 0.016 \text{ (m/s)}$$

(simplified from Mackenzie (1981) and Del Grosso (1974))

$$v = 1449 + 4.6t - 0.055t^2 + (1.39 - 0.012t)(s - 35) + 0.017d \text{ (m/s)}$$

(Wilson, 1960)

The sound velocity in water can also be directly measured by using a sound velocity probe (SVP). This probe consist of a cylindric tube which mainly consists of batteries with the actual measuring sensor at the base. When lowering this probe the sound velocity is directly measured in function of the depth.

It must however be noted that through experience of the CSS over the years the sound velocity is almost uniform in the North Sea. This because the water is almost always well mixed and so no thermoclines or haloclines are to be found. Therefore these above described methods to find velocity profiles are not used for bathymetric measurements at the Thornton bank, Hinder bank and Flemish banks. For these measurements vertical constant velocity profiles are used that match the measured sound velocity at the transducers. For measurements in the Scheldt Estuary, still the normal above described procedure is used.

A depth value is of no use if its location is not known. Therefore the exact position of the research vessel and the offsets of different component relative to the GPS have to be known. For this we have to know the position of the GPS, motion sensor and transducer in a reference system when multibeaming. It is common to take the position of the motion sensor as zero, and therefore the offsets of the GPS and transducers have to be measured when the vessel is in drydock. These offsets for RV Simon Stevin can be found in table 1.

Table 1. Location offsets on RV Simon Stevin. The motion sensor is used as zero point of the whole system.

Location Offset (m)	Forward (X)	Starboard (Y)	Downward (Z)
Position GPS antenna	0.2972	0.5025	-13.5341
TX Transducer	0.052	-0.369	2.167
RX Transducer	0.049	-0.064	2.153

The rotating movements of a vessel can occur around different axis. The sign convention for a reference system of a vessel is that the y-axis is positively directed to the bow of the ship, the x-axis positively directed to the left, looking to the port side of the ship, and the z-axis positively directed perpendicular to the x and y axis, in direction of the sky. The rotation around the x-axis of the vessel is called the pitch, the roll is the rotation around y-axis, and the yaw is the rotation around z-axis. These different motions are corrected for in real-time by means of a motion sensor.

Offset angles of the transducers have to be known as otherwise wrong depth values will be acquired due to alignment errors. The offset angles are determined by running patch test lines (Mann, 1998).

First of all the positioning time delay has to be corrected for. This delay is caused by time lags between the receival of the position by the system and the time this position is processed in the logging module. Time delay can be determined by detecting a slope along the same line in the same direction, but each

time with a different speed. In this way considering figure 7 the time delay formula can be calculated (Mann, 1998):

$$TD = \frac{d_a}{v_h - v_i}$$

With TD = time delay in seconds, d_a = the along-track displacement, v_h = the higher vessel speed and v_i = the lower vessel speed.

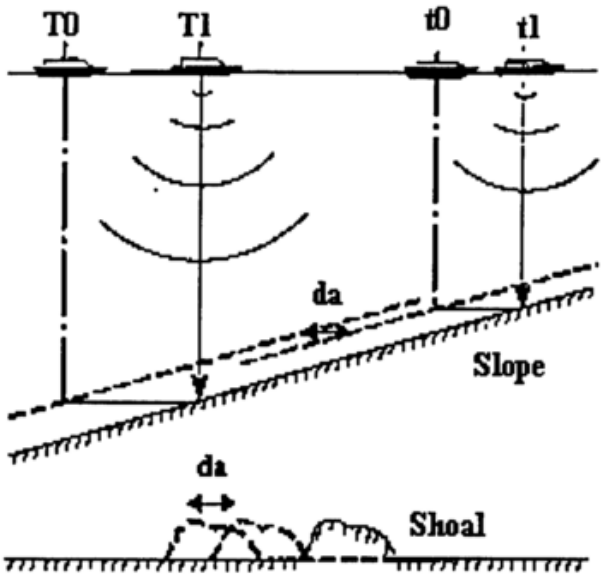

Figure 7. Patch line test to determine the time delay. Figure from Mann (1998) *modified after* (Godin, 1996).

After the time delay correction the pitch offset is determined. For this a suitable feature has to be found on the seafloor. A wrong mounting angle of the transducers directing ahead or to the rear can cause the detection of two virtual objects whereas there is only one real object when doing lines back and forth. This pitch bias (Fig. 8) can be calculated using the following formula (Mann, 1998):

$$d\alpha = \arctan\left(\frac{d_a}{2z}\right)$$

with z = depth, d_a = separation of target and dα = pitch offset.

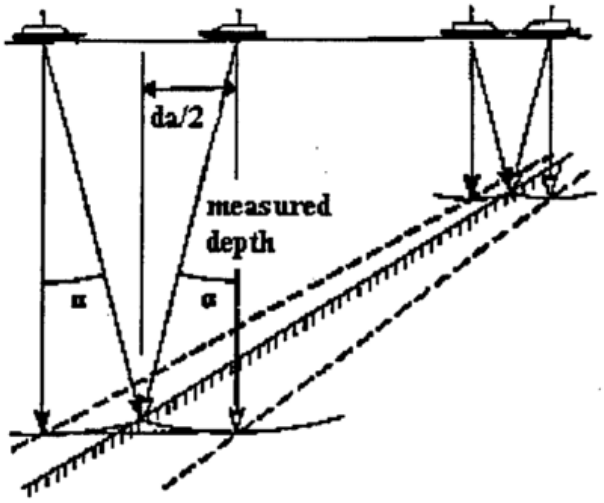

Figure 8. Patch line test to determine the pitch bias. Figure from (Mann, 1998) *modified after* (Godin, 1996).

A yaw/ heading offset again leads to the detection of two virtual objects when doing lines back and forth next to a feature. The angle of this offset can easily be calculated by using geometric formulas. Considering figure 9 it can be stated that:

$$\propto_1 = \arctan\left(\frac{y_1}{x_1}\right)$$

With $\propto_1$ = offset angle, y_1 = the distance between the centres of the real and virtual object and x_1 = the lateral distance from the navigated track to the virtual object. However, y_1 cannot be measured, so therefore another relationship has to be used:

$$\left(\frac{x_1}{y_1}\right) = \left(\frac{x_2}{y_2}\right) = \left(\frac{x}{y}\right)$$

In this way it can be stated that:

$$\propto_1 = \arctan\left(\frac{y}{x}\right)$$

And x = distance between the two track lines = $x_1 + x_2$; y = separation distance between the two virtual objects = $y_1 + y_2$. This yaw/ heading offset has to be measured for port side by measuring the object along track one and two, whereas for the starboard side tracks three and four will have to be navigated.

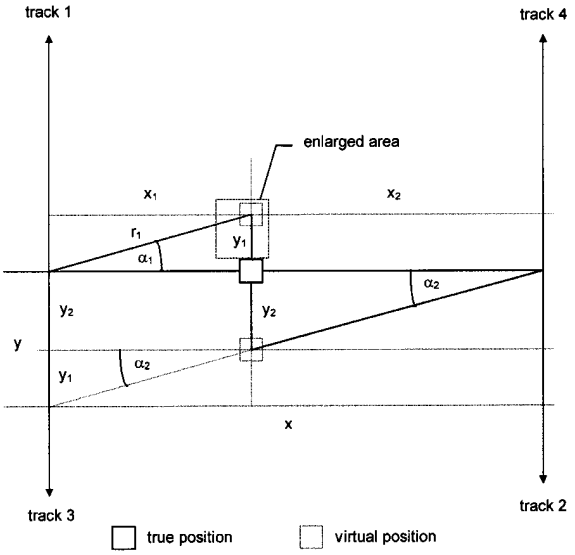

Figure 9. Calculation of the yaw bias. Figure by courtesy of L3 Communications ELAC Nautik.

At last also the offset angle for the roll has to be determined, as this can cause large depth errors at the outer beams it is the most critical one. The cause for a roll bias can be unequal mounting angles and leads to a virtual slope on the seafloor. The roll offset angle can be found by surveying reciprocal lines in shallow water at a low constant speed on a flat surface. By using the following formula the angle can be calculated (Mann, 1998):

$$\theta = \frac{\arctan\left(\frac{d_z}{d_a}\right)}{2}$$

In which θ = roll offset, d_z = depth difference, d_a = the across-track distance.

An overview of the calibration results of the Kongsberg EM2040 on RV Simon Stevin is given in table 2.

Table 2. Offset angles in degrees for the calibration of the EM2040 echosounder of RV Simon Stevin.

Offset angles (deg.)	Roll	Pitch	Heading
TX transducer	0.250	0.815	0.240
RX transducer	0.300	-2.220	0.325
GPS antenna	0.200	0.000	0.100
Motion sensor	0.000	0.000	0.000

When everything is calibrated well and every offset is known relative to the zero point of the reference system, precise location data can be acquired with the on board positioning system. Real Time Kinematic (RTK) corrections were also received to enhance the precision. Due to the availability of RTK corrections no tide or draught corrections had to be performed in the processing, as these were already included in the RTK corrections.

3.2.2. Bathymetry and Seafloor backscatter

The data on board was acquired using the Kongsberg Seafloor Information System software (Kongsberg Maritime AS, 2007). It has a user friendly interface and visualises the data in real-time. During all campaigns bathymetry was logged which is automatically calculated by means of the two-way travel time and the speed of sound in the water. This is not the only thing that is logged. Also the intensity of the reflected ping is stored. This is commonly known as the backscatter value and is represented by a value in decibels (dB). The scattering of an emitted ping can occur in the water column itself or at the seafloor. The SBS is commonly logged together with the bathymetric information and gives more information about the characteristics of the underground, as it can be used for habitat mapping and to detect changes in lithology (Lurton, 2002). The on board ADCP of RV Simon Stevin was switched of due to interference with the WCBS.

3.2.3. Water column backscatter

Due to the large storage capacity needed to store water column data compared to the amount of information in it (Gee et al., 2012), and the difficulty of processing and calibrating it (Lamarche et al., 2017), the water column data is mostly not acquired. During the September campaign in this work however, this data was logged to visualise and process the caused sediment plumes by dredging. The MBES was set to acquire the data in three sector mode. In this section an overview will be given of the applications and fields in which WCBS is currently being used.

Water column data is being used in the last decades for the detection of several targets. A detection in the water column is dependant of two main things: the system and the target. The MBES can be controlled by changing sonar frequency, vessel speed, acquisition settings, whereas the target that has to be detected cannot be controlled. Target strength in the water column is dependent on density, size, orientation, geometry, depth and behaviour of the target itself.

One of the most used applications of water column data from MBES is the detection of gas bubbles. Imaging of natural gas seepage has already been performed in a lot of instances, mainly for the detection of methane at seeps in sea (Greinert et al., 2010; Jones et al., 2010; Nikolovska et al., 2008;

Ostrovsky et al., 2008; Skarke et al., 2014), methane vents in lakes (Scandella et al., 2016) or mud volcanoes (Greinert et al., 2006) .

A way of data processing for bubble detection at seeps and black smoker have already been proposed by Schneider Von Deimling and Papenberg (2012) and Rona et al. (1998). Because of the strong impedance level between gas bubbles and the water a strong backscatter occurs of the transmitted acoustic pulse (Greinert, 2008) which makes them fairly easier to detect and process than other targets. Scandella et al. (2016) gave a more in depth view of the multibeam backscatter physics of the gas bubbles. By using echo-integration algorithms bubble abundance can be approached instead of simply counting the individual bubble echoes (Bayrakci et al., 2014), in this way the gas vents can be quantified. By using split-beam echosounders bubble flow rates have been quantified (Veloso et al., 2015).

Water column data can also be used for research into submerged vegetation. Mapping the seafloor vegetation can have benefits for easier environmental monitoring and even enhances the performance of mine hunting sonars in littoral regions (McCarthy and Sabol, 2000). Echosounders have been proven useful for environmental monitoring, mainly spatial distribution and biomass analysis of algae (Kruss et al., 2015, 2011, 2008). Fisherman have used several acoustic methods to enhance their fish gaining. Sonars can be used for detection of mammals (Pyć et al., 2016), for a density calculation of krill (Cox et al., 2011) and for normal acoustic observations of several normal sorts of fish (Weber et al., 2009). Cochrane et al. (2003) and Melvin and Cochrane (2014) go deeper into the physics of using MBES for fishery research. Other targets studied in the water column are shipwrecks, to detect the least depths (Wyllie et al., 2015), and water mass differences to determine thermoclines and freshwater influx (Schneider Von Deimling and Weinrebe, 2014).

More important for this specific work is previous research into the study of sediment plumes using MBES. The knowledge in this field of science is rather scarce as most research is executed using ADCP and OBS (Battisto and Friedrichs, 2003). Simmons et al. (2010) showed an early quantitative and temporal characterisation of sediments in a river mixing interface. By using MBES water column data and water calibration samples a rough SPM concentration was calculated. However it was stated that further research was needed in a range of environments and a suitable way had to be found to calibrate the whole system. This was further applied by Best et al. (2010) to a specific case, namely the leeside of a low-angle sand dune. Both papers state a workflow that could be applied and propose further research. However in this work itself the setting is more complex as a detection of the sediment plume formed by dredging is more difficult as several parameters have to be taken into account.

3.2.4. Sampling

During the March campaign (TBMAB16-310) nine samples were taken on the Thorntonbank. These were named SPI 1-9 as at that place also Sediment Profile Images (SPI) were taken. Sampling was performed using a Reineck box corer, with subsampling of the above 15 cm in a plastic bags. Location and remarks of these samples can be found in table 3.

Three additional samples were taken during the September campaign (TBMAB16-730) along the dredged track of the Ruyter. This was performed using the same procedure. Info about location of the samples on the Thorntonbank can be found in table 4.

Table 3. Location, date and remarks of the 9 samples acquired during survey TBMAB16-310..

Sample	LAT (theorical)	LONG (theorical)	Date	Mean Time (UTC)	Remarks	IMAGE FILE NUMBER
SPI 1	51.49071070	2.76368120	12-Apr-16	13:41	Sandy gravel with shells, coarse heterogenous	2552 2553
SPI 2	51.49361122	2.76612752	12-Apr-16	14:02	Sandy gravel with shells, coarse heterogenous	2554 2555
SPI 3	51.49556843	2.76962040	12-Apr-16	14:18	Gravel, soft cobbles of mud	2556 2557
SPI 4	51.49611780	2.77870642	12-Apr-16	14:39	Sand with fragmented shells, homogenous	2558
SPI 5	51.49660047	2.78400605	12-Apr-16	14:49	Sand with fragmented shells, homogenous	2560
SPI 6	51.50009977	2.79099617	12-Apr-16	15:00	Sand with fragmented shells, homogenous	2561 2562
SPI 7	51.50437455	2.80252893	12-Apr-16	15:22	Fine rippled sand, few fragmented shells, homogenous	2563 2564
SPI 8	51.50573652	2.80413288	12-Apr-16	15:34	Fine rippled sand, few fragmented shells, homogenous	2565 2566
SPI 9	51.51114288	2.82219887	12-Apr-16	15:37	Fine rippled sand, few fragmented shells, homogenous	2567 2568

Table 4. Location, date and remarks of the 3 samples acquired during survey TBMAB16-730.

Sample	LAT (theorical)	LONG (theorical)	Date	Mean Time (UTC)	Remarks	IMAGE FILE NUMBER
R1	51.50445	2.845406	14-Sep-16	10:57	/	/
R2	51.50925	2.852442	14-Sep-16	11:29	/	/
R3	51.51266	2.863126	14-Sep-16	11:57	/	/

3.3. Processing of acoustic data

Due to the large extent of the whole dataset, several types of data were combined using multiple software packages. Qimera and FMGT were used to study the direct impact of dredging (bathymetric and SBS grids respectively). To study the indirect impact (the suspended sediment plumes caused by the dredging) FMMidwater, Sonarscope and Voxler were used to visualize the intensity of the plume in 2D, 3D and even roughly quantify the plume volume. As the processing of water column data in relation to the specific case of sediment plumes is not common, the methodology in this work will be an important part and therefore explained more thoroughly.

Firstly all the software processing will be explained with an overview of which features of each program were used and the to what values the parameters were set. Lastly also the whole processing of the sand samples to obtain the grain size will be explained.

3.3.1. Processing in Qimera

Qimera is a program developed by QPS (QPS hydrographic and marine software solutions, 2016). It can be used to process both bathymetry and water column data but was only used for the processing of the bathymetry in this specific study. The bathymetric raw data consist of all the 'pings', which are points that are georeferenced. The raw data can therefore be simply imagined by a point cloud that has to be converted to a grid. First step was to import the raw bathymetric data files as they were acquired in SIS on board of the survey ship. These are the files which have an '.all' extension. After all the files were imported, the vertical reference separation model was selected. This file was available at the CSS for the whole BCS. By using the vertical reference separation model all the depth values of the pings were recalculated from the original depth on the WGS84 ellipsoid to a depth value in Lowest Astronomical Tide (LAT). Also the real time corrected positions were selected so no additional tide or draft correction had to be applied as they were already interbedded in the RTK corrections.

After this correction, the point data could be gridded. This was processed with a Combined Uncertainty and Bathymetry Estimator (CUBE) algorithm (Calder and Wells, 2003). The algorithm focuses on estimation of true depth, rather than selecting the best soundings. The algorithm uses an estimation of bathymetry using all the information at hand combined with the uncertainty on that depth estimate. The use of the CUBE algorithm tremendously improved the speed and efficiency of bathymetric data processing and provides a quality control needed to optimise surveying (Ladroit et al., 2012). The CUBE algorithm was applied to all the raw data to provide a dynamic surface. This reduced the amount of 'faulty' pings and outliers. The CUBE algorithm settings were 'shallow water' as all data acquired was max 25 m depth LAT, the fixed distance was set on 0.35 m, the number of samples offset 2.00. Resolution for al grids was set to 1 m in x and y direction as this will give a good equilibrium between what is needed for discussion of the features and storage capacity needed and calculating time of the computers on the other side.

At last the pings were visually checked for leftover outliers and if needed flagged out. The eventual dynamic grids were then definitively exported in asci format to be visualised in Surfer. In the end also the processed information files where exported in '.gsf' format to be used in FMGT.

3.3.2. Processing in FMGeocoder Toolbox (FMGT)

The Fledermaus Geocoder Toolbox module (QPS hydrographic and marine software solutions, 2017) designed by QPS was used to process the SBS. In this module the files with '.gsf' format were imported which were already filtered by the CUBE (Calder and Wells, 2003) algorithm and visually corrected further. No additional processing was required as the SBS mosaic could directly be calculated. The resolution was set to 1 m and the radius of search to obtain the gridded value was set to 10 m. FMGT then directly shows the needed memory space. In case the resolution is set to high, the needed mosaic memory will show up in red and the resolution should be changed accordingly. The end result of the processing in FMGT is a mosaic with SBS intensity in decibel value.

3.3.3. Processing in FMMidwater

To process the water column data the Fledermaus Midwater module developed by QPS was used (QPS hydrographic and marine software solutions, 2017). The raw water column data files which have the '.wcd' extension were imported, together with the '.all' files which contain all seafloor pings. In FMMidwater the water column can be visualized in different ways. It can be visualized as a slice perpendicular on the survey vessel track like in figure 10.

Visualization can also be performed in stacked view, which is the nadir view along the track of the vessel (Fig. 10). In all these views the different colours stand for different WCBS values in decibel. In both figures the sediment plumes can be observed in green as when the dredging vessels were not followed, so when no sediment is present, these views were plain blue. On the stacked view (Fig. 11) the seafloor can be observed as a very high scatter (positive decibel values). When looking in fan mode the seafloor is also detected (the red line in figure 10). Next step is to select the right range to filter out all the side lobe interference and multiples. This to only have the pure water column itself in the end.

The histogram (Fig. 12) shows that the backscatter values of the sediment plume were filtered out by trial and error on sight. For the Ruyter track only the backscatter values between -60 to -30 dB were retained as this represented the first peek in the histogram and corresponded roughly with the sediment plumes on sight.

At last the remaining backscatter values were exported in text format to be further processed (additional filtering) and visualized in Voxler. This resulted in a text file with four columns, the first one the coordinates along x-axis in meter in UTM 31N, the second column the coordinates along y-axis in meter in UTM 31N, the third axis the depth in meter LAT and the fourth column the backscatter value in decibels.

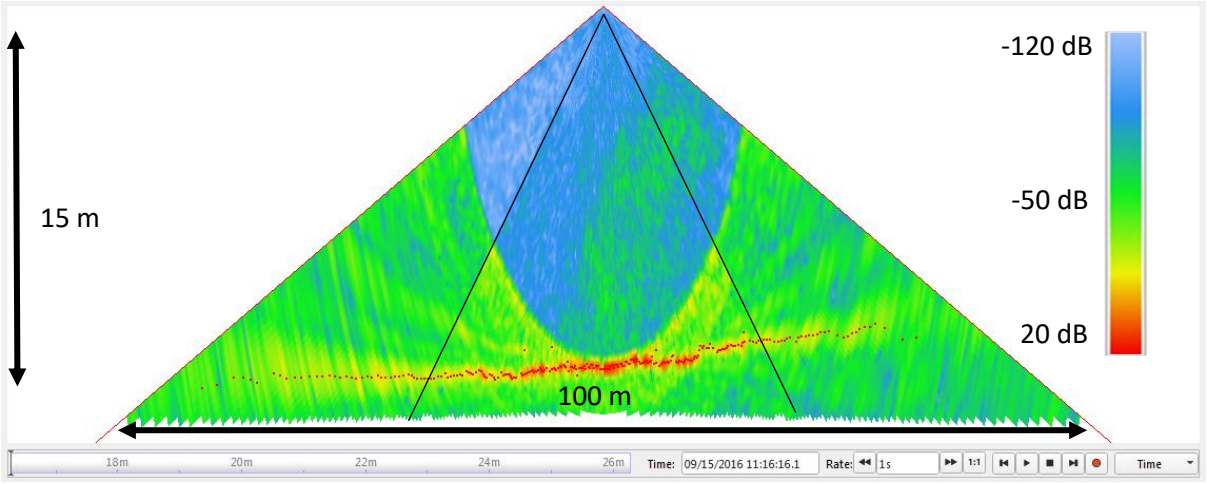

Figure 10. Screenshot from FMMidwater. Fan view of the water column. The centre blue part with green scatters are the actual water column with the sediment plume in green. The red line at the bottom is the seafloor detection. All the additional green at the sides is due to side lobe interference and multiples. The two black lines show the boundaries between the three sectors in which the water column was recorded.

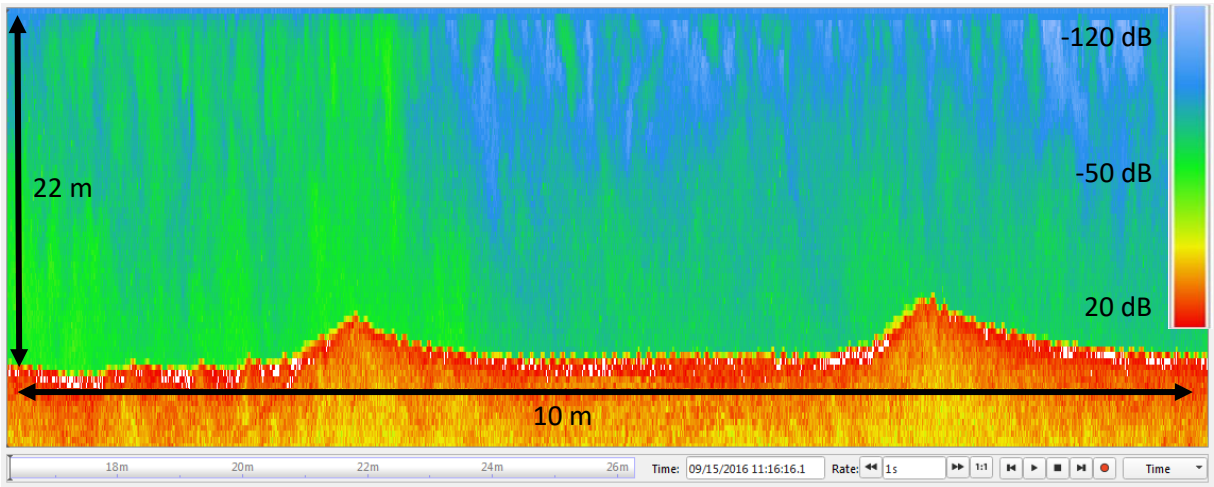

Figure 11. Screenshot from FMMidwater. Stacked view of the water column. The bottom red part is the seafloor with above the water column containing the sediment plume (in green).

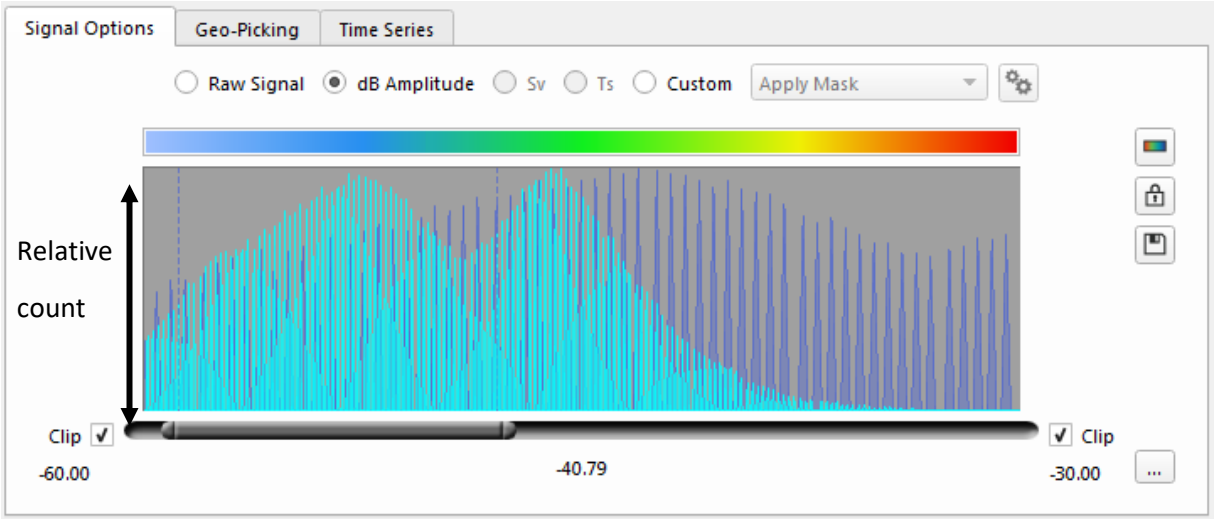

Figure 12. Screenshot of the water column backscatter histogram. The turquoise shows the distribution of the decibel values. The first peak corresponds to the sediment plumes on sight.

3.3.4. Processing in SonarScope

SonarScope is a software package which is developed by the French Institut Français de Recherche pour l'Exploitation de la Mer (IFREMER) in France (IFREMER, 2017). The software is programmed in MATLAB, which makes it very modifiable. The sediment plume was processed by the CSS using the echo-integration algorithm. In this process a vertical average of backscatter intensity is calculated from a time angle ring where the specular echo (due to side lobe interference) was already filtered out (Fig. 13). The result of this algorithm is a colour intensity value ranging from 0 to 255 which means that the original backscatter value is not retained in decibels. The result of the echo-integration can be visualized for each echogram i.e. ping as a graph in which the echo-integration intensity is plotted in function of the across distance. A two-dimensional grid can also be made which then shows the intensity of the sediment plume georeferenced in x and y direction.

From all the water column files the ring in between time angle 0 and 96 was used. This means that the resulting grids represent the sediment plume generated in the whole water column. Additionally also echo-integrated grids were computed where not the whole coverage of the water column was used. The outer 35 degrees on each side of the normal coverage were filtered out as these parts already have a large degree of interference.

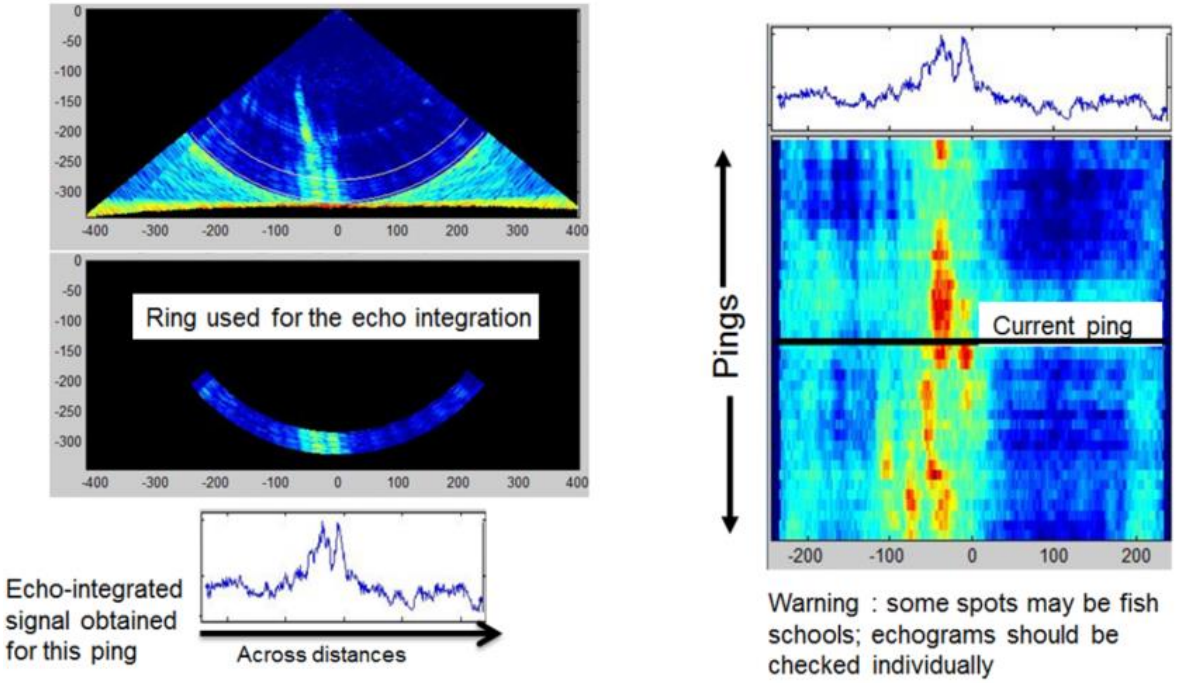

Figure 13. The echo-integration principle. The left upper figure represents the filtering of the side lobe interference and the extraction of the time-angle ring of interest. The left lower graph shows the result of the echo-integration algorithm for each ping. When stacking these pings next to each other, a two-dimensional grid can be made with the plume intensity (right figure) (Figure by courtesy of IFREMER).

3.3.5. Processing in Surfer 12

All the two-dimensional visualisations were performed using Surfer 12 software (Golden Software Inc., 2012a). The bathymetric and backscatter grids are just imported as they were exported in the processing software. Additional data can be visualized on top of these grids such as current files. Current data at the time of the campaign was retrieved from the website of BMM. This was saved as a text file with three columns, one with the date, the time and the tide in TAW in centimetre. It is important to note that the retrieved tide data is from the measuring station 'De Wandelaar' which is at about a distance of 20 kilometres.

Next step in the making of the current vector files was by combining the navigation files of the survey ship with the current file. The resulting current vector file was therefore prepared by using the time as connecting factor. The coordinates of the survey ship at the time of each current measurement were searched and put in a text file with four columns: x coordinates in UTM 31N, y coordinates in UTM 31N, the current orientation in degrees relative to the north in clockwise rotation and the current velocity in meters per second. This file could then be visualized as a 2-grid vector layer which results in an overlay with the direction of the arrows indicating the current direction and with their length a relative measure of the current velocity strength.

Additional methods helped to visualize certain features more clearly. Rather than just importing the bathymetric and backscatter two-dimensional grids as they were, shaded relief visualizations could be used to enhance the dredging induced changes. In a shaded relief map the bathymetry is enlightened from a certain wind direction (in this case the north-western direction), at an angle of 45 degrees with the horizontal plane. This makes the dredging induced trace more clearly visible, mostly if the dredging track is perpendicular on the enlightening direction.

Part of the research question was to study the dredging trace and study how fast it changes or becomes replenished. This is studied by making difference maps between moments in time, represented by the data acquired at two different campaigns. By making a difference map between the bathymetry of a campaign before dredging and right afterward, the dredging traces in that time interval can be visualised. The replenishment of the trace can be studied in the same way by making a difference map between the situation right after dredging and bathymetry of a campaign afterward.

At last also other data can be plotted such as navigational data of both the dredging vessel, which is to be found in the EMS data, and the navigational data of the survey vessel. This is performed by adding as a 'post' map and then selecting the right columns of the data file for x coordinates and y coordinates.

3.3.6. Processing in Voxler

Voxler is a software package developed by GoldenSoftware that makes it possible to visualize 3D data (Golden Software Inc., 2012b). It was used to make a three dimensional model of the already pre-filtered backscatter data in FMMidwater. The data was converted to voxels, which are a short for volume pixel, that's the smallest distinguishable box-shaped part of a three-dimensional image.

First step was to import this data as a text file which consists of four columns like exported in FMMidwater (X, Y, Z and backscatter value). Once imported an additional filter was applied which filtered the data further based on the backscatter value. This applied filter was tested using several ranges, but eventually for all results a filter that only retained the backscatter values in between -40 and -55 was used. As these data were still point data after this operation, the next logical step was to grid the data. This is executed by the gridder module implemented in Voxler. The voxel geometry was

set to 1 m along x and y axis, whereas along z-axis the resolution was set to 0.5 m (due to the smaller range in depth). The gridding method was an isotropic inverse distance to power algorithm, with power two. This means that for each value the pings closest to that point will weigh more on the eventual calculated value than the other pings further away. A one meter radius was used in which minimum 1 ping and maximum 50 pings were used to calculated a grid value.

At last several output geometries were created using several modules. The most important one of these is the FaceRender module which displays non-interpolated cubes of the gridded input lattice. Each unit of the grid is visualized as a block with a colour value corresponding to the component value which is in this case the WCBS value itself. The component value presented are calculated by summing the values at each of the corner points and dividing them by eight. If one of these neighbouring components has a null value, the cube will not be displayed. This module actually visualized the sediment plume as blocks of half a cubic meter, with their colour corresponding to a backscatter value. The workflow chart as used in Voxler is shown in figure 14. Additionally also other visualization methods can be used to explore the data more thoroughly like the 'Contour module' and the 'OrthoImage module'. The 'VolRender module' was used but did not work out as the volume was not smooth enough like some other objects in the water column as fish and mines.

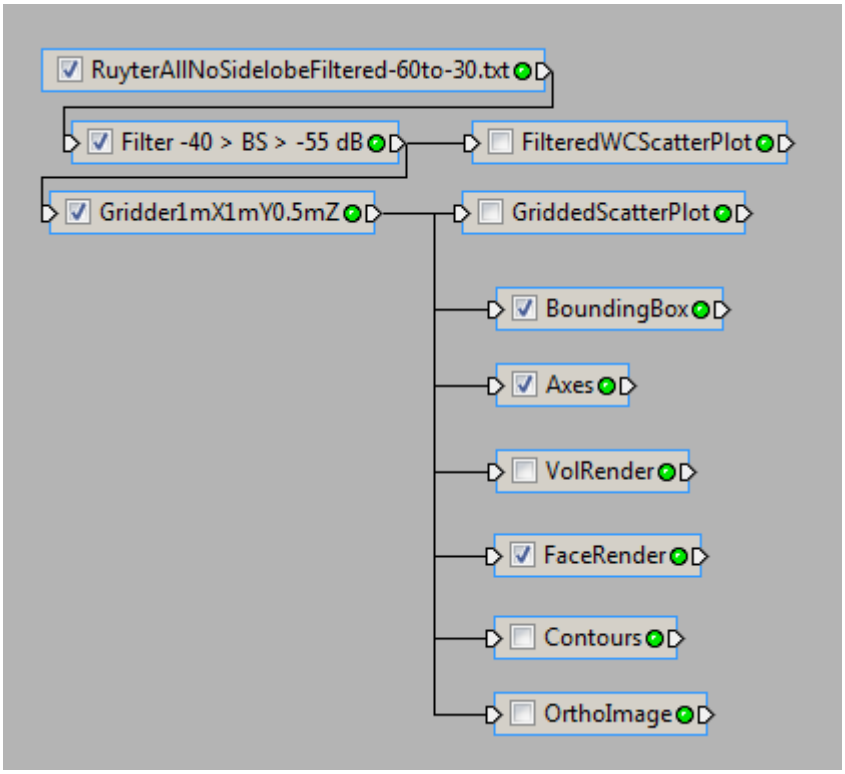

Figure 14. Workflow chart of the processing in Voxler. Firstly and additional filter is applied on the already pre-filtered data exported from FMMidwater, then the gridding is performed with then finally the visualisation methods.

3.4. Processing of the sand samples

Firstly the bags with approximately a weight of 2 kg each were oven dried at 40 degrees Celsius to remove the water content. As the passive plume, processing of the sand samples was firstly performed by sieving of all the bags on a 1 mm dry sieve. Both fractions, the one higher than 1 mm and the one smaller than 1 mm were weighed. The fraction smaller than 1 mm was further prepared to then be put in a Malvern Mastersizer 3000 to be analysed in greater detail. This preparation consisted of an organic

matter removal by adding H_2O_2. (35% solution) and then boiling the mixture until the reaction stopped. After allowing the sediment to settle again (approximately one day) the liquid was decanted. Carbonates and/or biogenic silica was not removed as this was not deemed necessary within the requirements of this study. At last the samples were also treated with Calgon ($(NaPO_3)_6$) to make sure the particles do not stick together when analysed by the Malvern Mastersizer.

Gradistat Version 8.0 (Blott and Pye, 2001) was used to process grain size data. It is freely available and is mostly used for the rapid analysis of grain size statistics. Several parameters are automatically calculated such as mean grain size, mode and skewness. Additionally other statistics are calculated logarithmically (phi units) (Krumbein and Pettijohn, 1938), geometrically (metric units) and arithmetically using Folk and Ward methods (Folk and Ward, 1957). Also frequency and ternary plots can be made. It can also provide a description of the textural group and the name of the sediment (Folk, 1954). The program itself runs in excel which makes everything easy to modify by just pasting the desired statistics and manipulate them. The raw data is the text file provided from the Malvern Mastersizer 3000. This file contains general information as operator name, date and time, sample name, laser obscuration and mode count plus the results of the grain size which is in format of percentage above certain values. It is only these data that is imported in Gradistat to perform the processing. As only the general characteristics of all samples were needed, the 'Multiple Sample Data Input' was used to calculate all the parameters.

Additional data was at hand of the grain sizes of the dredged material for all fractions. As this had to be compared to the in-situ grain size data (of the fraction smaller than 1 mm) all the cumulative percentages had to be recalculated so that 1 mm corresponded to 100%. By using the grain sizes of both the in-situ material along the track of the Interballast and this additional grain size data of the dredged material, the possible fraction that forms the sediment plume can be found.

3.5. Processing of navigation files and EMS

Two main correlations were researched by using the EMS-data files of the dredger and the navigational data of the survey vessel combined with the echo-integrated grids made in SonarScope. This was researched by using self-written programs of the CSS, manipulation of all these data and making graphs and correlation coefficients later-on in Microsoft Office Excel. Two coefficients were calculated, a Spearman's ranking coefficient and a Pearson's correlation coefficient, if possible.

The Pearson's correlation coefficient, which is mostly symbolised as 'r' measures the linear relationship between two quantitative variables. It is the covariance of the variables divided by the product of their standard deviations. It can be calculated by the correlation function in Excel. The outcome value lies always in between -1 and +1, with a total non-correlation at 0 and a positive correlation at +1 and negative correlation at -1. Some assumptions for the Pearson's correlation have to be made, with the most important one here that the variables are approximately normally distributed. This is most of the time not the case as non-detection of the plume shows extremely low values whereas detection of it shows high backscatter values. Therefore one should be sure that the plume is relatively well detected before the relationship between plume intensity and the distance/ time is researched.

The Spearman's rank correlation, symbolised as the Greek letter ρ (rho) is a non-parametric measure of rank correlation. It gives a measure of how well the ranked values of both variables correlate to each other and is therefore less sensitive for outliers than the Pearson's correlation. Also the variables shouldn't necessarily be normally distributed. In this work the Pearson's correlation coefficient was

always calculated, whereas only for the Ruyter track the Pearson's correlation coefficient could be calculated.

3.5.1. Influence of distance on the detection of sediment plumes

Firstly the dependency of distance between survey vessel and dredger on the detection of the sediment plume was investigated. For this an excel spreadsheet was made in which the coordinates of the survey ship and dredger were put for each point in time. So time was used as connecting factor in this case. As these coordinates were still in latitude/ longitude form, these had to be converted first to UTM 31N. A screenshot of this coordinate transformation program written by the CSS is shown in figure 15. By using the Pythagoras formula which states that in a right angled triangle the square of the hypotenuse is equal to the sum of the squares of the other sides, the distance between survey ship and dredger can be calculated from the X and Y coordinates in meters. Therefore the resulting distance is also in meters.

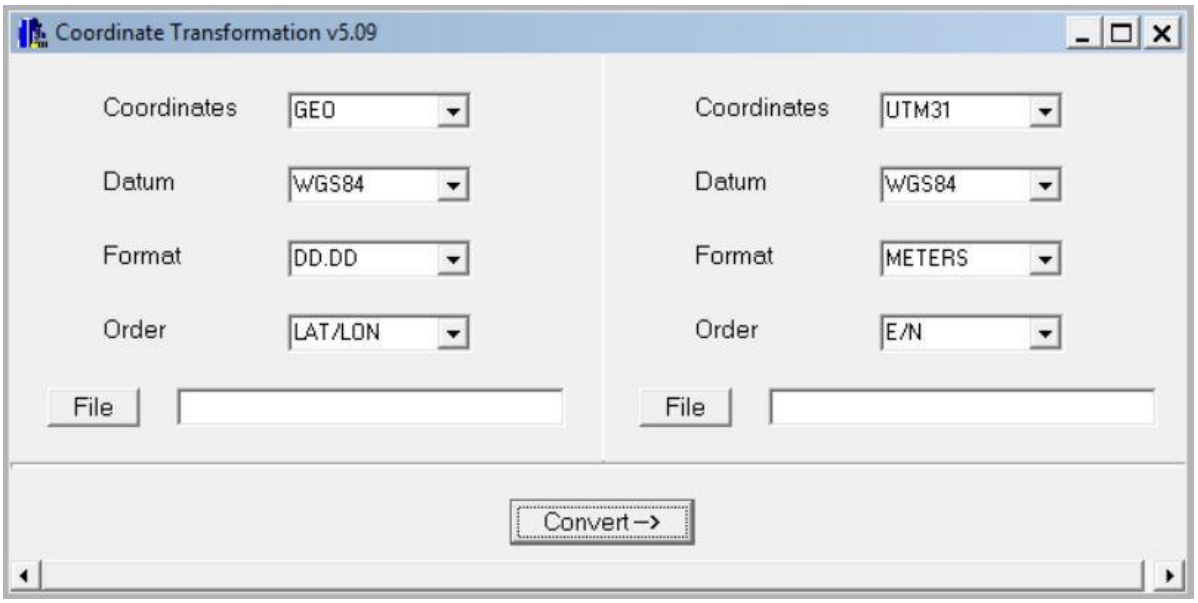

Figure 15. The coordinate transformation program written by the CSS. Coordinates were converted from latitude/longitude coordinates in degrees to UTM 31N coordinates in meters.

As the influence of distance on the detection of the sediment plume is investigated, the plume intensity value has to be extracted from the echo-integrated grids. This was performed by using another self-written program of the CSS named 'BSextraction' (Fig. 16). A search radius was applied of 2.5 m to obtain an relative intensity level of the sediment plume. Afterwards the resulting scatterplot graph was made and a Spearman's rho coefficient and Parson's coefficient was calculated to investigate the correlations.

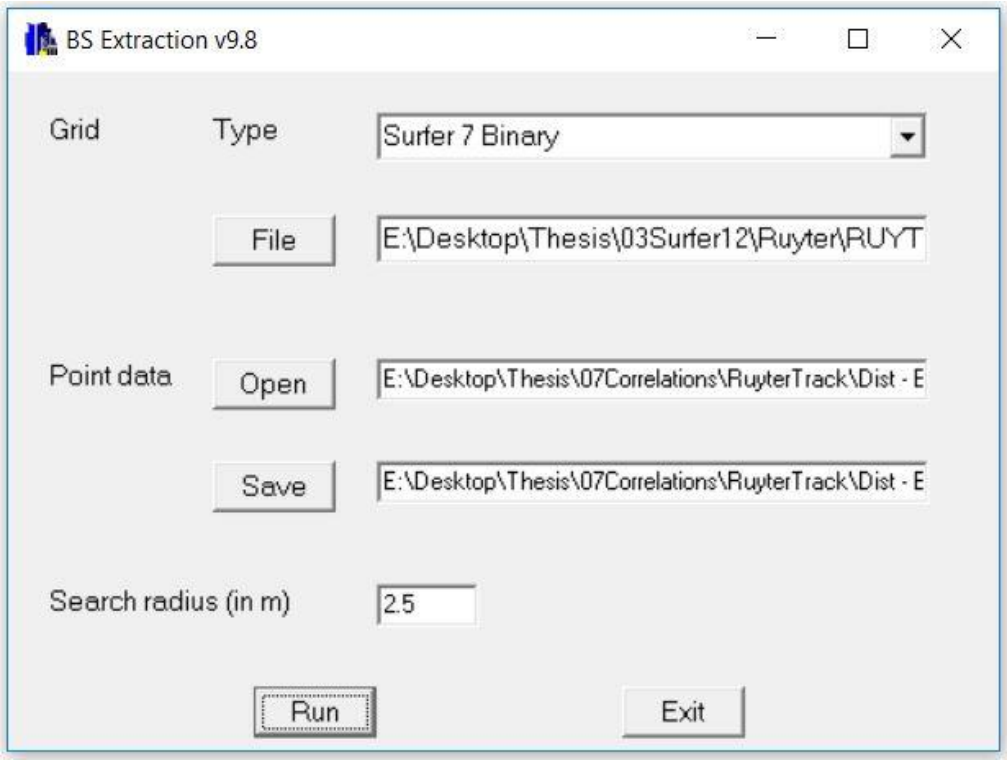

Figure 16. The backscatter extraction program written by the CSS. This program is used to extract the intensity values of the echo-integrated sediment plume maps.

3.5.2. Influence of time since passing on the detection of sediment plumes

Secondly also the dependency of the time that has passed since the dredging took place and the passing of the survey vessel, and its influence on the detection of the sediment plume was researched. This was mainly performed in the same way as in the previous paragraph, by using a self-made program of the CSS and processing of raw text data files in Excel. A program Vesseltracks (Fig. 17) was used to search for each position of the dredging vessel for the position of the surveying vessel that was the closest to that track. From both logs then the time at which they passed at that point was used to calculate a time difference. Next step was to again extract sediment plume intensity values from the echo-integrated grids and draw out the scatterplot which shows the plume intensity in function of the time since passing.

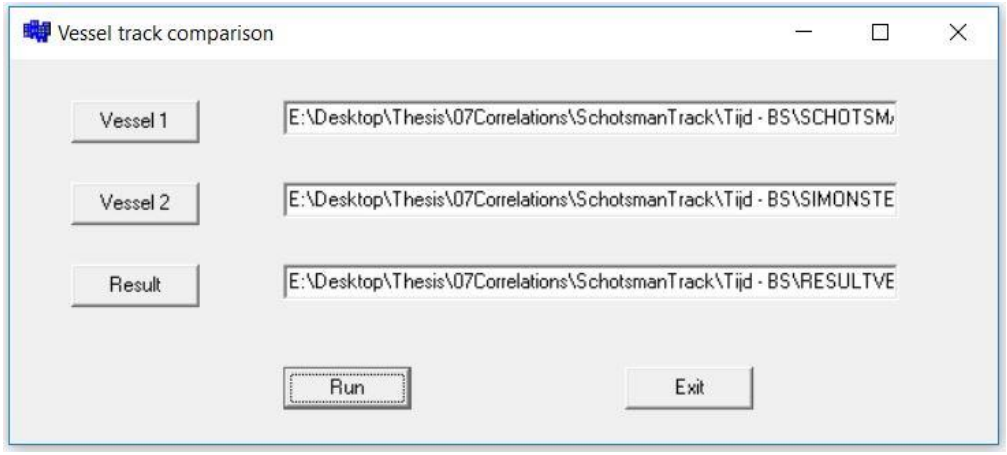

Figure 17. The vessel track comparison program written by the CSS. This program is used to calculate the time difference between two the two nearest data point between the track of the dredger and the survey ship.

In this chapter all the results are shown starting with the bathymetric and SBS results and the comparison with before and after the dredging. This is followed by the results from the water column data in both two and three dimensions. In the last two sections the results of the grain size analysis and the researched correlations are shown.

4.1. Bathymetry

All the shown grids in the following paragraphs are grids applied to the specific situation of following TSHD Ruyter. These data most clearly show the dredging induced changes. The resolution of all the grids shown is 1 meter. All coordinates are in WGS 84 UTM 31N format which means they also show the scale as these coordinates are expressed in meters. All depth values are expressed with respect to the Lowest Astronomical Tide (LAT).

4.1.1. Bathymetry right before dredging

The bathymetry that was acquired before TSHD Ruyter was followed in this area shows several longitudinal depressions in the entire area (the mainly blue fine lines on figure 18). Clear sand dune crests (red) with their accompanying throughs (blue) can be distinguished which are crosscut by longitudinal depressions that mainly have a NW-SE orientation or E-W orientation. Note that in the zoom-in box all crests are undisturbed.

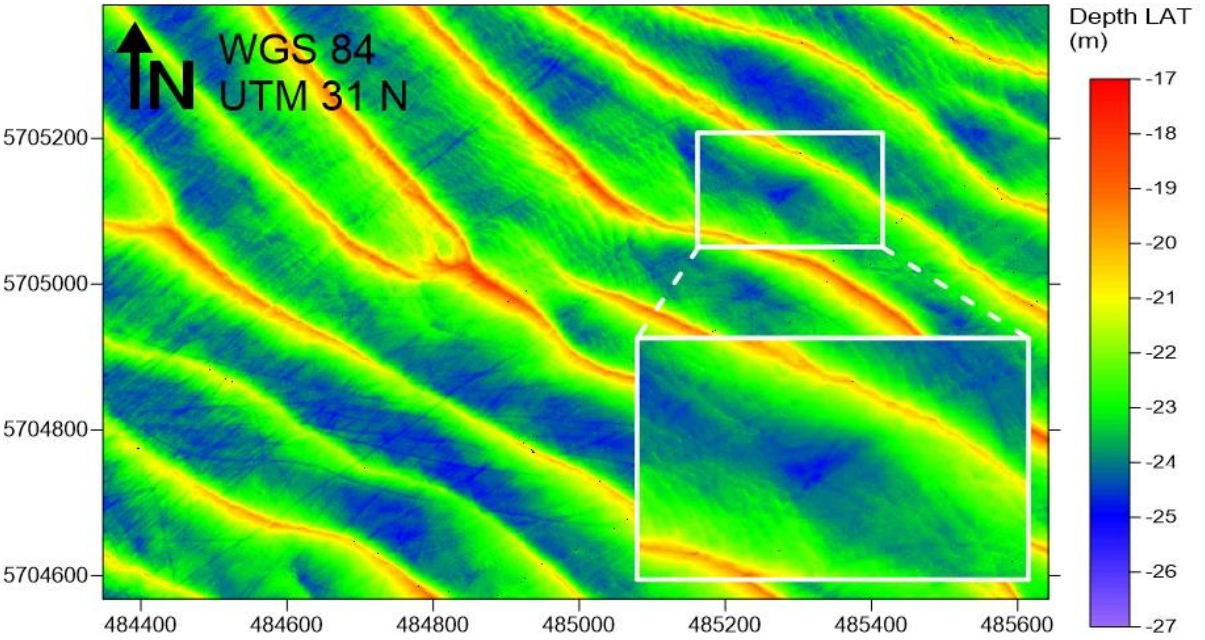

Figure 18. Bathymetry of a part of the Thorntonbank which shows the general outline of this particular area with an outlet in which later-on the TSHD will pass.

4.1.2. Bathymetry directly after dredging

The bathymetric situation moments after the dredging of TSHD Ruyter can be observed in figure 19. Important is the fact that a new longitudinal depression is to be observed (encircled area on figure 19) which clearly crosscuts the sand crests which were previously undisturbed in figure 18. This longitudinal depression is even more distinctive on a shaded relief grid on which the feature is depicted

as enlightened from the north-eastern corner under a vertical angle of 45 degrees with the horizon (Fig. 20).

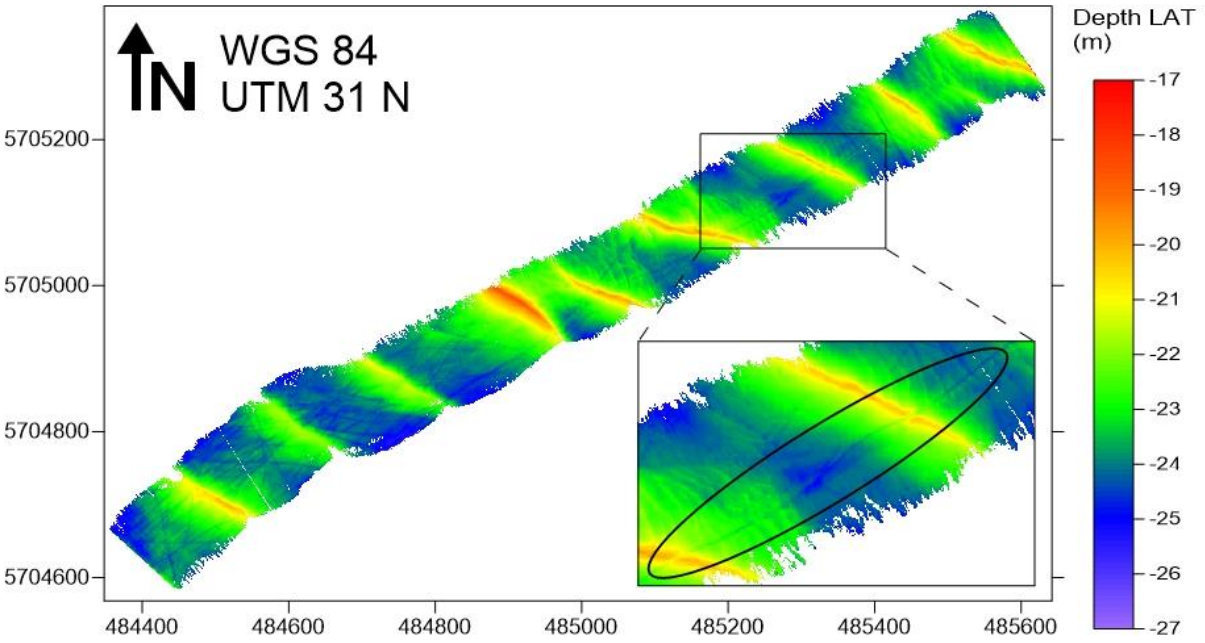

Figure 19. Bathymetry of the track following the Ruyter (TBMAB16-730). The encircled in the zoom-in box is a depression line which crosses the sand crests. In the south-western part of the track, several of these lines can be differentiated.

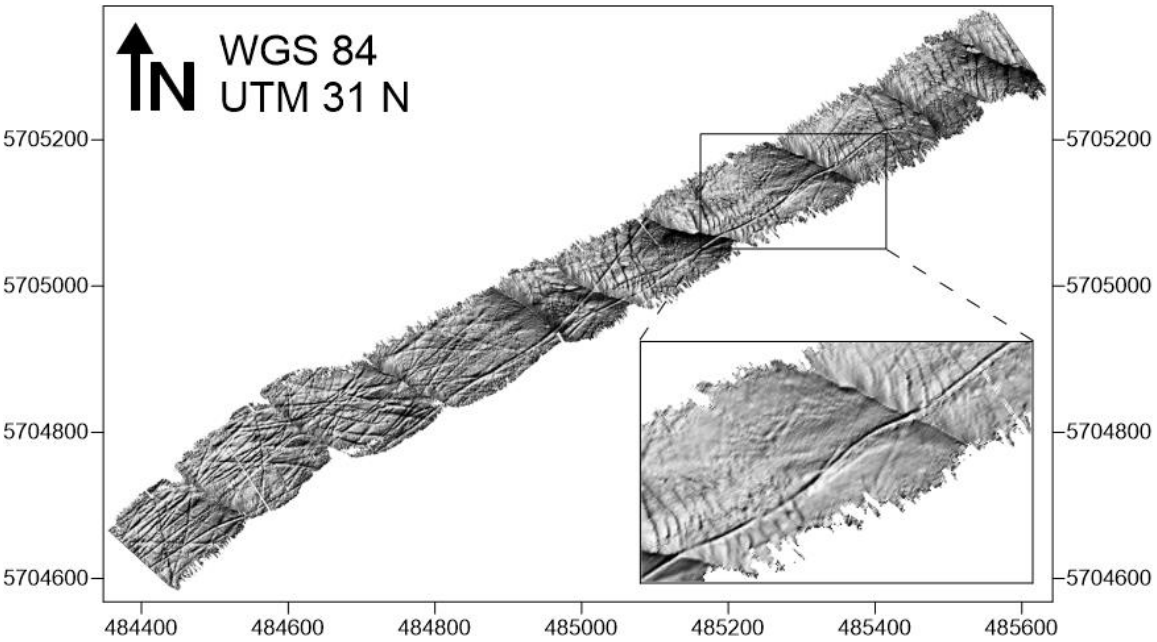

Figure 20. Shaded relief grid of the track following the Ruyter (TBMAB16-730). The grid is enlightened from the northwest, under a degree of 45° with the horizon. The depression features are best visualised on this grid, as again in the zoom-in one track can be visualised whereas in the southwestern part of all the data a hot spot of depressions can be found.

The depth of the depression can be estimated by calculating a difference map between bathymetric charts of two different moments in time. The calculated difference between the bathymetric situation right before and right after dredging shows that the depressions mainly have a depth ranging from 0.20 m to 0.30 m (greenish to yellow colour) (Fig. 21). At some points the depression even adds up to 0.50 m. At the outer sides of the grid the differences add up to more than 0.5 m (red and greenish colour). The width of the depression was measured in Surfer itself by counting about two pixels, which

means the width is one to two meters. This has also been confirmed by making a cross section in Qimera.

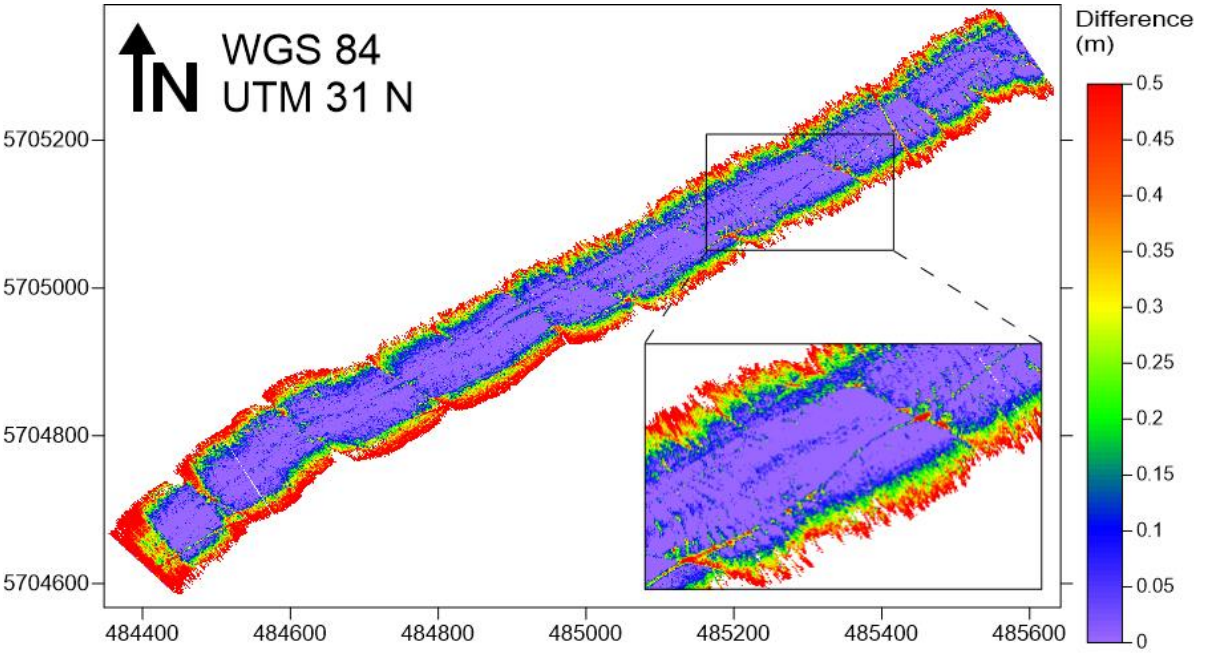

Figure 21. Difference grid of the Ruyter track (1m resolution). Bathymetry of the September campaign (TBMAB16-730) was subtracted from the previous April campaign bathymetry (TBMAB16-310). Therefore the positive difference is sand that was dredged.

4.1.3. Bathymetry two months after dredging

At last also the bathymetry that was surveyed two months after the studied dredging can be shown (Fig. 22). This shows that the sand crests are replenished again, the previous depressions on the crests are not visible anymore. In the through some bit of the dredging track can still be observed.

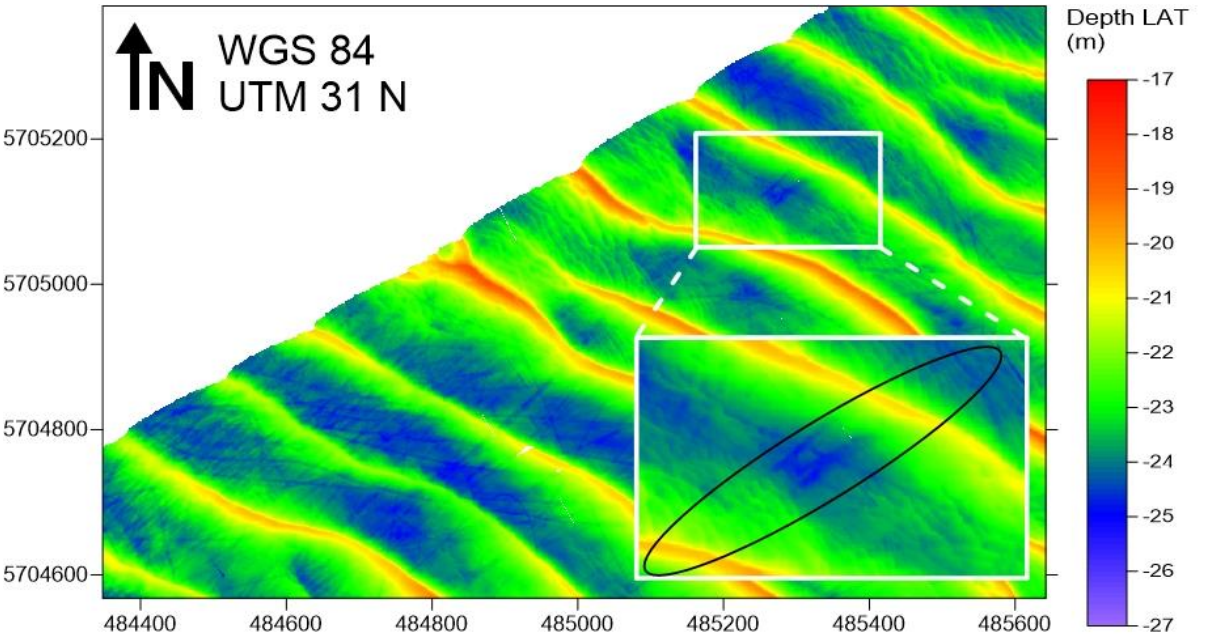

Figure 22. Bathymetry of the Thorntonbank two months after the studied dredging took place. The sand crests are again replenished although the depression in the troughs remain

4.1.4. Overview all tracks

An overview off all the bathymetric results is summarized in table 5.

Table 5. Overview of the bathymetric results for all the tracks.

Bathymetry (in Qimera)			
Track	**Situation before dredging**	**Situation right after dredging**	**Situation half hour/ two months after dredging**
Ruyter	Lot of dredging traces throughout the whole area	Real-time dredging furrow found on 85% of the bathymetric line, clearly visible	Data not available/ fading of the dredging furrow on the crest, rest of the depression stays
Interballast	Dredging traces throughout the whole area, but less to be seen than Ruyter line	Real-time dredging furrow found on 5% of the bathymetric line, but poorly visible	Data not available/ no dredging furrow to be seen anymore
Schotsman	Lot of dredging traces throughout the whole area	Real-time dredging furrow found on 50% of the bathymetric line, clearly visible	Same dredging furrow visible/ bathymetry unavailable (track outside monitoring zone)

4.2. Seafloor backscatter

To describe the SBS mosaics, mainly the track of the Ruyter was used to illustrate certain features.

4.2.1. Seafloor backscatter right before and two months after dredging

In this section the situation right before dredging and a long time after dredging are described together as both grids simply show the same features. No clear difference can be observed between both situations. Both the mosaics made in FMGT and SonarScope yield the same grids and show that backscatter is almost uniform in the whole area (Fig. 23) as there is no sharp boundary somewhere which should implicate a change of lithology.

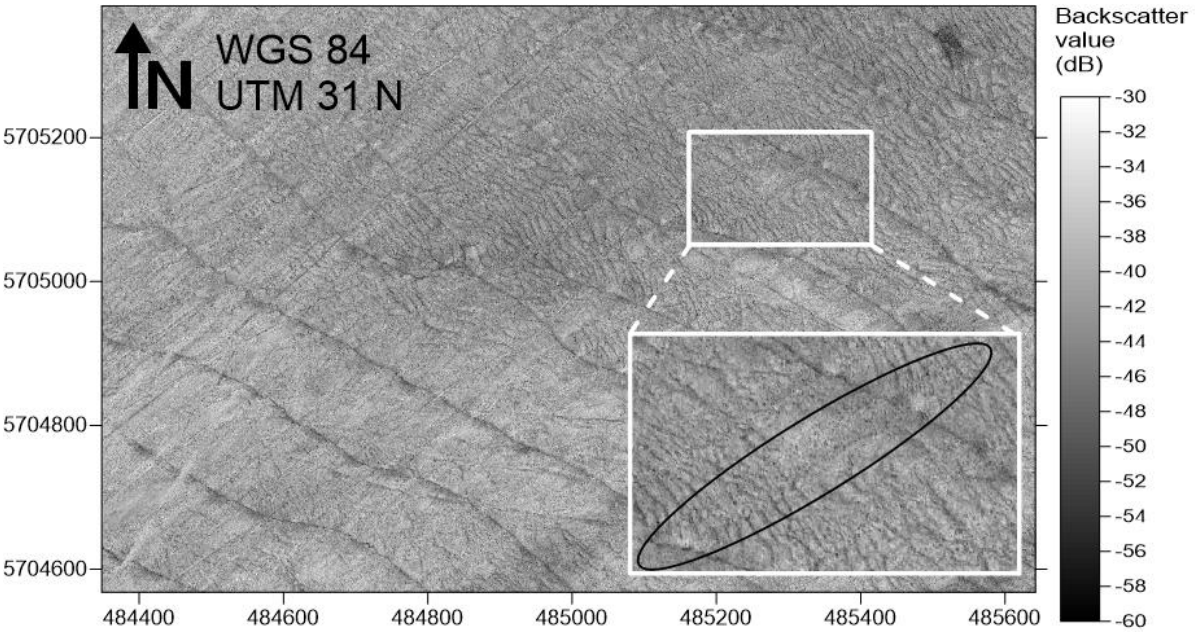

Figure 23. Backscatter mosaic of a part of the Thorntonbank which shows the uniform backscatter. Also in the enlarged part of our study area nothing is to be observed yet.

4.2.2. Seafloor backscatter directly after dredging

The backscatter mosaic of the situation directly after dredging however reveals more interesting things. Backscatter grids were performed using both FMGT and Sonarscope. Figure 24 shows the resulting SBS grid made in FMGT whereas figure 25 shows the resulting backscatter grid made using the SonarScope software. The small depression lines can once again be differentiated (the small thin line of high scattering values).

However there is a remarkable fact when comparing the FMGT and SonarScope grid. Although the resolution of both grids is one meter, there is a difference to be observed between figure 24 and figure 25. On figure 25 the depression is accompanied with a 'halo' of high scatters on the south-eastern side. This 'halo' consists of scatters which yield a value between -32 to -40 dB and is found throughout the whole track next to the depression line (Fig. 20). This 'halo' is not visible on the FMGT mosaic (Fig. 24).

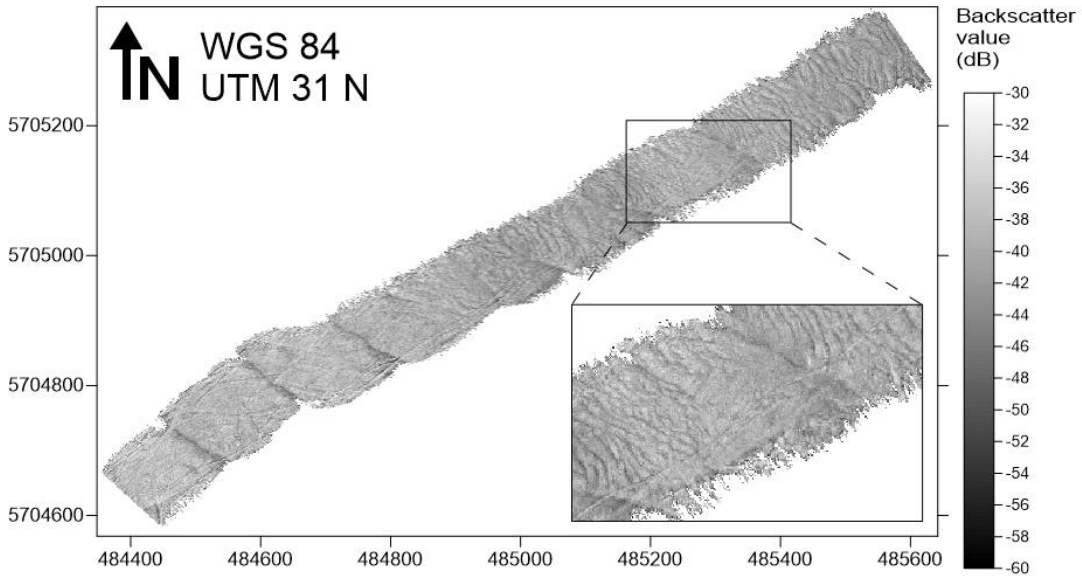

Figure 24. Backscatter grid of the Ruyter track (TBMAB16-730) made using FMGT.

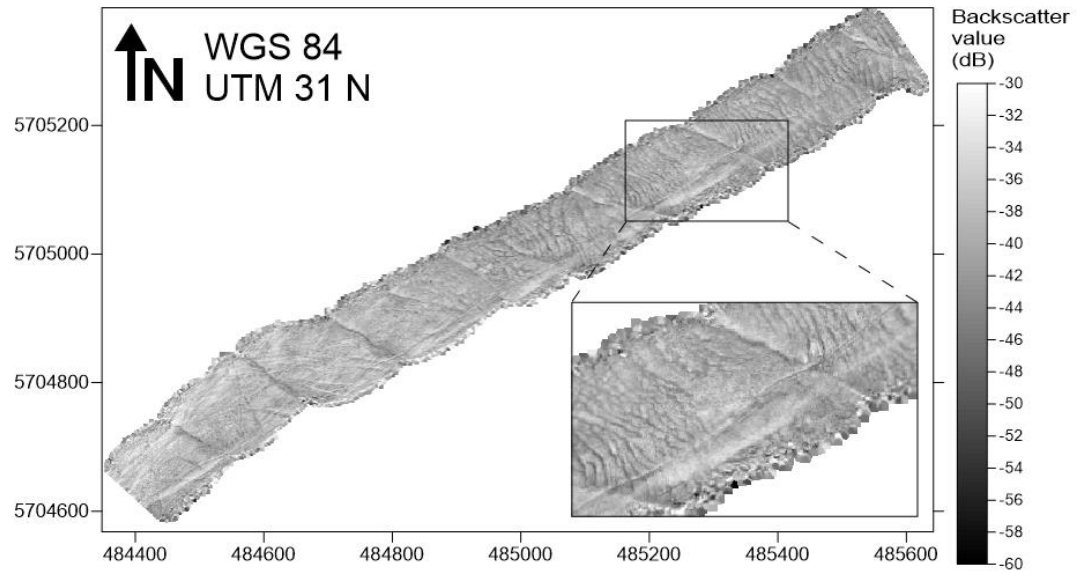

Figure 25. Backscatter grid of the Ruyter track (TBMAB16-730) made using Sonarscope. Note the 'halo' of high scatters at the south-eastern side of the depression line.

4.2.3. Overview of all tracks

An overview of all the backscatter data of all tracks processed in this study and their results is shown in table 6 and table 7. It shows that the 'halo' is not to be observed on the FMGT grids, whereas they are observed directly after dredging on the SonarScope grids.

Table 6. Overview of the seafloor backscatter results for all the tracks in FMGT.

Seafloor backscatter (in FMGT)			
Track	**Situation before dredging**	**Situation right after dredging**	**Situation half hour/ two months after dredging**
Ruyter	Uniformous backscatter, in the NE slightly higher backscatter overall	Higher backscatter in the real-time dredging furrow, accompanied by a lower backscattervalues next to it, no halo	Data not available/ nothing special to be seen, some interference
Interballast	Uniformous backscatter	Higher backscatter in the real-time dredging furrow, accompanied by a lower backscattervalues next to it, no halo	Data not available/ nothing special to be seen
Schotsman	Uniformous backscatter, slightly higher backscatter in the centre of the track	Higher backscatter in the real-time dredging furrow, accompanied by a lower backscattervalues next to it, no halo	Nothing special to be seen / nothing Special to be seen

Table 7. Overview of the seafloor backscatter results for all the tracks in SonarScope.

Seafloor backscatter (in SonarScope)			
Track	**Situation before dredging**	**Situation right after dredging**	**Situation half hour after dredging/ two months**
Ruyter	Uniformous backscatter, in the NE slightly higher backscatter overall, no halo	Higher backscatter in the real-time dredging furrow, accompanied by a lower backscattervalues next to it, halo	Not available/ no halo visible
Interballast	Uniformous backscatter, no halo	Higher backscatter in the real-time dredging furrow, accompanied by a lower backscattervalues next to it, halo	Not available/ no halo visible
Schotsman	Uniformous backscatter, slightly higher backscatter in the centre of the track, no halo	Higher backscatter in the real-time dredging furrow, accompanied by a lower backscattervalues next to it, halo	Half an hour later, the halo of higher backscatter values is gone / no halo visible

4.3. Water column backscatter

Water column processing mainly resulted in the visualization of it in two dimensions and possibly in three dimensions. A calculation of sediment plume volume was performed using the amount of sediment plume voxels, this will give a rough quantification of the sediment plume. Firstly the results of processing in FMMidwater and SonarScope will be shown, followed by the three dimensional visualizations in Voxler.

4.3.1. Two-dimensional results

The water column was processed using two software packages. By using the echo-integration algorithm in SonarScope a grid could be made with the plume intensity. This intensity is not retained in original decibel value but converted to a colour value between 0 and 256. The results of this echo-integration for the plume of the Ruyter can be observed in figure 26. The centre part of the grid shows high plume intensities whereas at the border blue bands of low intensity are found. The plume intensity value diminishes from centre to the border of the footprint.

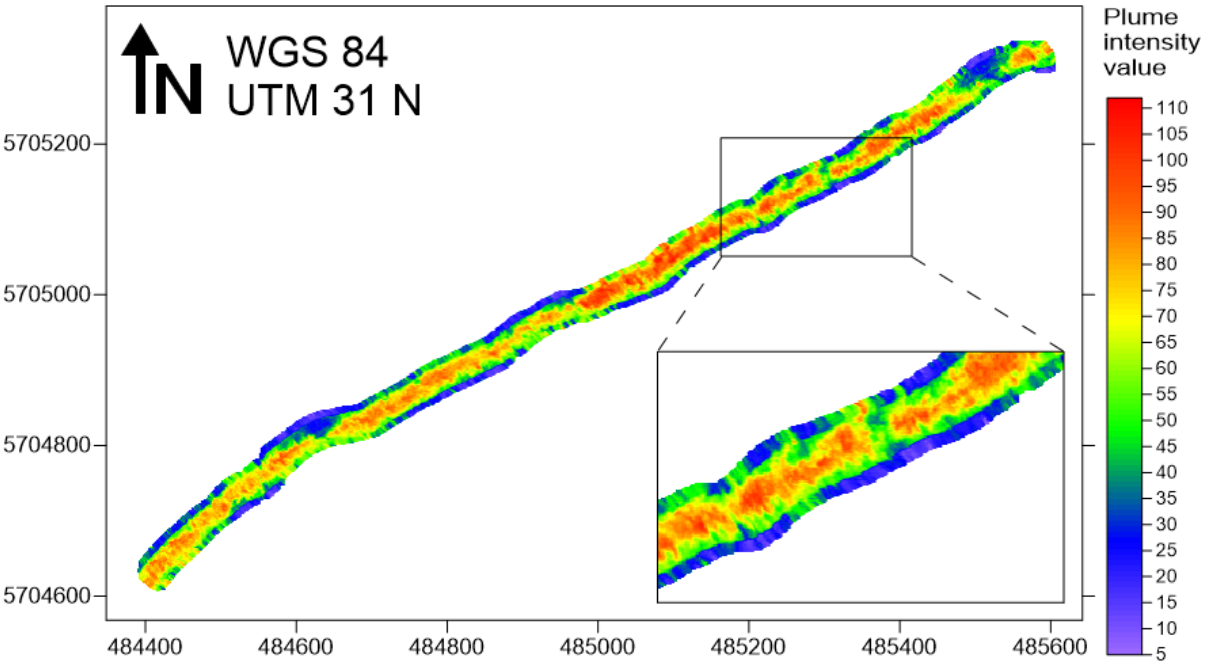

Figure 26. Intensity of the sediment plume resulting from the SonarScope echo-integration algorithm. All sectors of the water column were used. The original decibel backscatter values are not retained.

4.3.2. Three-dimensional results

To better visualize the made three dimensional model, only a part of the sediment plume caused by TSHD Ruyter will be shown in the following figures. In this case the data from line 31 was used.

Figure 27 shows the first step in making the model, namely the raw pre-filtered backscatter values ranging from -60 to -30 decibels, exported from FMMidwater. Therefore it is important to note that all the values that are observed are already the sediment plume itself, as most of the backscatter values of the water column were already filtered out in FMMidwater.

Figure 28 shows the results of the VolumeRender module that was applied on the gridded values. The resulting model shows the sediment plume in a transparent way. In this way it can be found where the higher intensities are inside the sediment plume itself. The question in this case is if these higher values ranging from -49 to -40 decibels are related to a denser sediment plume (higher sediment concentration) or related to fish which cause the higher values.

The results of the FaceRender module are shown in figure 29. This shows the sediment plume modelled in blocks of half a cubic meter (1 m resolution in x and y, 0.5 m resolution in z direction). The colour once again shows the mean backscatter value for that block, which are here at the outside in the range of -55 to -52 decibels. In the FaceRender module itself an approximate calculation was shown of the volume of voxels. This results in an approximate volume of 2003 m^3 for line 31 of the data of following the Ruyter. In analogy this was calculated for the whole track (so all lines from the Ruyter track). This resulted in a volume of 48520 m^3.

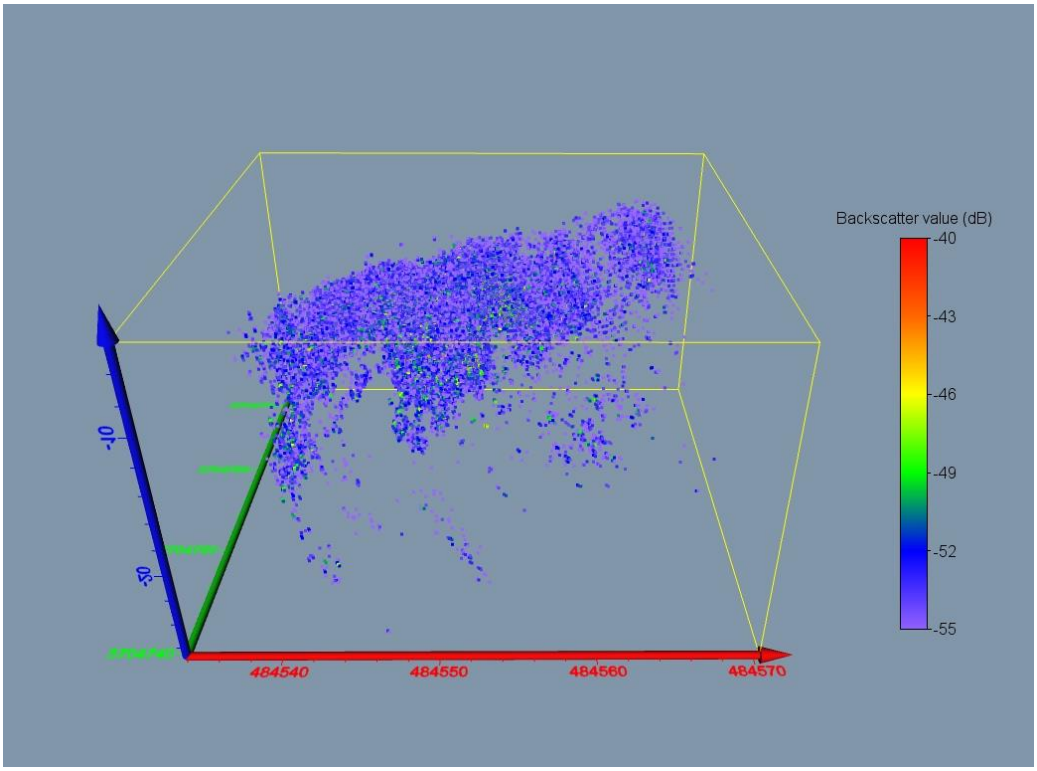

Figure 27. The raw backscatter values from a part of the sediment plume caused by TSHD the Ruyter. Colours correspond to the backscatter values in decibel, which are mainly in the range of -52 to -55 decibels.

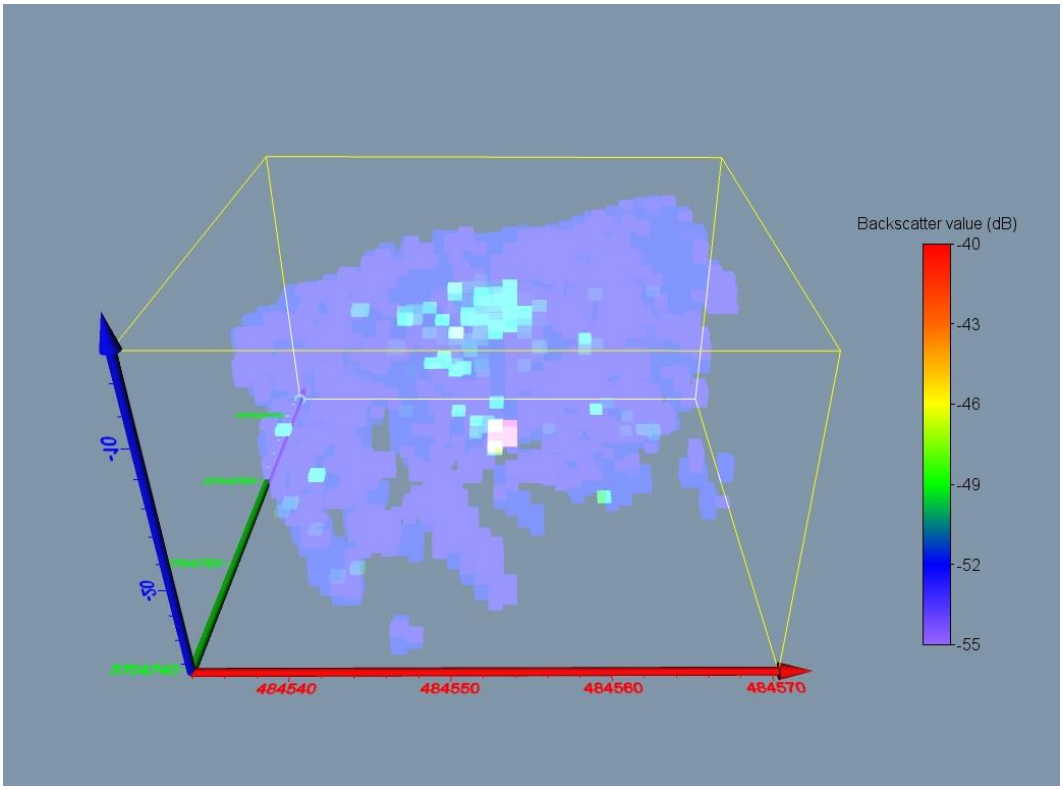

Figure 28. Volume render of the sediment plume caused by TSHD the Ruyter. In the inside of the plume high scattering values are to be found (ranging from -49 to -40 decibels).

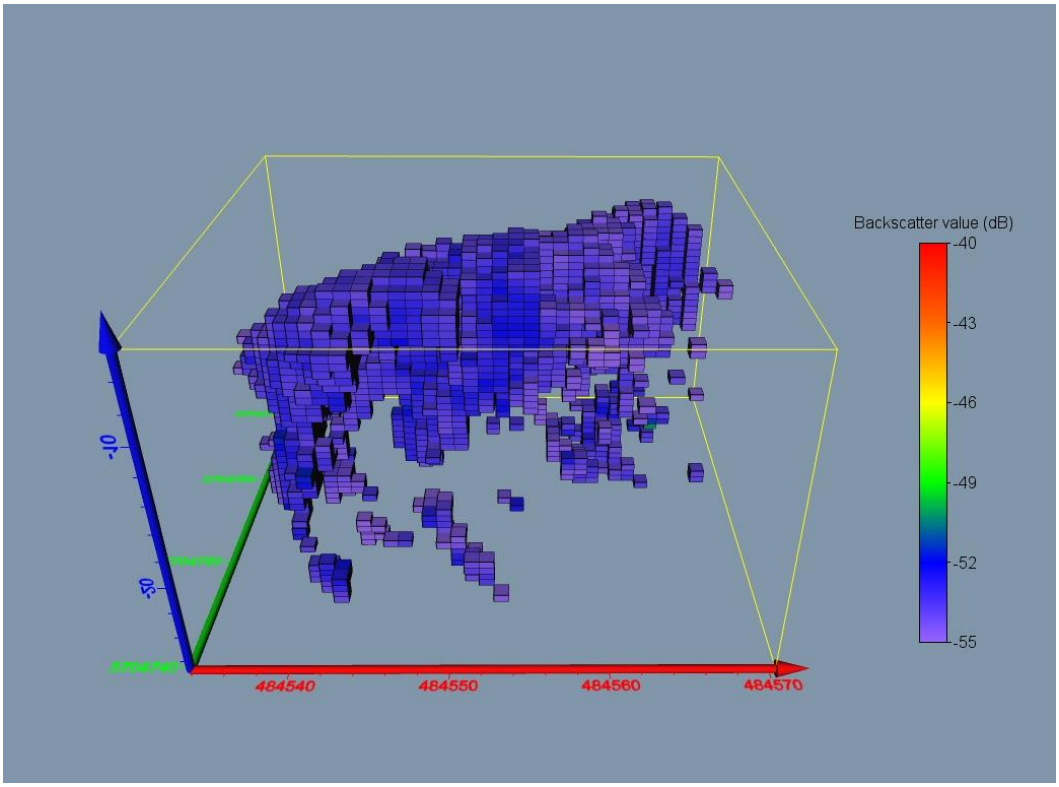

Figure 29. Face render of the sediment plume caused by TSHD the Ruyter. The sediment plume is visualised as built up from blocks of half a cubic meter (one meter resolution in x and y, half a meter resolution along z axis. Their intensities is again show by their colour (mainly purple and blue on the outside).

4.4. Influence of time or distance between vessels on the plume intensity

4.4.1. Results for TSHD Ruyter

The first of the two key correlations that were researched was to research if the distance between dredger and survey ship had an influence on the intensity of the sediment plume (Fig. 30). It shows a cluster of points with the majority of plume intensities ranging in between 60 and 100. The distance at which the Ruyter was followed was always in between 400 and 600 m. Additionally also a Spearman's rho rank correlation coefficient and a Pearson's correlation coefficient was calculated. These were -0.20 and -0.14 respectively.

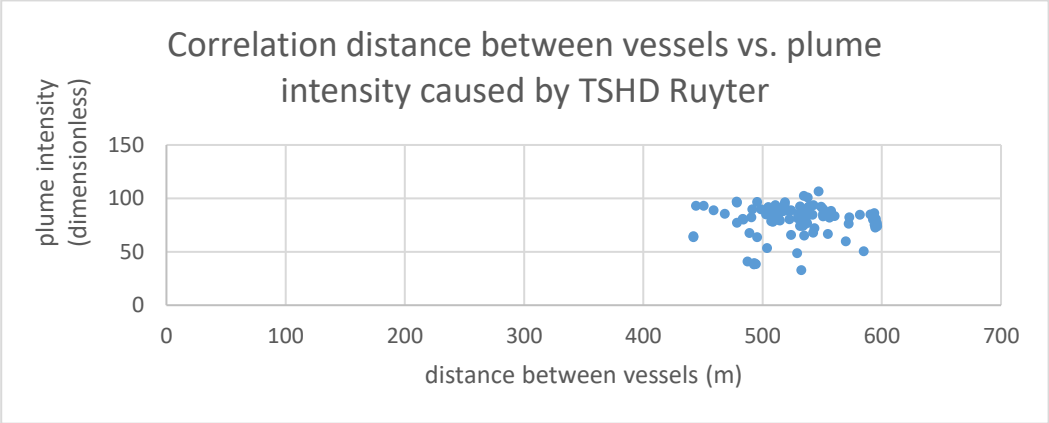

Figure 30. Plume intensity in function of the distance between TSHD the Ruyter and RV Simon Stevin.

The second correlation investigated was to investigate what the influence was of the time since passing on the intensity of sediment plumes. The resulting scatterplot of this can be found in figure 31. The time difference was as in the previous correlation constant, ranging in between 900 and 1200 seconds that have passed since the dredging ship passed. Intensities of the sediment plume lie mainly in between 60 and 110, with one outlier around 40. For this correlation the Spearman's rho rank correlation coefficient was -0.41, and the Pearson's r correlation could not be calculated as the time values were not normally distributed, which was one of the requirements of calculating a Pearson's r coefficient.

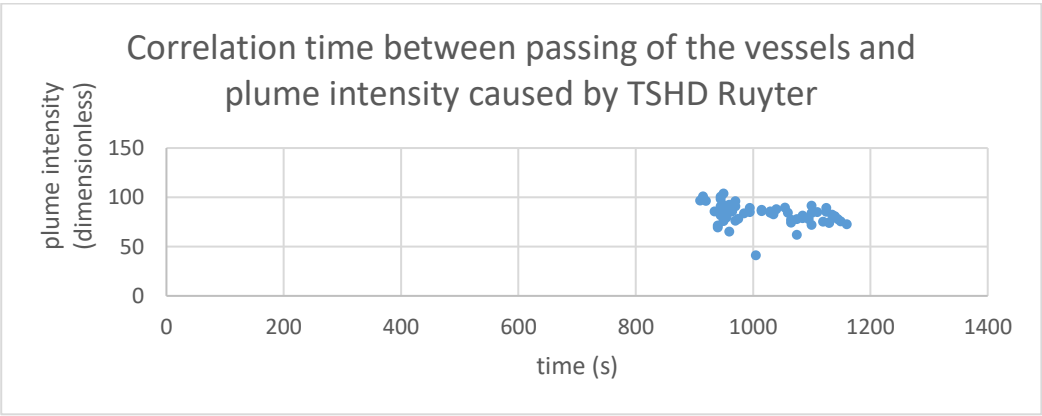

Figure 31. Plume intensity in function of the distance between TSHD the Ruyter and RV Simon Stevin.

4.4.2. Overview results for the other tracks

The results from the other tracks (Table 8) show that for the Interballast track nothing correlates at all, whereas for the Schotsman higher Spearman's correlation coefficients are found than those shown for the Ruyter track. As in the discussion time range and distance range will be of an importance, these are also given in table 8. Only for the distance – plume intensity correlation of the Ruyter track a Pearson's coefficient was calculated as in other cases, either the distance or time or plume intensity was not normally distributed.

Table 8. Overview of the correlation coefficient results for all tracks.

Track	Correlation	Spearman's coefficient	Pearson's coefficient	Time range (s)	Distance range (m)
Ruyter	Distance - plume intensity	-0.20	-0.14		400-600
	Time - plume intensity	-0.41	not normally distributed	850-1200	
Interballast	Distance - plume intensity	0.01	not normally distributed		200-400
	Time - plume intensity	0.04	not normally distributed	250-450	
Schotsman	Distance - plume intensity	-0.60	not normally distributed		150-550
	Time - plume intensity	-0.36	not normally distributed	0-550	

4.5. Grain size analysis

The grain size analysis of the fraction smaller than 1 mm of the samples 'SPI1-9', the samples that were taken on the Thorntonbank in the April campaign, show that the sand fraction is dominantly medium sand. A brief summary of some selected statistical parameters is given in table 9Table 9.

Table 9. Grain size results of the fraction less than 1 mm from the samples on the Thorntonbank.

SAMPLE NAME:	**SPI 1**	**SPI 2**	**SPI 3**	**SPI 4**	**SPI 5**	**SPI 6**	**SPI 7**	**SPI 8**	**SPI 9**
SEDIMENT NAME:	Moderately Well Sorted Medium Sand	Moderately Well Sorted Medium	Moderately Well Sorted Medium	Well Sorted Medium	Well Sorted Medium	Well Sorted Medium	Well Sorted Medium	Well Sorted Medium	Moderately Well Sorted Medium
MEAN	360.18	304.21	370.24	384.27	406.16	389.71	393.80	361.51	385.07
SORTING	1.51	1.60	1.43	1.38	1.39	1.37	1.39	1.36	1.46
SKEWNESS	-0.03	-0.09	-0.02	0.00	0.00	0.00	-0.01	-0.01	0.03
KURTOSIS	0.96	1.04	0.93	0.96	0.95	0.96	0.95	0.95	0.95
D_{10} (μm):	209.39	163.17	231.32	253.43	265.92	257.97	256.51	242.77	238.76
D_{50} (μm):	361.83	308.39	371.26	384.20	406.71	389.66	394.06	361.90	383.41
D_{90} (μm):	608.73	536.83	586.00	579.75	620.81	584.72	600.87	540.38	634.83
(D_{90} / D_{10}) (μm):	2.91	3.29	2.53	2.29	2.33	2.27	2.34	2.23	2.66
(D_{90} - D_{10}) (μm):	399.34	373.66	354.68	326.32	354.89	326.75	344.35	297.61	396.07
(D_{75} / D_{25}) (μm):	1.78	1.87	1.66	1.56	1.58	1.55	1.58	1.54	1.70
(D_{75} - D_{25}) (μm):	210.31	195.11	190.64	172.22	186.39	173.22	181.61	157.20	205.46

Results of the grain size analyses of the samples taken in the September campaign along the track of TSHD Interballast are shown in table 10. Table 11 shows the mean grain size distribution of the dredged material (46 samples) on the Thorntonbank that in the end is used in building materials. This data was provide by the CSS. In both cases the highest increase in cumulative percentage can be found in the fraction between roughly 250 to 500 μm which means that the main grain size is medium sand (Fig. 32). However the dredged material also appears to be coarser overall. This is confirmed by the grain size at 50 percent (D50). D50 for the in-situ seafloor material is 364.33 μm whereas it is 397.99 μm for the dredged material.

Table 10. Grain size results of the three taken samples after dredging along the track of the TSHD Interballast. Only the fraction smaller than 1mm was analysed.

Grain size (µm)	98.1	111	127	144	163	186	211	240	272	310	352	400	454	516	586	666	756	859	976	1000
Cumulative % I1	0.00	0.00	0.00	0.09	0.74	2.80	7.23	14.71	25.31	38.34	52.51	66.25	78.17	87.38	93.66	97.35	99.15	99.82	99.98	100.00
Cumulative % I2	0.00	0.05	0.50	2.09	5.76	12.33	22.11	34.68	48.90	63.19	75.98	86.11	93.12	97.25	99.21	99.88	100.00	100.00	100.00	100.00
Cumulative % I3	0.00	0.00	0.00	0.23	1.26	3.87	8.83	16.58	27.04	39.54	52.95	65.95	77.35	86.37	92.75	96.71	98.81	99.70	99.97	100.01
Average cumualtive %	0.00	0.02	0.17	0.80	2.59	6.33	12.72	21.99	33.75	47.02	60.48	72.77	82.88	90.33	95.21	97.98	99.32	99.84	99.98	100.00

Table 11. Grain size results of a total of 46 samples taken from the dredged material that is used in building applications. Everything was recalculated to the fraction smaller than 1mm to be able to compare with the in-situ data. Data from the CSS.

Grain size (µm)	63	125	250	500	1000
Average cumulative %	0.59	0.92	15.95	89.41	100.00

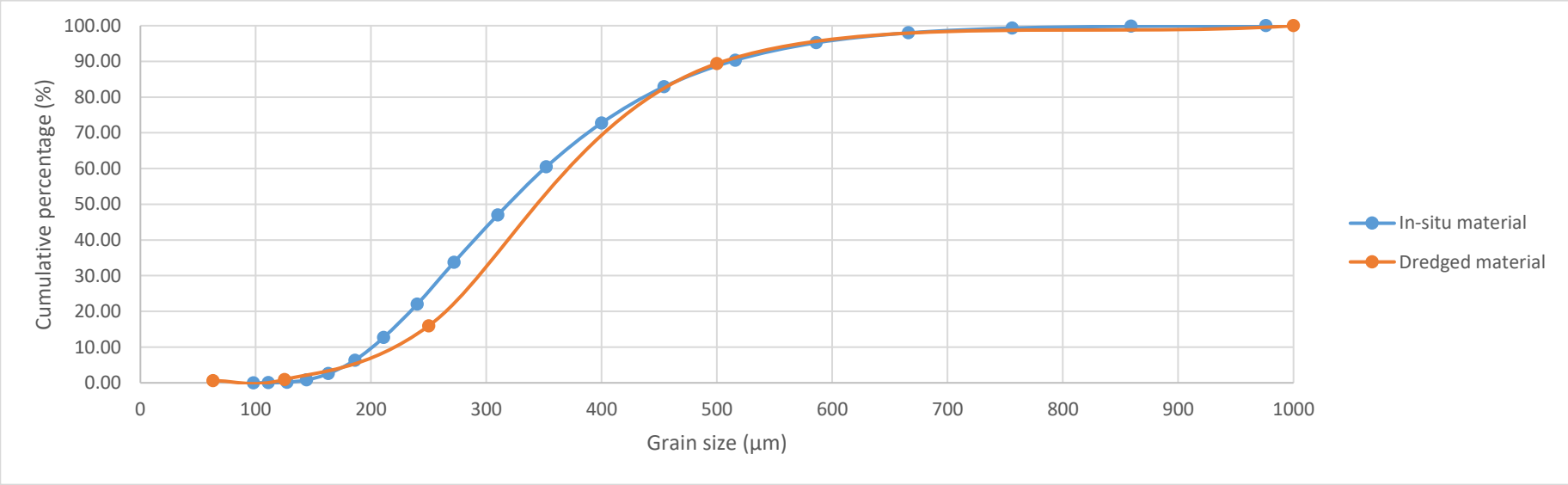

Figure 32. Comparison between the in-situ grain size data and the grain size data from the dredged material itself. The largest difference between the two curves lies mainly in the 200-400 µm category.

5.1. Evolution of the tracks on bathymetry

The depressions found on the bathymetric grids are clearly caused by the TSHD. When the navigation data is plotted on the shaded relief map, one particular trace stands out that matches the track of TSHD Ruyter. This can be observed in figure 33 where the navigation data of the Ruyter (in green) corresponds to a clear longitudinal depression. The approximate dredged depth of about 0.2 to 0.3 m corresponds to the typical amount of sand that is scraped from the bottom by a TSHD (Mills and Kemps, 2016). The track was not yet visible on the situation before dredging (Fig. 18). Moreover the width of the track is in the same order of magnitude as the width of the suction head of a TSHD. In the specific case of the Ruyter, the width of the suction head is not known, but the diameter of the suction pipe is 0.65 m (Dredgepoint, 2017a). The suction head will therefore be approximately 1 to 2 m wide and this is almost the same and at least in the same order of magnitude as the width of the longitudinal depression.

The estimation of how well the dredging furrow was observed in table 5 was performed in the same way as in figure 33. The data of the Ruyter represents the dredging induced changes the best as along that track almost 85% of the real-time dredging furrow was captured. The data acquired following the Interballast only shows an estimated 15% of the dredging track which makes it difficult to study the dredging induced consequences as to be observed on SBS and possibly also the WCBS as the surveyed track was further of the dredged furrow. Also only 50% of the dredging track was captured when following TSHD Schotsman which makes it also less ideal to be studied.

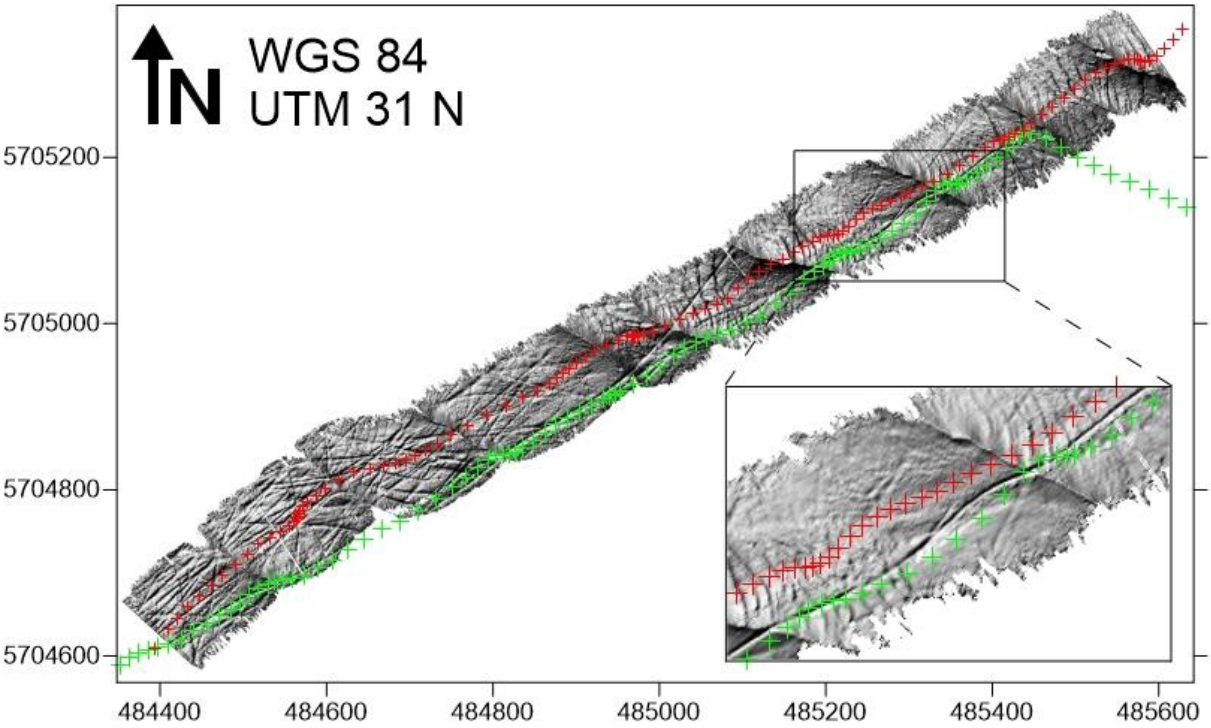

Figure 33. Plot of the navigation data on the shaded relief map following TSHD Ruyter. The red crosses form the track of RV Simon Stevin whereas the green crosses form the track of TSHD Ruyter. One clear dredging trace matches the navigation data of TSHD Ruyter

As for the fading of the dredging track this could just be due to the instability of the crest together with the influence of currents. Previous research already showed that the sand crests move and generally become lower due to the extraction in that area (Roche et al., 2017)). Sand does not replenish as once again recent publications of the CSS showed (Degrendele et al., 2010; Roche et al., 2013), but small depressions appear to fade probably due to current.

It can therefore be proven that the real-time impact of dredging is recorded and therefore the backscatter data acquired from the water column and seafloor can be investigated to research what the consequences of dredging give on these type of data.

5.2. Impact and evolution on seafloor with SBS

Firstly the difference between the backscatter grid made in FMGT and the one made in SonarScope has to be explained. On the grid made using SonarScope a clear 'halo' of high scatters was observed next to the real-time dredging trace. This 'halo' is not observed on the FMGT grid. Both grids have a one meter resolution so this difference is not caused by a different resolution. As the 'halo' was also observed on the SonarScope grids next to the real-time dredging track following TSHD Interballast and TSHD Schotsman, it can firstly be said that the 'halo' of high scatters really is there and is caused by the dredging operation itself. The question that arises then is why this 'halo' is not visible on the grid made in FMGT.

As stated in the report of the GEOHAB working group about calibration and processing of SBS data, most post-processing software's implement a long processing chain to reach the resulting backscatter mosaic (Lurton and Lamarche, 2015). This chain of processing the raw data, going from decoding of raw measurements to the whether or not correcting for static and time-varying gain, source level and transmit and receive level, propagation losses, correcting for ensonified areas or volumes and/or correcting for angular dependence can be the cause of this difference between the two grids.

As in FMMidwater only the resolution and search radius have to be set, one does not always know what goes on when the backscatter mosaic is created. Therefore further research is needed into these specific processing chains of both software packages as it could be important in this case, and in the general case of processing SBS. Especially in the case of the research and attempts in the recent years to calibrate the SBS (Lurton and Lamarche, 2015) to be able to compare results acquired with different systems, this proves once again that also software processing can lead to large differences in outcome grids, even when using the same raw data.

For the cause of the observed 'halo' several hypothesis were made. First of all it should be noted that this 'halo' is a really temporary thing which is clearly dredging induced and which also fades a half hour after dredging. One hypothesis that was discussed with members of the CSS to explain this onset of higher scatters and the following fading afterwards, was the possibility of temporal relative enrichment of the coarse fraction (shells and gravel) due to the finer fraction going temporarily into suspension because of the dragging of the suction head on the seafloor. The drag head of the TSHD causes turbulence which leads to a sediment plume and temporarily less fine sediment on the seafloor. The following disappearance of the 'halo' could then be explained by the settlement of the sediment plume again which will lead to an again normal SBS value.

As shown in the next section also the sediment plume will be gone, so the sediment cloud settles in more or less the same place and is not transported with the current, additional proof of this is shown by the vector map (Fig. 34). This shows that the sediment plume was transported for several meters

by the current, although after calculations with the current speed at hand and the mean time difference between the dredging operation and the actual surveying, the sediment plume should be way of the place where it was detected here. The mean time is around 1000 seconds, the mean current around 0.4 m/s which means that the cloud should have drifted off for 400 m whereas here it only drifted off for 50- 100 meter. A possible explanation for this is that the plume is stable, which means that it is not very much influenced by the current. This would also fit in the hypothesis of the 'halo', which states that the sediment plume has to settle at more or less the same place in order to explain the disappearance of the 'halo' half an hour after dredging.

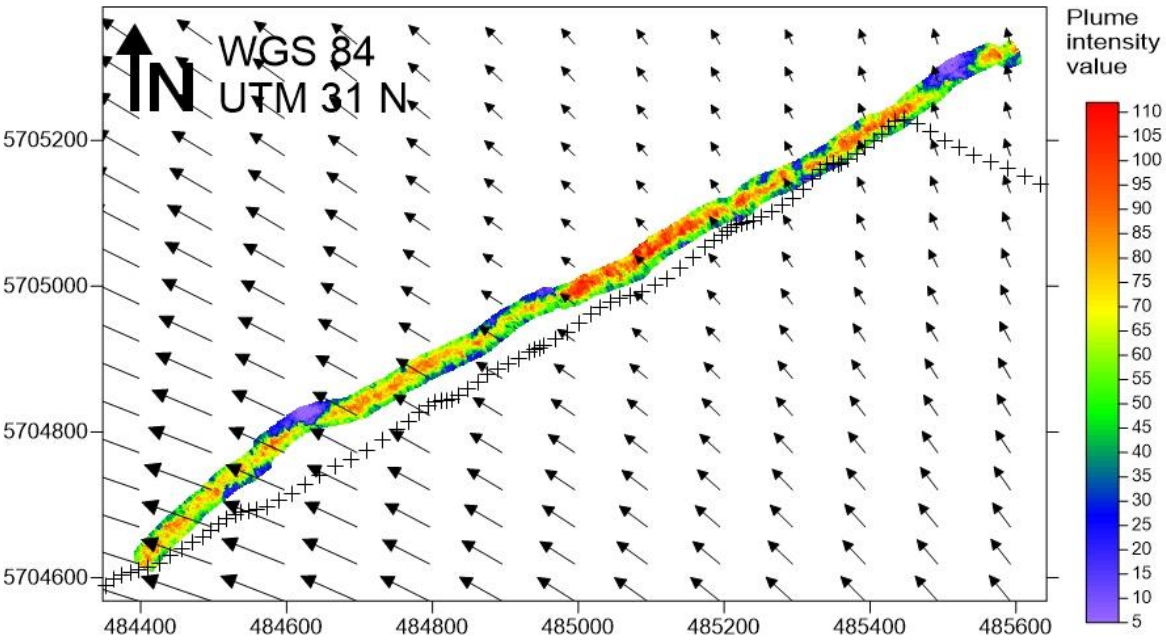

Figure 34. Plume intensity along TSHD Ruyter track. The vectors show the current direction. The black crosses show the navigation data of the dredger. Current info retrieved for measuring station 'De Wandelaar' (Meetnet Vlaamse Banken, 2017).

5.3. Visualization of the sediment plumes

Processing of the water column resulted in clear representations of the water column in both two dimensions and three dimensions. During the processing and interpretation several problems were encountered and advantages and disadvantages were found which will be discussed in the next section.

5.3.1. Quality of the visualizations in two and three dimensions

The resulting grids of the echo-integration in SonarScope give a more or less decent representation of the sediment plume intensity in two dimensions although insights were gathered in some flaws incorporated in it. Figure 26 showed the echo-integration of almost the whole water column (upper 96 percent). What stands out on that grid were the bands of lower plume intensity at the sides of the track with a clear abrupt shift in plume intensity value. This shift was hypothesised to have three possible causes.

Firstly one can think of an actual decrease of plume intensity, this would mean that the sediment plume was perfectly captured and the blue colour values at the sides would then actually mean a non-detection of the sediment plume. However this would be a lot of coincidence. It would mean that throughout the whole track the sediment plume was followed and recorded perfectly. It would be

more logical that the boundary between detection and non-detection of sediment plume would be a gradual one instead of an abrupt as is the case now. Therefore this explanation was abandoned.

Second possible explanation was that it could be due to nature of the echo-integration principle itself as it takes a vertical mean intensity, and therefore at the sides of the water column there are simply less points to take the mean intensity from. This would explain the lower value but not the abrupt change from high to low intensity. So in this case it is not possible as explanation for the abrupt shift, but it shows that false or faulty pings will gradually have a larger impact to the sides of the grid. It could therefore be stated that the accuracy and therefore the quality of the grid diminishes from the centre to the sides.

A more likely explanation is that this abrupt change at the sides of the grid is an artefact of the water column data being recorded in three sector mode. A similar shift in backscatter values due to the three sector mode could already be observed in the echogram view (Fig. 10). Therefore it is recommended to record water column data for the detection of sediment plumes in single sector mode in the future or to keep on recording in three sector mode, but filter out the outer sectors in the processing. A new and probably more correct representation of the two-dimensional grid is shown in figure 35 where the outer 35 degrees of the water column are not considered. The encircled parts in this figure then actually mean that the sediment plume is not detected as a plume intensity of 10 to 30 corresponds to the intensity of the water column background as detected along the Schotsman track half an hour after dredging when the sediment plume was already gone.

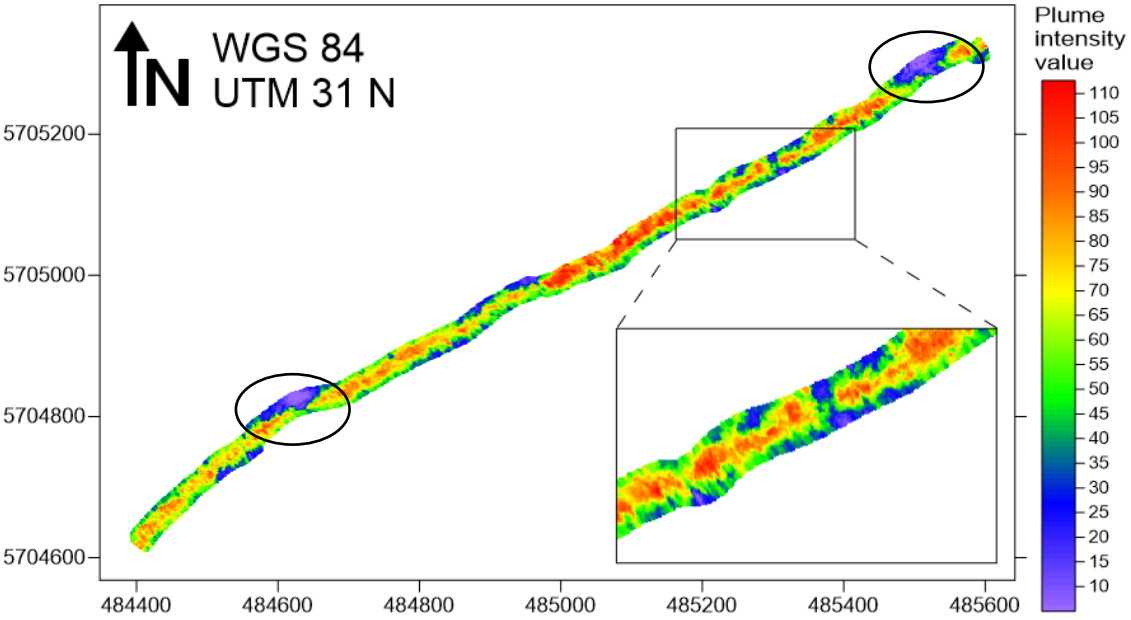

Figure 35. Intensity of the sediment plume resulting from the SonarScope echo-integration algorithm. Not the whole water column was used, the beams in the outer 35 degrees on both sides were not considered to filter out the outer sectors. The original decibel backscatter values are not retained.

The eventual end result of processing of the water column was a three dimensional model of the sediment plume in voxels of half a cubic meter. A visual comparison between the stacked view in FMMidwater of the raw water column data of line 32 (Fig. 36), with a sideway look on the eventual face render model in Voxler of line 32 in figure 37 could be performed. This shows that the made model is a good representation of the sediment plume as the morphology of the sediment plume in the stacked view can be recognised in the sideway view of the model of the same line in Voxler.

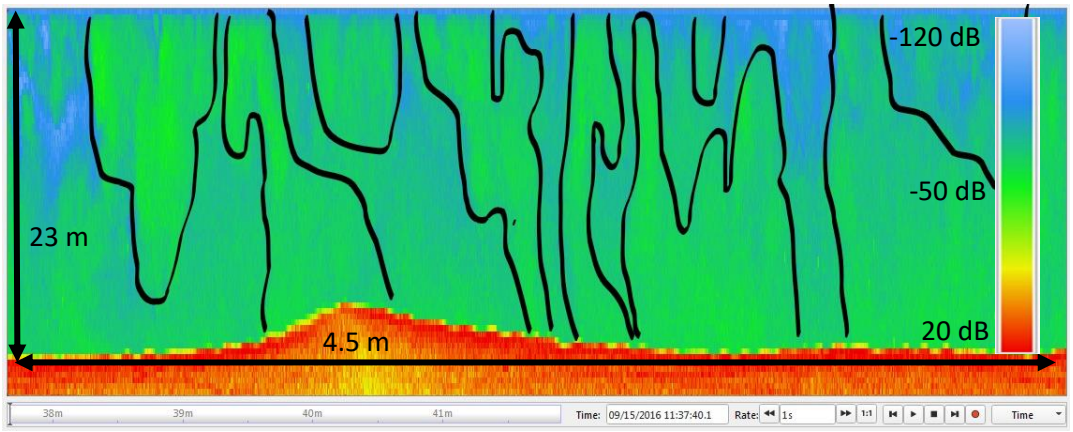

Figure 36. Stacked view of line 32 of the Ruyter track. The green values are the sediment plume. Contours of the biggest clouds are shown in black. These corresponds roughly with the model in figure 37.

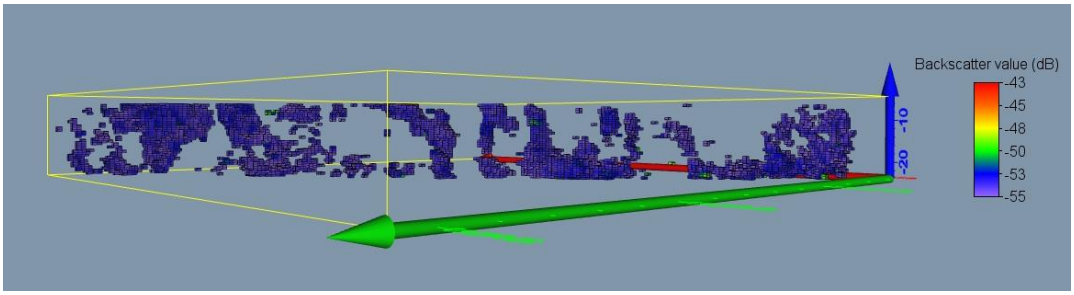

Figure 37. Sideway look on the resulting face render model for line 32 of the Ruyter track.

A big debating point on the three-dimensional models made is the threshold at which the backscatter values were filtered to solely represent the sediment plume. In this work a first rough filtering threshold of -60 to -30 dB was established for the data of the Ruyter track, based on both a peek in the histogram of backscatter values which showed the distribution of the backscatter values and a visual comparison between background WCBS without sediment and a backscatter profile with sediment on the other hand. This first pre-filtering was absolutely necessary before importing the data in Voxler as otherwise Voxler crashed due to restrictions of calculating capacity. It must be noted here that by using the same method as stated above, the backscatter values in the histogram of the water column of the Interballast track lay way lower than the -60 to -30 dB for the Ruyter track, namely ranging from -65 to -40 dB.

As observed in figure 28 also several spots of a higher backscatter value (ranging from -49 to -46 dB) were found within the sediment plume itself. This could be small fish which have a typical target strength of -60 to -44 decibels (Ostrovsky, 2009). As fish generally avoid sediment plumes due to the reduced visibility which makes feeding more difficult (Nieuwaal, 2001), a more likely explanation is just the fact that the sediment plume has a higher intensity over there which leads to a higher backscatter value. The need for a new campaign in which water samples are taken to grab a hold on the SPM concentration within the sediment plume is therefore big and further research into this is needed.

5.3.2. The difficulty of processing water column data with sediment plumes

First of all it should be noted that processing of the water column takes a lot of storage capacity relative to normal bathymetric data. One minute of water column data recorded along track on the Thorntonbank takes around 25 Mb. This means that one hour of recording already adds up to 1.5 Gb. This led to problems when processing the raw point data, with sometimes calculating times of several minutes when processing one line at a time. Especially when visualizing all the raw data Voxler crashed most of the times. It was only by pre-filtering to reduce the size of the files by an order magnitude that the several modules in Voxler could be applied to the data to be further processed. This problem can be solved in two ways. Either supercomputers have to be used with higher calculating and visualising capacities or the water column data acquiring software needs an implementation to reduce or compress the water column data.

The biggest minor side of the two-dimensional grids in SonarScope that show the plume intensity is the fact that the echo-integration algorithm in SonarScope does not retain the original backscatter value in decibels. It recalculates the values to a colour intensity value which is actually loss of information. It would therefore be an interesting feature if the developers update the software to make sure it retains the original backscatter value. In that way also the influence of scatters in the water column on the SBS can be investigated directly.

One last big problem was the inability of FMMidwater to automatically select the right range for each echogram. When in fan view (Fig. 38) this range can be manually set to specifically match that echogram. However this range will not be the right range for every echogram as the water column height is never constant due to sand dunes and ripples. This will lead to a situation in stacked view as observed in figure 39 where in a part of the water column the range will be set to high which leads to plume and water column data being lost when exporting. At other parts the range will be set to low, which means that parts of the seafloor and side lobe interference will be incorporated in the exported data.

In all the models of this work the range was set high enough so not to incorporate the seafloor and side lobe interference. This means that the models made in Voxler miss some small lower part of the water column data and that the volume calculations in the face render module are actually underestimated. An automatic detection of the right range for each echogram would therefore be a useful feature in the future.

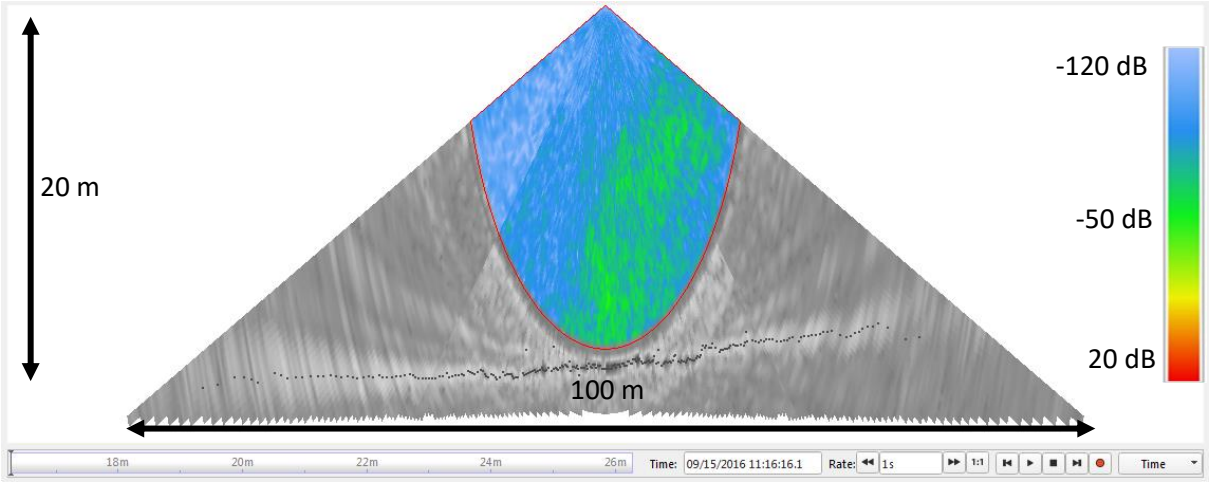

Figure 38. Echogram of water column with a good range set to filter out side lobe interference. The red line is the boundary, only the coloured part is retained.

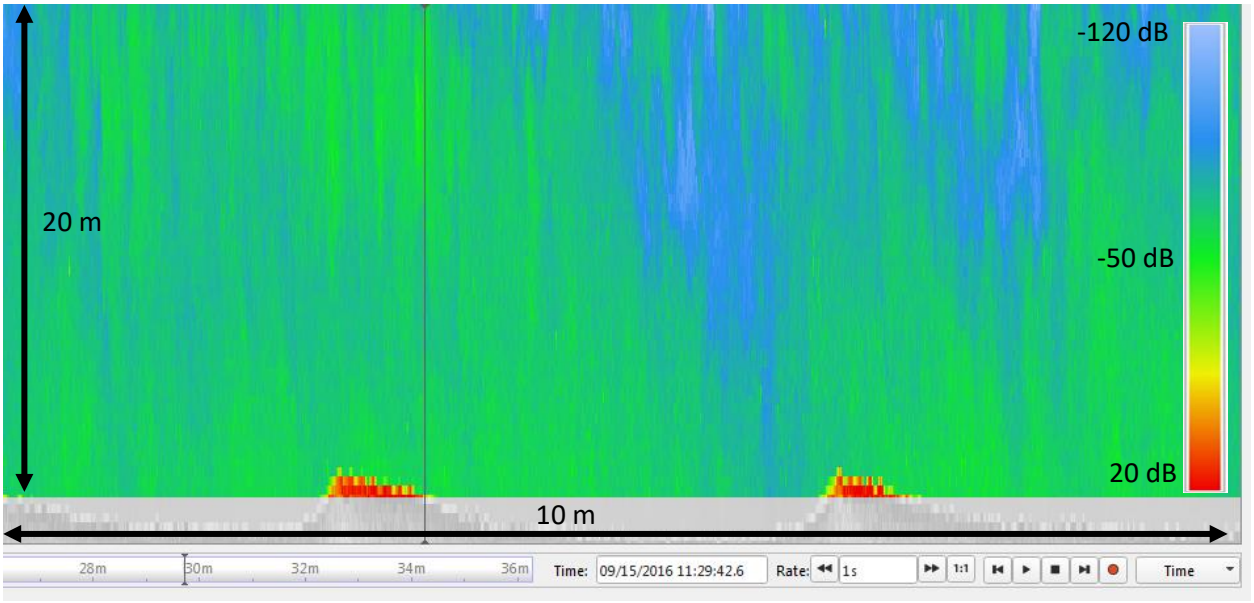

Figure 39. The accompanying stacked view of figure 38. Only the parts above the grey zone were retained. The thin central black line corresponds to echogram shown in figure 38.

5.4. Possible grain size of the sediment plume

Figure 32 showed the difference in grain size distribution between what is available at the seafloor on the Thorntonbank, and the eventual grain size of the dredged material. Although less data of this dredged material was available (only cumulative percentages of five grain sizes) a cautious statement can be made. As the difference between the cumulative percentages in figure 32 becomes bigger in between a grain size of approximately 175 µm and 250 µm, this could possibly indicate the grain size of the SPM in the water column, being medium sand.

It will be important in future research to have more extended grain size data of the dredged material to exactly compare it and calculate what the fraction is of the SPM. Maybe more accurate would be the direct measurement of SPM concentration in the water column using water samples. When this concentration is known it can be further researched what the influence is of the concentration of that actual suspended fraction on the backscatter values.

5.5. Impact of measurement conditions on results

First of all it should be noted that the effective capture of the sediment plume is a prerequisite to research the correlation between distance/time and plume intensity. A non-detection of sediment plume (intensity ranging from 5 to 30) will only add random water column noise data points. Therefore when looking to the two-dimensional plume intensity grid only the data from the Ruyter track was considered and only these calculated coefficients should be used. This because only along that track the sediment plume was captured along the whole water column.

The researched dependence of distance between survey and dredging vessel and the plume intensity for the Ruyter track shows that in that case it seems to not matter much for the intensity of the sediment plume if the survey vessel navigates close by or further away from the dredger. With a Pearson's correlation coefficient of -0.14 and a Spearman's rho rank correlation coefficient of -0.20 an almost non-correlation is proven. A fixed or varying distance between both vessels will have no implications on the acquired backscatter strength value of the sediment plume.

The dependence of time since passing between dredger and survey vessel versus the intensity of the sediment plume shows a moderate negative Spearman's rho rank correlation coefficient of -0.41. This means that the longer the time in between dredging and surveying, the lower the intensity of the plume will be. This implicates that the time since passing of dredger before detection by the survey ship has a 'moderate' relation to the plume intensity. This is in one way also logical as this is probably due to the sediment plume that disperses with a lower backscattering of the SPM as consequence.

Combining both points shows that there is a certain flexibility in detecting sediment plumes. Distance can vary in some way, there is no need to always stay at a certain fixed space behind the dredger. As for time there is a slightly higher dependence but this data showed that even after 1000 seconds the sediment plume is still visible. All this shows that the sediment plume has a certain consistency and is more or less stable and does not change or disperses that fast.

CHAPTER VI CONCLUSION

The main scope of this work was to investigate the dredging induced changes on the BCS in real time with a higher focus on what is happening in the water column and how a caused sediment plume can be better monitored using a MBES. The studying of the sediment plume in the water column using a MBES was relatively unexplored. A broad dataset was acquired and processed by combining the different separate types of data to extract information.

Firstly the dredging induced consequences on bathymetry and SBS were studied to choose which track represented the dredging furrow the best. This led to mainly the data of following TSHD Ruyter being used. The study of the bathymetry showed the real-time dredging furrow and the evolution of it. The SBS grids for each track showed the appearance of a 'halo' of high scatters right after dredging, which disappeared later-on. A possible theory to explain this was that turbulence temporarily causes a fine fraction to go into suspension, leaving the seafloor coarser, which shows off as a higher scattering. The fine fraction eventually settles, after a short time, on the same place, leading to the normal situation again.

A clear methodology was searched and described in this work to process raw water column data of sediment plumes. The final results of this were two-dimensional and three-dimensional grids. The two-dimensional grids from SonarScope showed the vertical mean intensity through the water column and gave a good indication of the plume intensity. Setbacks of these grids were the fact that remnants of the recording sectors were visible and that less values are taken into consideration at the sides which leads to a loss of accuracy at the outer sides of the grid. Additional to this the possibilities of treating water column in FMMidwater and Voxler were explained and showed a way to make a three-dimensional model of the sediment plume. Setbacks here were problems with calculating capacity due to the high memory needed and not being able to automatically detect the right range in FMMidwater. In Voxler a FaceRender was performed which represented the plume as blocks of a half cubic meter and a VolumeRender gave an insight in the internal parts of the sediment plume which show higher backscatter values possibly due to higher SPM concentration.

At last also several key correlations were researched to investigate if distance or time between dredger and survey ship and the plume intensity are in relation to each other. Mostly Spearman's rank coefficients were calculated which show no correlations between these parameters. Due to the complexity of the whole system it is also very difficult to put a cause/consequence relation on it.

During this investigation it became more clear that several key data was missing, or that some data had to be of a higher quality to asses and solve the whole problem of linking sediment plumes with WBS values. Therefore an ideal survey campaign could be proposed to better and more extensively research this topic, with the premature experience of this study in mind.

One setback was the interference of the on board ADCP of the survey vessel with the multibeam echosounding itself. Therefore the working frequencies of both systems will have to lie far enough from each other so they do not interfere. Current data to plot current vectors on the two dimensional grids was in this work at hand, but not from the survey site itself. Therefore a real time current measurement by using ADCP during the detection of the sediment plume could be useful.

During this study it became very clear that water samples from which the concentration of SPM could be retrieved was a missing link. Therefore water samples to obtain the SPM concentration should be taken. This at times that one is sure that the survey vessel lies above the sediment plume. This means

that the ideal time to take these samples is in between high and low tide as the current is minimal at that moment. This way of directly measuring of what the sediment plume consists will be more accurate than calculating the difference between the in-situ results and the grain size results of the dredged material. The data of water samples can then be used in the calibration process and to research if the higher backscatter values inside the plume correspond to higher SPM concentration within that plume

One of the things that has to be monitored further is the behaviour and stability of the sediment plume. This research already showed that there is a flexibility in the distance at which a dredger is followed and the time since passing of the dredger. By following a sediment plume and staying stationary above it one could maybe study how fast or slow the SPM settles or disperses.

Due to the complexity of the whole SPM and its backscatter in the water column and the still too poorly known factors influencing it, the usage of MBES to obtain a SPM concentration will require more extensive studies, although this work provides a small base to start from in this great endeavour.

REFERENCES

Scientific paper references

Battisto, G., Friedrichs, C., 2003. Monitoring suspended sediment plume formed during dredging using ADCP, OBS and bottle sample. Coastal Sediments 2003: Crossing Disciplinary Boundaries 1–12.

Bayrakci, G., Scalabrin, C., Dupré, S., Leblond, I., Tary, J.-B., Lanteri, N., Augustin, J.-M., Berger, L., Cros, E., Ogor, A., Tsabaris, C., Lescanne, M., Géli, L., 2014. Acoustic monitoring of gas emissions from the seafloor. Part II: a case study from the Sea of Marmara. Marine Geophysical Research 35, 211–229.

Best, J., Simmons, S., Parsons, D., Oberg, K., Czuba, J., Malzone, C., 2010. A new methodology for the quantitative visualization of coherent flow structures in alluvial channels using multibeam echo-sounding (MBES). Geophysical Research Letters 37, 1–6.

Blott, S., Pye, K., 2001. Gradistat: A grain size distribution and statistics package for the analysis of unconcolidated sediments. Earth Surface Processes and Landforms 26, 1237–1248.

Booth, J., Miller, R., Mckee, B., Leathers, R., 2000. Wind-induced bottom sediment resuspension in a microtidal coastal environment. Continental Shelf Research 20, 785–806.

Briere, C., Roos, P., Garel, E., 2010. Modelling the morphodynamics of the Kwinte Bank , subject to sand extraction. Journal of Coastal Research SI, 117–126.

Calder, B., 2003. Automatic statistical processing of multibeam echosounder data. The International Hydrographic Review 4, 53–68.

Calder, B., Wells, D., 2007. CUBE User's Manual. Technical report. Center for Coastal Ocean Mapping, and NOAA/UNH Joint Hydrographic Center, University of New Hampsire, pp. 54.

Carr, S.J., Holmes, R., Van Der Meer, J.J.M., Rose, J., 2006. The Last Glacial Maximum in the North Sea Basin : micromorphological evidence of extensive glaciation. Journal of Quaternary Science 21, 131–153.

Cochrane, N.A., Li, Y., Melvin, G.D., 2003. Quantification of a multibeam sonar for fisheries assessment applications. The Journal of the Acoustical Society of America 114, 745–758.

Colbo, K., Ross, T., Brown, C., Weber, T., 2014. A review of oceanographic applications of water column data from multibeam echosounders. Estuarine, Coastal and Shelf Science 145, 41–56.

Cox, M.J., Borchers, D.L., Demer, D.A., Cutter, G.R., Brierley, A.S., 2011. Estimating the density of Antarctic krill (Euphausia superba) from multi-beam echo-sounder observations using distance sampling methods. Journal of the Royal Statistical Society Series C-Applied Statistics 60, 301–316.

De Backer, A., Hillewaert, H., Van Hoey, G., Wittoeck, J., Hostens, K., 2014. Structural and functional biological assessment of aggregate dredging intensity on the Belgian part of the North Sea, in: Which Future for the Sand Extraction in the Belgian Part of the North Sea. FPS Economy, Brussels, pp. 29–58.

De Batist, M., 1989. Seismostratigrafie en struktuur van het Paleogeen in de zuidelijke Noordzee. PhD Thesis, Ghent University, Ghent, 107 pp.

De Moor, G., 1996. De zanden van de Vlaamse Vallei, in: Delfstoffen in Vlaanderen. Brussel Ministerie van de Vlaamse Gemeenschap. Departement Natuurlijke Rijkdommen 1996, pp. 63–68.

De Moor, G., 1986. Het continentaal platform van de Noordzee gedurende het Kwartair. Tijdschrift over Waterproblematiek 31, 6–9.

Degraer, S., Brabant, R., Rumes, B., 2013. Environmental impacts of offshore wind farms in the Belgian part of the North Sea. Royal Belgian Institute of Natural Sciences (RBINS), Operational Directorate Natural Environment, Marine Ecology and Management Section, Brussels, 239 pp.

Degrendele, K., Roche, M., De Mol, L., Schotte, P., Vandenreyken, H., 2014. Synthesis of the monitoring of the aggregate extraction on the Belgian Continental Shelf from 2011 till 2014, in: Which Future for the Sand Extraction in the Belgian Part of the North Sea. FPS Economy, Brussels, pp. 3–29.

Degrendele, K., Roche, M., Schotte, P., Van Lancker, V., Bellec, V., 2010. Morphological evolution of the Kwinte Bank central depression before and after the cessation of aggregate extraction. Journal of Coastal Research SI, 77–86.

Degrendele, K., Roche, M., Vandenreyken, H., 2017. New limits for the sand extraction on the Belgian part of the North Sea, in: Belgian Marine Sand: A Scarce Resource? FPS Economy, Brussels, pp. 135–147.

Del Grosso, V.A., 1974. New equation for the speed of sound in natural waters (with comparisons to other equations). The Journal of the Acoustical Society of America 56, 1084.

Duelos, P.A., Lafite, R., Le Bot, S., Rivoalen, E., Cuvilliez, A., 2013. Dynamics of turbid plumes generated by marine aggregate dredging: an example of a macrotidal environment (the Bay of Seine, France). Journal of Coastal Research 29, 25–37.

Erftemeijer, P., Riegl, B., Hoeksema, B., Todd, P., 2012. Environmental impacts of dredging and other sediment disturbances on corals : a review. Marine Pollution Bulletin 64, 1737–1765.

Evangelinos, D., 2015. Dispersion and deposition of sediment plumes, resulting from intensive marine aggregate extraction. Master Thesis, University of Ghent, Ghent, 42 pp.

Flemish Government Department Coastal Safety, 2014. Het masterplan kustveiligheid. Flemish Government, Ostend, 32 pp.

Folk, R.L., 1954. The distinction between grain size and mineral composition in sedimentary-rock nomenclature. The Journal of Geology 62, 344–359.

Folk, R.L., Ward, W.C., 1957. Brazos River bar: a study in the significance of grain size parameters. Journal of Sedimentary Research 27, 3–26.

FPS Economy S.M.E.s Self-employed and Energy, 2014. Zand- en grindwinning in het Belgische deel van de Noordzee. FPS Economy, Brussels, Belgium, pp. 30.

Gabrielson, J., Lukatelich, R.J., 1985. Wind-related resuspension of sediments in the Peel-Harvey estuarine system. Estuarine, Coastal and Shelf Science 20, 135–145.

Gee, L., Doucet, M., Parker, D., Weber, T., Beaudoin, J., 2012. Is multibeam water column data really worth the disk space? “Hydro12 - taking care of the sea,” in: Conference Proceedings 12-15 November 2012. Rotterdam, the Netherlands, pp. 81–86.

Godin, A., 1996. Field procedures for the calibration of shallow water multibeam echo-sounding systems, in: Canadian Hydrographic Conference 1996. Canadian Hydrographic Service, Halifax, Nova Scotia.

Golden Software Inc., 2012a. Surfer 11 Quick Start Guide. Technical Report. Golden Software Inc, Colorado, U.S.A., pp. 60.

Golden Software Inc., 2012b. Voxler User’s Guide. Technical Report. Golden Software Inc, Colorado, U.S.A., pp. 72.

Greinert, J., 2008. Monitoring temporal variability of bubble release at seeps: the hydroacoustic swath system GasQuant. Journal of Geophysical Research: Oceans 113, 1–20.

Greinert, J., Artemov, Y., Egorov, V., De Batist, M., McGinnis, D., 2006. 1300-m-high rising bubbles from mud volcanoes at 2080 m in the Black Sea: hydroacoustic characteristics and temporal variability. Earth and Planetary Science Letters 244, 1–15.

Greinert, J., Faure, K., Von Deimling, J.S., McGinnis, D.F., Kipfer, R., Linke, P., 2010. Methane seepage along the Hikurangi Margin of New Zealand: geochemical and physical data from the water column, sea surface and atmosphere. Marine Geology 272, 170–188.

Group De Cloedt N.v., 2011. Interballast III. Technical Report. Group De Cloedt n.v., Brussels, Belgium, pp. 2.

Henriet, J.-P., De Moor, G., De Batist, M., 1989. The Quaternary and Tertiary geology of the Southern Bight, North Sea. Ministry of Economic Affairs, Belgian Geological Survey, Brussels, 241 pp.

Jones, A.T., Greinert, J., Bowden, D.A., Klaucke, I., Petersen, C.J., Netzeband, G.L., Weinrebe, W., 2010. Acoustic and visual characterisation of methane-rich seabed seeps at Omakere Ridge on the Hikurangi Margin, New Zealand. Marine Geology 272, 154–169.

Jones, J., 1992. Environmental impact of trawling on the seabed : a review. New Zealand Journal of Marine and Freshwater Research 26, 59–67.

Kim, H., 2011. Effect of resuspension on the release of heavy metals and water chemistry in anoxic and oxic sediments. Soil, Air, Water 39, 908–915.

Kongsberg Maritime AS, 2007. Seafloor Information System: operator manual. Technical report. Kongsberg Maritime AS, Horten, Norway, pp. 551.

Krumbein, W.C., Pettijohn, F.J., 1938. Manual of sedimentary petrography I. sampling, preparation for analysis, mechanical analysis and statistical analysis. Appleton-Century-Crofts, New York.

Kruss, A., Blondel, P., Tegowski, J., 2011. Mapping macrophytes and habitats: single-beam and multibeam imaging in the Arctic, in: 4th International Conference and Exhibition on “Underwater Acoustic Measurements: Technologies and Results.” pp. 1687–1694.

Kruss, A., Blondel, P., Tegowski, J., Wiktor, J., Tatarek, A., 2008. Estimation of macrophytes using single-beam and multibeam echosounding for environmental monitoring of arctic fjords (Kongsfjord, West Svalbard Island). The Journal of the Acoustical Society of America 123, 3213.

Kruss, A., Madricardo, F., Sigovini, M., Christian, F., Montereale Gavazzi, G., 2015. Assessment of submerged aquatic vegetation abundance using multibeam sonar in very shallow and dynamic environment. The Lagoon of Venice (Italy) case study. 2015 IEEE/OES Acoustics in Underwater Geosciences Symposium (RIO Acoustics) 1–7.

Ladroit, Y., Lurton, X., Sintès, C., Augustin, J.M., Garello, R., 2012. Definition and application of a quality estimator for multibeam echosounders, in: Conference Proceedings 2012 Oceans - Yeosu. pp. 1–7.

Lamarche, G., Le Gonidec, Y., Greinert, J., Lucieer, V., Lurton, X., 2017. Building capability for in situ quantitative characterisation of the ocean water column using acoustic multibeam backscatter data, Workshop report - 25-28 April 2017 - Rennes France. The Water Column Imaging Working Group, Rennes, France.

Le Bot, S., Van Lancker, V., Deleu, S., De Batist, M., Henriet, J.P., 2003. Tertiary and quaternary geology of the Belgian Continental Shelf, in: Scientific Support Plan for a Sustainable Development Policy. PPS Science Policy, Brussels, p. 76.

Lebbe, L., Van Meir, N., Viaene, P., 2008. Potential implications of sea-level rise for Belgium. Journal of Coastal Research 24, 358–366.

Lurton, X., 2002. An introduction to underwater acoustics: principles and applications. Springer, New York.

Lurton, X., Lamarche, G., 2015. Backscatter measurements by seafloor - mapping sonars guidelines and recommendations, in: A Collective Report by Members of the GeoHab Backscatter Working Group. p. 200.

Mackenzie, K. V., 1981. Nine-term equation for sound speed in the oceans. The Journal of the Acoustical Society of America 70, 807.

Mann, R., 1998. Field calibration procedures for multibeam sonar systems. US Army Corps of Engineers Topographic Engineering Center, Virginia, 13p.

Mathys, M., 2009. The Quaternary geological evolution of the Belgian Continental Shelf, southern North Sea. PhD Thesis, Ghent University, Ghent, 382 pp.

McCarthy, E.M., Sabol, B., 2000. Acoustic characterization of submerged aquatic vegetation: military and environmental monitoring applications, in: Conference Proceedings 2000 Oceans. pp. 1957–1961.

Melvin, G.D., Cochrane, N.A., 2014. Multibeam acoustic detection of fish and water column targets at high-flow sites. Estuaries and Coasts 38, 227–240.

Mills, D., Kemps, H., 2016. Generation and release of sediments by hydraulic dredging : a review, in: WAMSI Dredging Science Node Report of Theme 2 - Project 2.1. Dredging Science Node, Western Australian Marine Science Institution, Perth, Western Australia, p. 97.

Nieuwaal, M., 2001. Requirements for sediment plumes caused by dredging. PhD Thesis, Delf University of Technology, Delft, 89 pp.

Nikolovska, A., Sahling, H., Bohrmann, G., 2008. Hydroacoustic methodology for detection, localization, and quantification of gas bubbles rising from the seafloor at gas seeps from the eastern Black Sea. Geochemistry, Geophysics, Geosystems 9, 1–13.

OD Nature, 2014. Oceanographic research vessel Belgica: technical description. Technical Report. OD Nature, Brussels, pp. 23.

Ostrovsky, I., 2009. Fish and methane bubbles in aquatic ecosystems: hydroacoustic separation and quantification. Verhandlungen des Internationalen Verein Limnologie 30, 870–873.

Ostrovsky, I., McGinnis, D.F., Lapidus, L., Eckert, W., 2008. Quantifying gas ebullition with echosounder: the role of methane transport by bubbles in a medium-sized lake. Limnology and Oceanography: Methods 6, 105–118.

Palanques, A., Guille, J., Puig, P., 2001. Impact of bottom trawling on water turbidity and muddy sediment of an unfished continental shelf. American Society of Limnology and Oceanography 46, 1100–1110.

Pilskaln, C.H., Churchill, J.H., Mayer, L.M., Pilskaln, C.H., Churchill, J.H., Mayert, L.M., 1998. Resuspension of sediment by bottom trawling in the Gulf of Maine and potential geochemical consequences. Conservation Biology 12, 1223–1229.

Pohlmann, T., Sündermann, J., 2011. A brief analysis of North Sea physics. Oceanologia 53, 663–689.

Pyć, C.D., Geoffroy, M., Knudsen, F.R., 2016. An evaluation of active acoustic methods for detection of marine mammals in the Canadian Beaufort Sea. Marine Mammal Science 32, 202–219.

QPS hydrographic and marine software solutions, 2017. Fledermaus 7.4 Documentation. Technical Report. QPS hydrographic and marine software solutions, Zeist, The Netherlands.

QPS hydrographic and marine software solutions, 2016. Qimera Reference Manual. Technical report. QPS hydrographic and marine software solutions, Zeist, the Netherlands.

Richards, S.D., Leighton, T.G., 2003. High frequency sonar performance predictions for littoral operations: the effect of suspended sediments and microbubbles. Journal of Defence Science 8, 1–7.

Roche, M., Degrendele, K., De Mol, L., Milano, R., Van den Branden, R., De Schepper, G., 2013. Essential facts of the monitoring of the sand extraction and its impact on the Flemish banks on the Belgian continental shelf from 2003 to 2012, in: Marine and River Dune Dynamics - Madrid IV - 15 & 16 April 2013. Bruges, Belgium, pp. 223–230.

Roche, M., Degrendele, K., Vandenreyken, H., Schotte, P., 2017. Multi time and space scale monitoring of the sand extraction and its impact on the seabed by coupling EMS data and MBES measurements, in: Belgian Marine Sand: A Scarce Resource? FPS Economy, Brussels, p. 164.

Rona, P., Bemis, K., Kenchammana-Hosekote, D., Silver, D., 1998. Acoustic imaging and visualization of plumes discharging from black smoker vents on the deep seafloor, in: Proceedings Visualization ’98. p. 4.

Scandella, B.P., Pillsbury, L., Weber, T., Ruppel, C., Hemond, H.F., Juanes, R., 2016. Ephemerality of discrete methane vents in lake sediments. Geophysical Research Letters 1–14.

Schneider Von Deimling, J., Papenberg, C., 2012. Technical note: detection of gas bubble leakage via correlation of water column multibeam images. Ocean Science 8, 175–181.

Schneider Von Deimling, J., Weinrebe, W., 2014. Beyond bathymetry: water column imaging with multibeam echosounder systems. Hydrographische Nachrichten 31 (97), 6–10.

Simmons, S.M., Parsons, R., Best, J.L., Orfeo, O., Lane, S.N., Kostaschuk, R., Hardy, R.J., West, G., Malzone, C., Marcus, J., Pocwiardowski, P., 2010. Monitoring suspended sediment dynamics using MBES. Journal of Hydraulic Engineering 136, 45–49.

Skarke, A., Ruppel, C., Kodis, M., Brothers, D., Lobecker, E., 2014. Widespread methane leakage from the sea floor on the northern US Atlantic margin. Nature Geoscience 7, 657–661.

Spearman, J., De Heer, A., Aarninkhof, S., Van Koningsveld, M., 2011. Validation of the TASS system for predicting the environmental effects of trailing suction hopper dredgers. Terra et aqua 125, 14–22.

Taylor, P., Wilber, D.H., Clarke, D.G., 2011. Biological effects of suspended sediments : a review of suspended sediment impacts on fish and shellfish with relation to dredging activities in estuaries. North American Journal of Fisheries Management 21, 37–41.

Todd, V.L.G., Todd, I.B., Gardiner, J.C., Morrin, E.C.N., Macpherson, N.A., Dimarzio, N.A., Thomsen, F., 2015. A review of impacts of marine dredging activities on marine mammals. ICES Journal of Marine Science 72, 328–340.

Van De Kerckhove, L., 2011. Sea-dredged sand in real terms, in: Marine Aggregate Extraction: Needs, Guidelines and Future Prospects. FPS Economy, Brussels, pp. 143–145.

Van den Branden, R., De Schepper, G., Naudts, L., 2014. Electronic Monitoring System (EMS) for sustainable management of sand and gravel resources, in: Which Future for the Sand Extraction in the Belgian Part of the North Sea. FPS Economy, Brussels, pp. 105–106.

Van Lancker, V., Baeye, M., Evangelinos, D., Eynde, D., 2014. Monitoring of the impact of the extraction of marine aggregates, in casu sand, in the zone of the Hinder Banks, in: Scientific Report 2 – January - December 2014. RBINS-OD Nature, Brussels, p. 384.

Van Lancker, V., Du Four, I., Verfaillie, E., Deleu, S., Schelfaut, K., Fettweis, M., Van Den Eynde, D., Francken, F., Monballiu, J., Giardino, A., Portilla, J., Lanckneus, J., Moerkerke, G., 2007. Management, research and budgetting of aggregates in shelf seas related to end-users (Marebasse). Belgian Science Policy, Brussels, p. 125.

Vanhellemont, Q., Ruddick, K., 2014. Turbid wakes associated with offshore wind turbines observed with Landsat 8. Remote Sensing of Environment 145, 105–115.

Veloso, M., Greinert, J., Mienert, J., De Batist, M., 2015. A new methodology for quantifying bubble flow rates in deep water using splitbeam echosounders: examples from the Arctic offshore NW-Svalbard. Limnology and Oceanography: Methods 13, 267–287.

Weber, T.C., Peña, H., Jech, J.M., 2009. Consecutive acoustic observations of an Atlantic herring school in the Northwest Atlantic. ICES Journal of Marine Science 66, 1270–1277.

Wilson, W.D., 1960. Equation for the speed of sound in sea water. The Journal of the Acoustical Society of America 32, 1357.

Wyllie, K., Weber, T., Armstrong, E., 2015. Using multibeam echosounders for hydrographic surveying in the water column: estimating wreck least depths, in: U.S. Hydrographic Conference 2015. National Harbor MD, p. 20.

Ziegler, P.A., 1992. North Sea rift system. Tectonophysics 208, 55–75.

Electronic references

Dredgepoint, 2017a, accessed 12 August 2017. Retrieved from:
https://www.dredgepoint.org/dredging-database/equipment/ruyter.

Dredgepoint, 2017b, accessed 12 August 2017. Retrieved from:
https://www.dredgepoint.org/dredging-database/equipment/schotsman.

Flanders Marine Institute, 2017, accessed 9 June 2017. Retrieved from:
http://www.vliz.be/en/technical-specifications.

IFREMER, 2017, accessed 1 August 2017. Retrieved from:
http://flotte.ifremer.fr/fleet/Presentation-of-the-fleet/Logiciels-embarques/SonarScope.

Jan De Nul, 2017, accessed13 March 2017. Retrieved from:
http://www.jandenul.com/en/equipment/fleet/trailing-suction-hopper-dredger.

Meetnet Vlaamse Banken, accessed 25 February 2017. Retrieved from:
http://meetnetvlaamsebanken.be/Measurement

APPENDIX

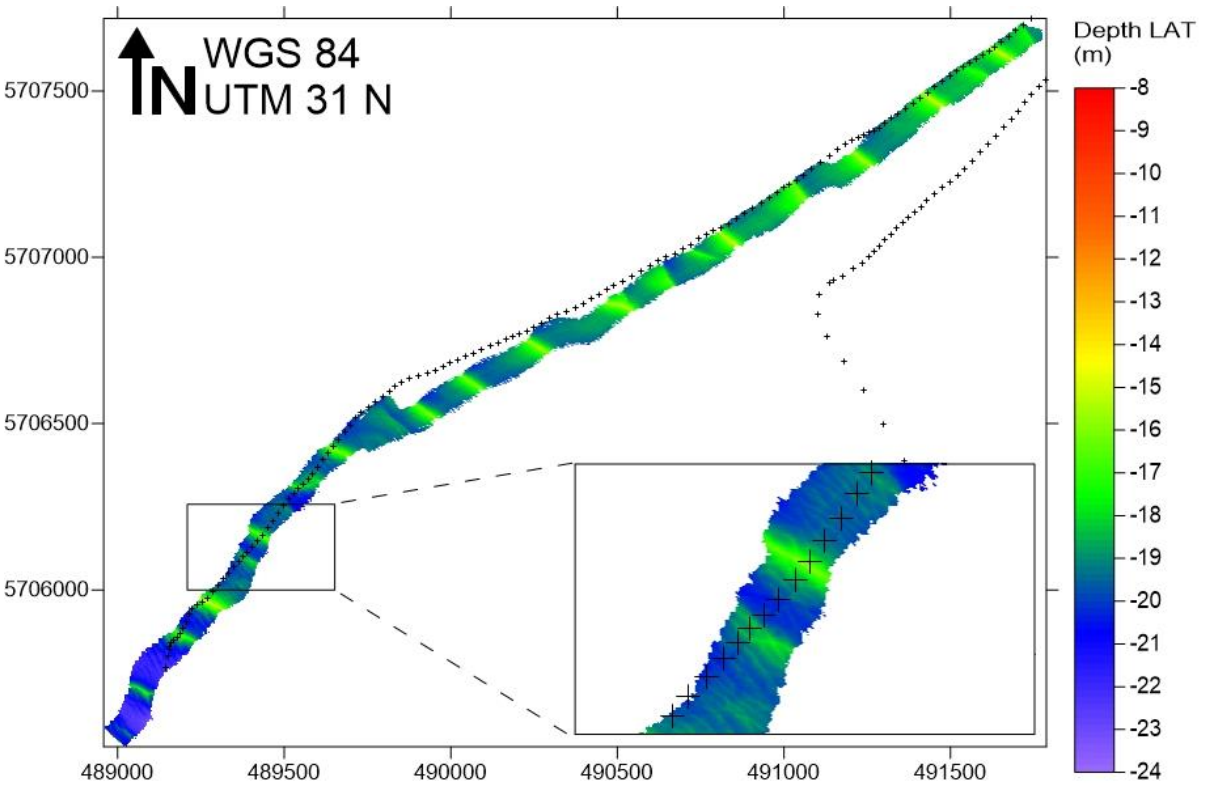

Appendix I. Bathymetry of the Schotsman track. The navigational data of the Interballast is represented with black crosses.

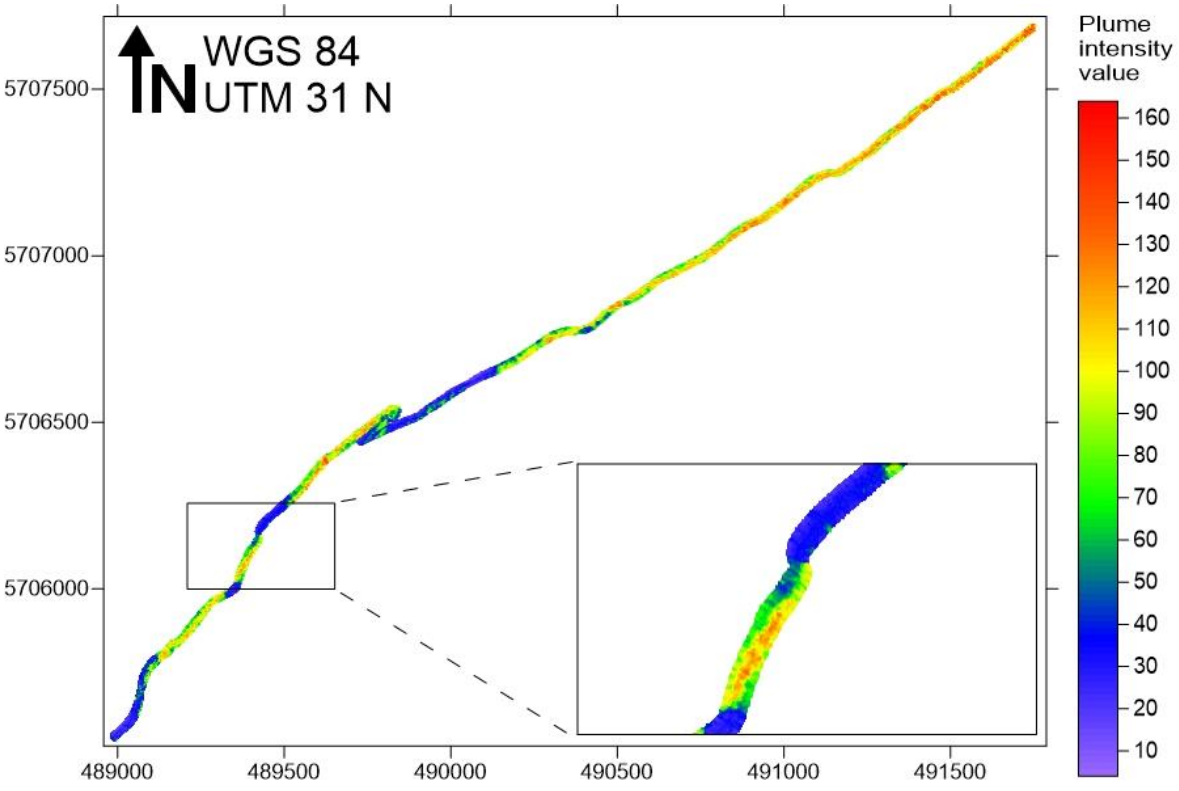

Appendix II. Echo-integration grid of the Schotsman track.

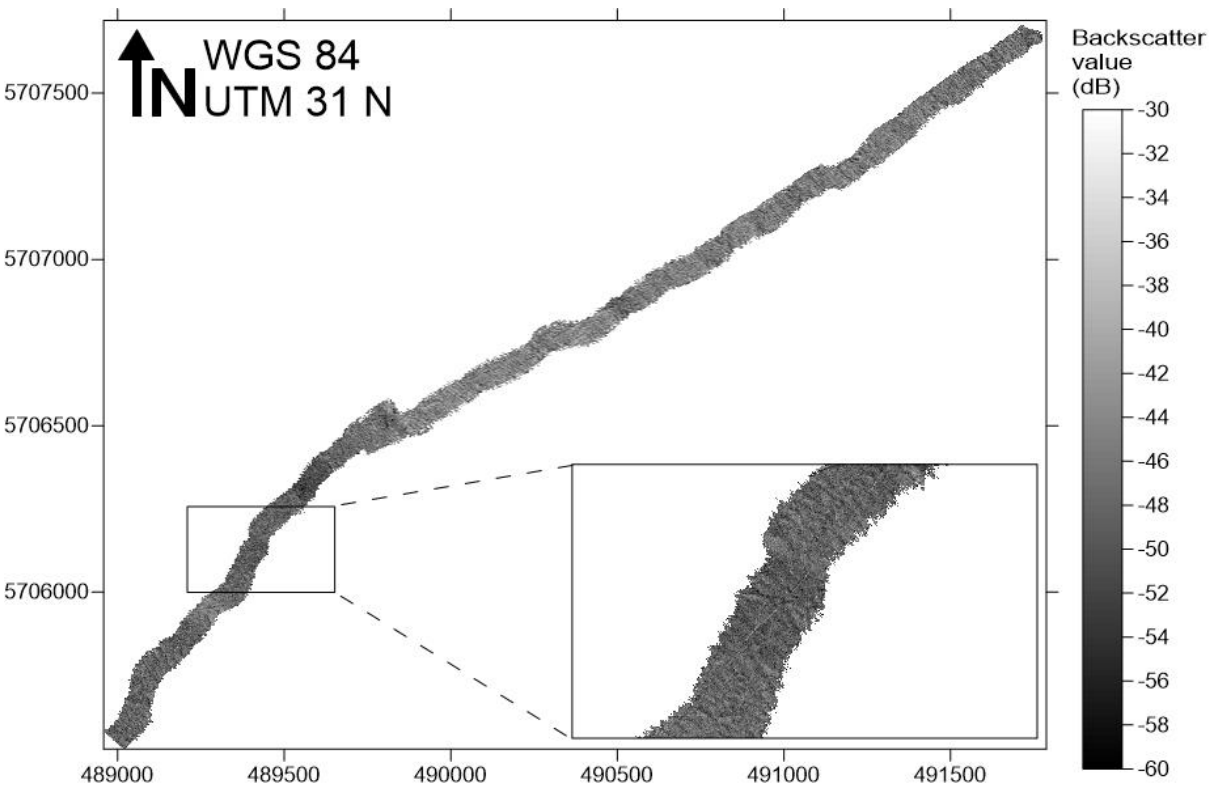

Appendix III. Backscatter map of the Schotsman track made using FMGT.

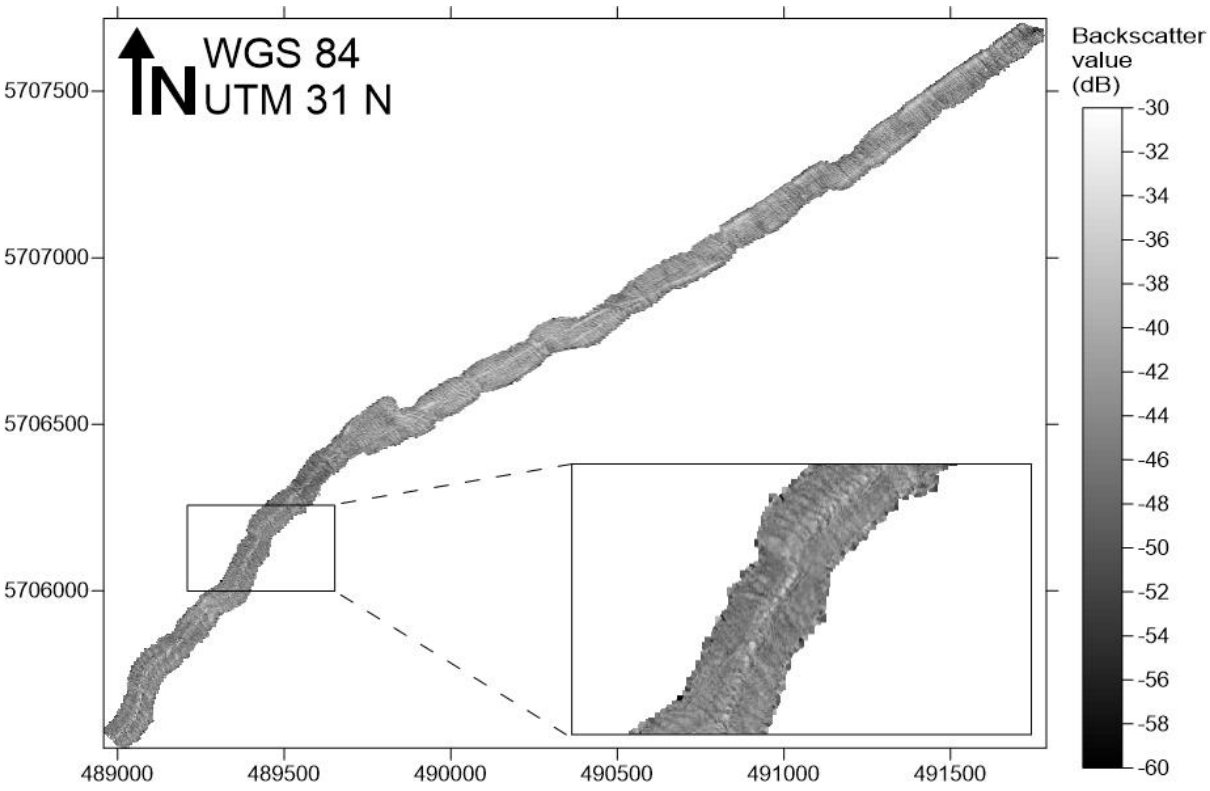

Appendix IV. Backscatter map of the Schotsman track made using SonarScope.

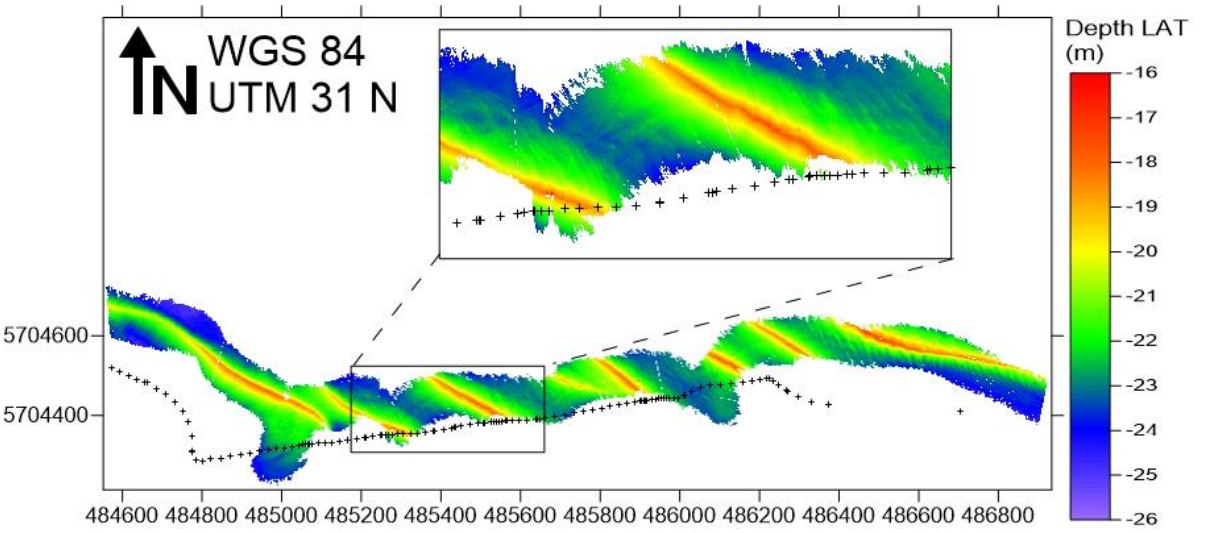

Appendix V. Bathymetry of the Interballast track. The navigational data of the Interballast is represented with black crosses.

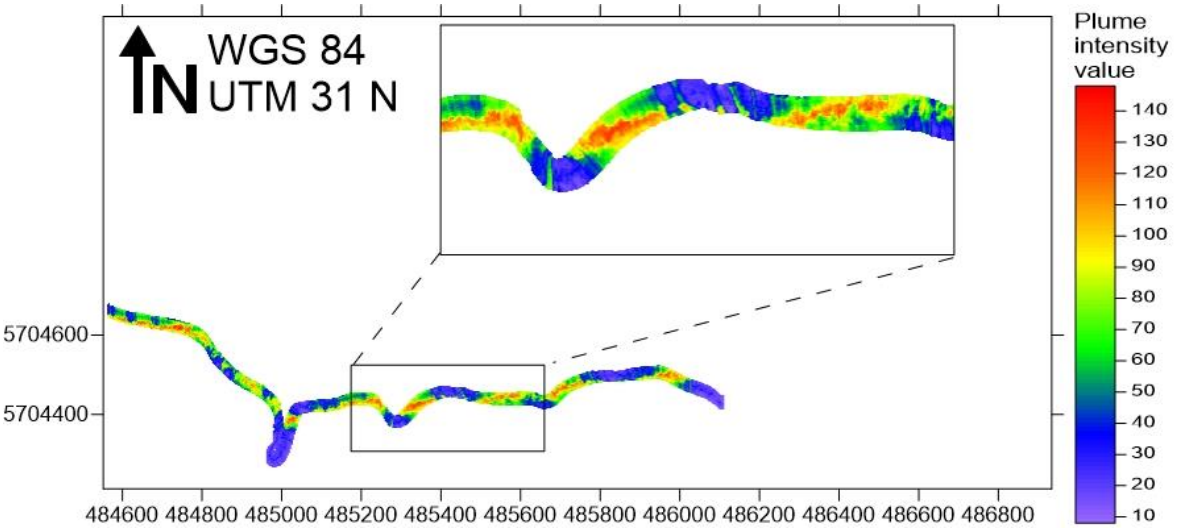

Appendix VI. Echo-integrated grid of the Interballast track.

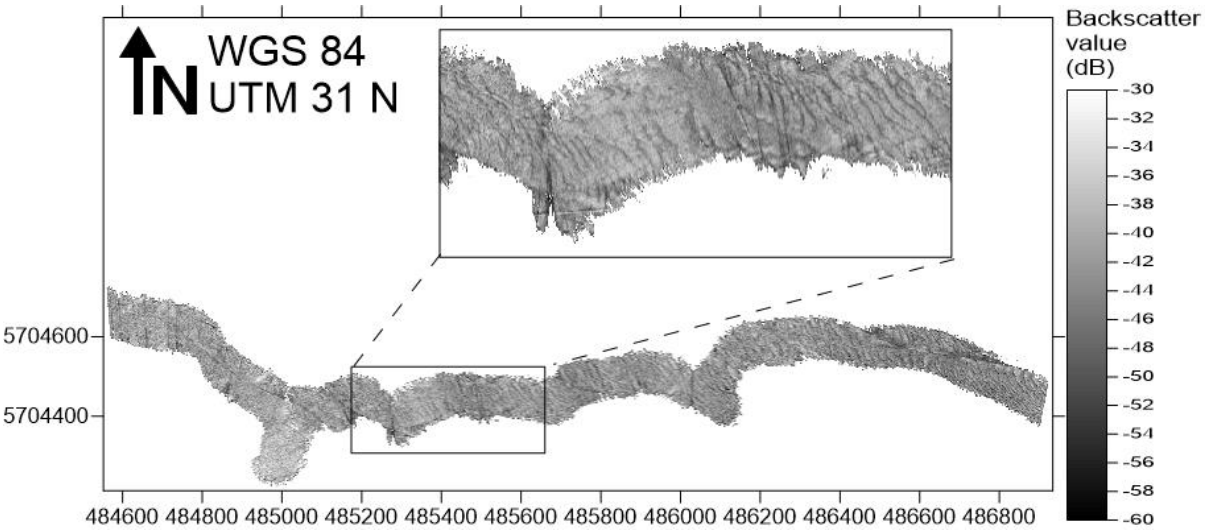

Appendix VII. Backscatter map of the Interballast track made using FMGT.

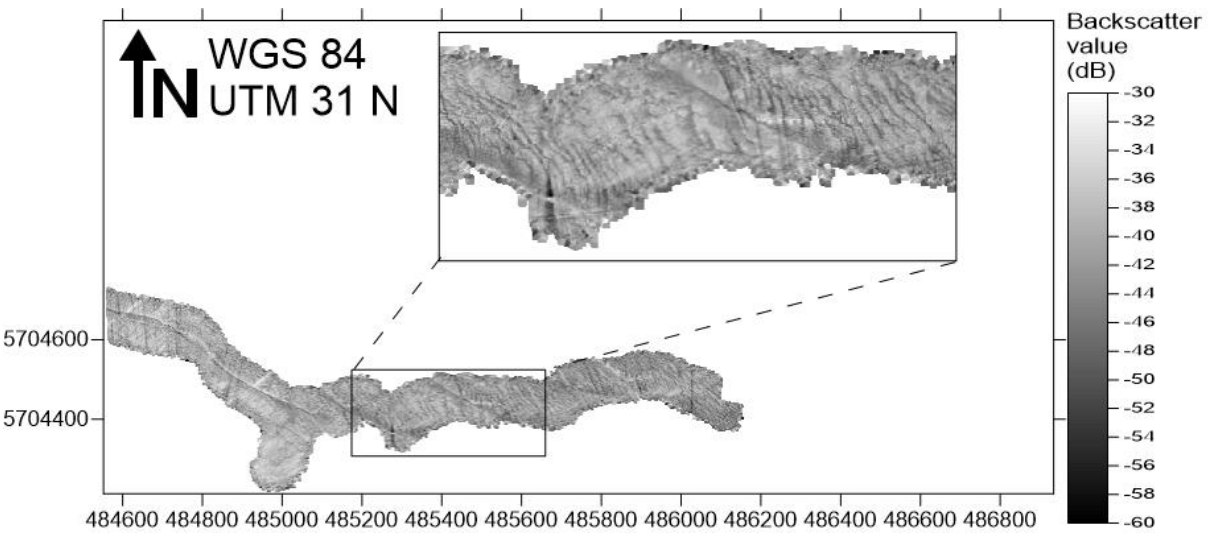

Appendix VIII. Backscatter map of the Interballast track made using SonarScope.

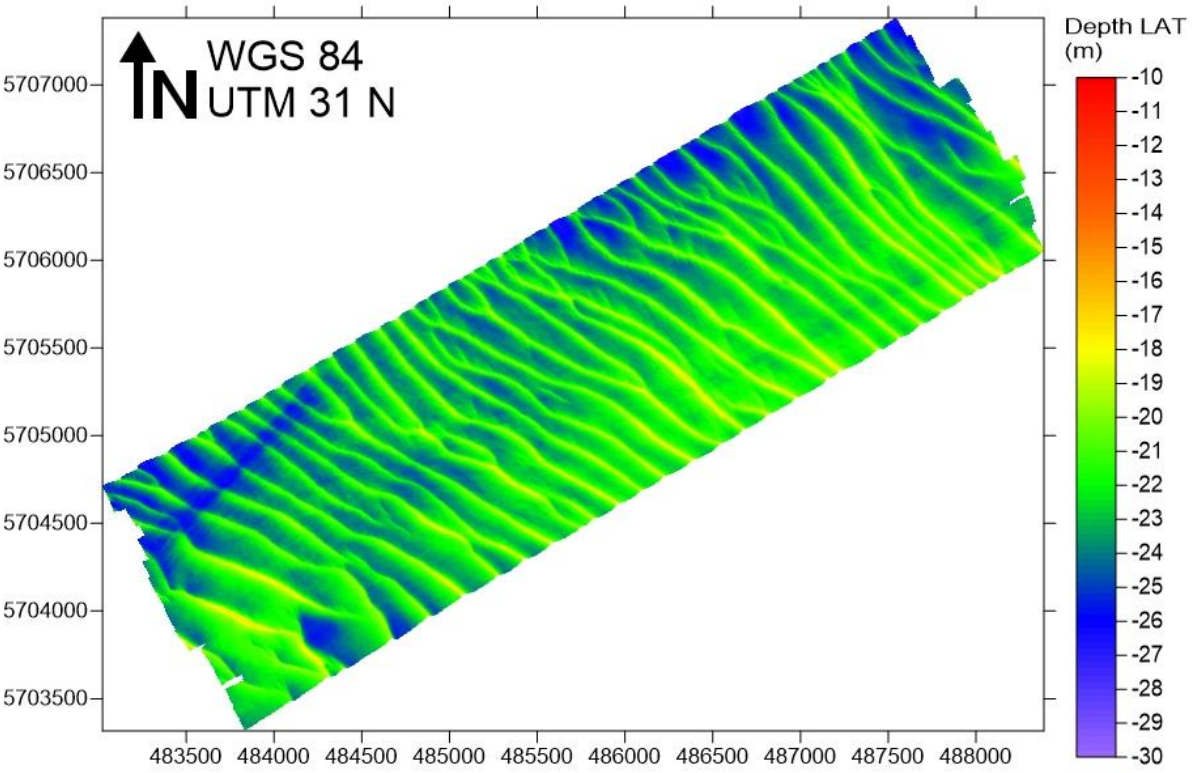

Appendix IX. Bathymetric grid from campaign TBMAB1610. Campaign conducted in March 2016.

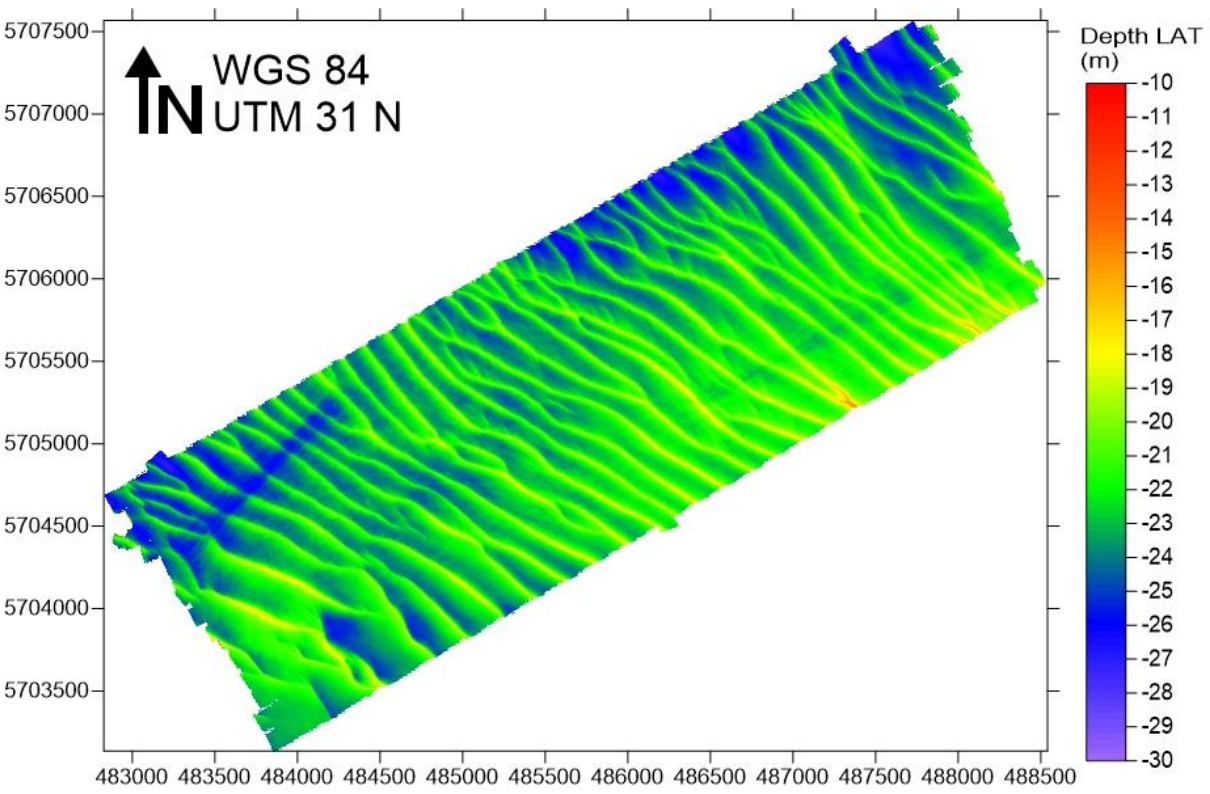

Appendix X. Bathymetric grid from campaign TBMAB16-310. Campaign conducted in April 2016.

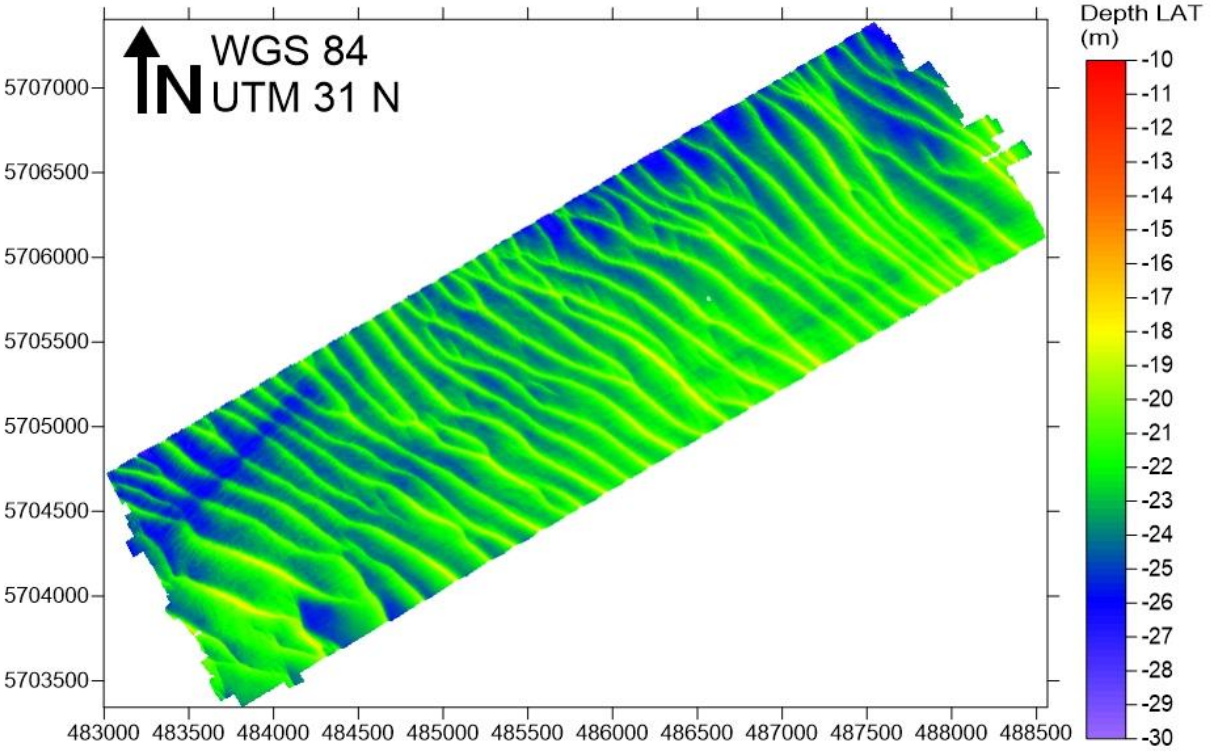

Appendix XI. Bathymetric grid from campaign TBMAB16-730. Campaign conducted in September 2016.

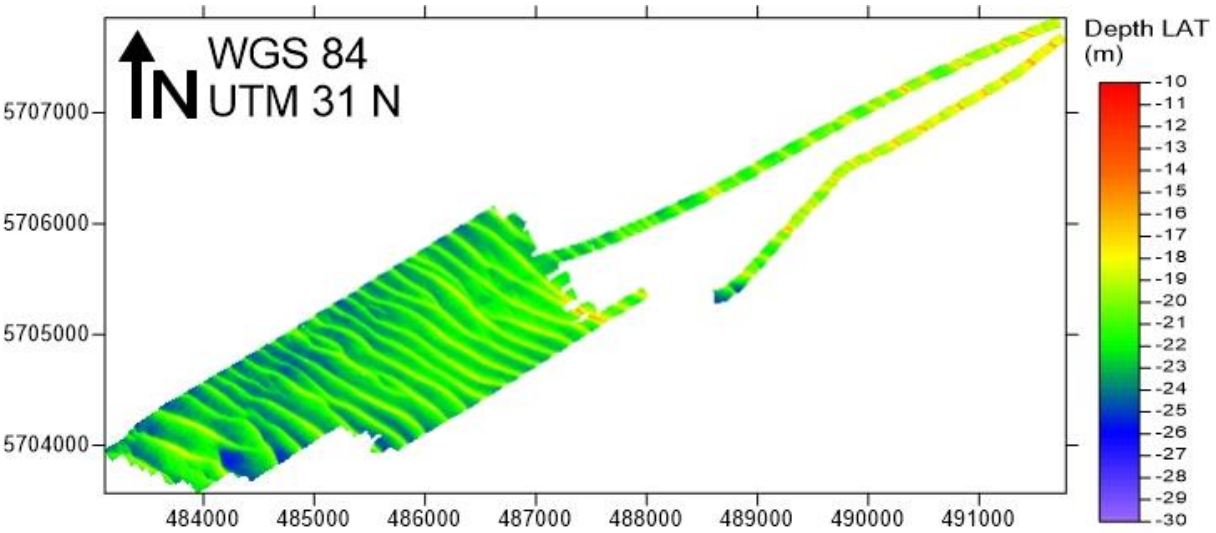

Appendix XII. Bathymetric grid from campaign TBMAB16-900. Campaign conducted in November 2016.

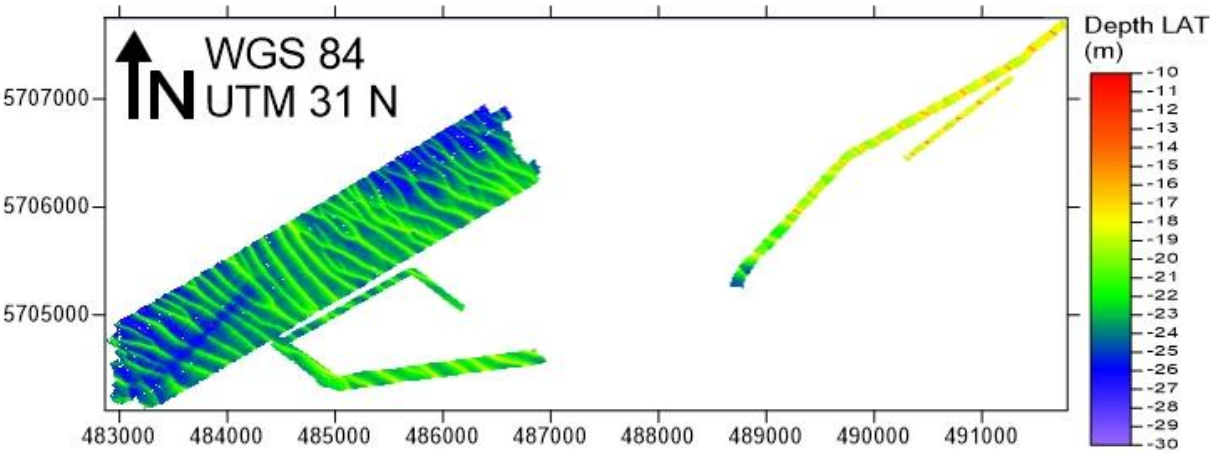

Appendix XIII. Bathymetric grid from campaign TBMAB16-930. Campaign conducted in December 2016.